

**INFLUENCE OF WO_3 ON GAMMA RAY SHIELDING
GLASS IN $30\text{BaO} - (50-x)\text{B}_2\text{O}_3 - 10\text{BG} - 10\text{CR} - x\text{WO}_3$
SYSTEM**

PATTARANIPA GUNHAKOON

**A THESIS SUBMITTED IN PARTIAL FULFILLMENT OF THE
REQUIREMENTS FOR THE DEGREE OF DOCTOR OF PHILOSOPHY
MAJOR IN PHYSICS
FACULTY OF SCIENCE
UBON RATCHATHANI UNIVERSITY
ACADEMIC YEAR 2020
COPYRIGHT OF UBON RATCHATHANI UNIVERSITY**

ACKNOWLEDGEMENT

I would like to express my sincere gratitude to several individuals and organizations for supporting me throughout my Ph.D. study. Firstly, I immensely grateful to my advisor Assoc. Prof. Raewat Laopaiboon and my co-advisor Assoc. Prof. Jintana Laopaiboon for the continuous support of my Ph.D. study, for their patience, motivation and immense knowledge. Their guidance helped me in all the time of research and writing of this thesis. Besides, I would like to thank my thesis committee Besides, I would like to thank my thesis committee Dr. Nuan La-ong Srakaew, Dr. Somkid Pencharee, Dr. Orathai Thumthan and Assoc. Prof. Dr. Supakorn Pukird for their insightful comments and encouragement, but also for the hard question which incented me to widen my research from various perspectives.

Special mention goes to Asst. Prof. Chadet Yenchai. I thank him wholeheartedly, for giving me so many wonderful opportunities about radiation shielding testing at department of Nuclear Engineering, faculty of Engineering, Chulalongkorn university. Similar, I am also hugely appreciative to Instructor Thon Thongklom, especially for sharing his microhardness testing expertise willingly at department of Industrial Engineering, faculty of Engineering, Ubon Ratchathani University. In addition, I am deeply indebted to the Science Achievement Scholarship of Thailand; this financial support has enabled me to complete my Ph.D. studies successfully. Also, I am grateful the department of Physics, Glass Technology Excellence Center, Scientific Equipment Center, Ubon Ratchathani university for research tools and places. I would like thanks to Dr. Ussadawut Patakham from National Metal and Materials Technology Center for EDS analysis. My sincere thanks also goes to many related laboratory staff, who gave access to the laboratory and research facilities. Without they precious support it would not be possible to conduct this research.

Last but not the least, I would like to thank my family and friends for unbelievable support throughout writing this thesis. They are the most important people in my world and I dedicate this thesis to them.

Pattaranipa Gunhakoon
Researcher

บทคัดย่อ

เรื่อง : ผลของ WO_3 ที่มีต่อแก้วกำบังรังสีแกมมาในระบบ $30BaO - (50-x)B_2O_3 - 10BG - 10CR - xWO_3$

ผู้วิจัย : ภัทรนิภา กันทะคุณ

ชื่อปริญญา : ปรัชญาคุณฐิบัณฑิต

สาขาวิชา : ฟิสิกส์

อาจารย์ที่ปรึกษา : รองศาสตราจารย์เรวัฒน์ เหล่าไพบูลย์

อาจารย์ที่ปรึกษาร่วม : รองศาสตราจารย์จินตนา เหล่าไพบูลย์

คำสำคัญ : แก้ว, เทคนิคอัลตราโซนิกแบบสัมผัส, สมบัติยืดหยุ่น, สมบัติทางรังสี

ระบบแก้วแบเรียม-บอเรต-ซานอ้อย-เหง้ามันสำปะหลัง-ทังสเตนออกไซด์ ได้รับการพัฒนาเพื่อใช้เป็นวัสดุกำบังรังสีแกมมา ระบบแก้วนี้ถูกเตรียมด้วยเทคนิคการหลอมแบบดั้งเดิมโดยหลอมที่อุณหภูมิสูงและปล่อยให้เย็นตัวลงอย่างรวดเร็ว ความหนาแน่นของตัวอย่างแก้วทั้งหมดถูกศึกษาโดยใช้หลักการของอาร์คิมิดีส ข้อมูลความหนาแน่นนี้ถูกนำไปใช้คำนวณหาปริมาตรโดยโมล ตัวอย่างแก้วทั้งหมดถูกนำมาตรวจสอบความเป็นเนื้อเดียวกันและลักษณะอสัณฐานด้วยเทคนิคการทำ X-ray mapping และเทคนิคการเลี้ยวเบนรังสีเอกซ์ ตามลำดับ นอกจากนี้ยังวัดความเร็วคลื่นเสียงอัลตราโซนิกโดยใช้เทคนิคอัลตราโซนิกแบบสัมผัส จากนั้นทำการคำนวณโมดูลัสยืดหยุ่นของทุกตัวอย่างแก้ว ผลลัพธ์ที่ได้ถูกนำมาเปรียบเทียบกับค่าทางทฤษฎีซึ่งคำนวณจากแบบจำลองของ Makishima-Mackenzie และแนวทางของ Abd El-Moneim-Alfifi ทำการบันทึกสเปกตรัมฟูเรียร์ทรานส์ฟอร์มอินฟราเรดเพื่อสนับสนุนผลลัพธ์ของความเร็วคลื่นเสียงอัลตราโซนิก ความแข็งแรงระดับไมโครของระบบแก้วนี้ได้รับการทดสอบและถูกนำไปเปรียบเทียบกับแก้วตะกั่วกำบังรังสีมาตรฐาน สำหรับสมบัติทางรังสีของระบบแก้วนี้ได้ทำการศึกษาสัมประสิทธิ์การลดทอนเชิงมวลด้วยเทคนิคการส่งผ่านแบบไม่บังคับลำรังสีที่พลังงานโฟตอน 60, 122 และ 662 กิโลอิเล็กตรอนโวลต์ ข้อมูลที่ได้ถูกนำมาใช้คำนวณความหนาแน่นค่าและระยะปลอดการชนโดยเฉลี่ย ผลที่ได้ถูกนำไปเปรียบเทียบกับค่าที่ได้จากการคำนวณโดยโปรแกรม WinXCom ผลการวิจัยแสดงให้เห็นว่า สมบัติทางกายภาพ สมบัติทางโครงสร้าง สมบัติยืดหยุ่น และสมบัติทางรังสีมีความสัมพันธ์กับการปรับเปลี่ยนในโครงสร้างแก้ว ซึ่งมีการเปลี่ยนแปลงอย่างมีนัยสำคัญของจำนวนของออกซิเจนที่ไม่ได้เชื่อมต่อกันในเครือข่ายแก้ว เนื่องจากการเพิ่มความเข้มข้นของทังสเตนออกไซด์ และสมบัติทางรังสียังขึ้นอยู่กับพลังงานโฟตอนด้วย สำหรับการคำนวณสมบัติยืดหยุ่นด้วยแบบจำลองของ Makishima-Mackenzie มีโมดูลัสยืดหยุ่นบางค่าที่ใกล้เคียงกับค่าที่ได้จากการทดลอง แต่แนวทางของ Abd El-Moneim-Alfifi ให้ความสัมพันธ์ที่ไม่สอดคล้องกับค่าที่ได้จากการทดลอง

ABSTRACT

TITLE : INFLUENCE OF WO_3 ON GAMMA RAY SHIELDING GLASS IN
30BaO - (50-x) B_2O_3 - 10BG - 10CR - x WO_3 SYSTEM
AUTHOR : PATTARANIPA GUNHAKOON
DEGREE : DOCTOR OF PHILOSOPHY
MAJOR : PHYSICS
ADVISOR : ASSOC. PROF. RAEWAT LAOPAIBOON
CO-ADVISOR : ASSOC. PROF. JINTANA LAOPAIBOON
KEYWORDS : GLASS, ULTRASONIC CONTACT TECHNIQUE, ELASTIC
PROPERTIES, RADIATION PROPERTIES

Glasses of system barium-borate-bagasse-cassava rhizome- WO_3 are developed for gamma ray shielding materials. This glass system was prepared by a conventional melt-quenching technique. The density of all glass samples was studied using the principle of Archimedes, then their molar volume was calculated. The homogeneity and amorphous nature of this glass system were examined using X-ray mapping and X-ray diffraction techniques, respectively. In addition, the ultrasonic velocities were measured using the ultrasonic contact technique and then their elastic moduli were calculated. The results obtained were compared with theoretical values through the Makishima-Mackenzie model and Abd El-Moneim-Alfifi approaches. FTIR spectra were also recorded to support the result of ultrasonic velocities. The microhardness of this glass system was tested and compared with standard radiation shielding lead glass. The mass attenuation coefficient was studied using a broad-beam transmission technique at 60, 122 and 662 keV photon energies. The data obtained was used to calculate the half value layers and mean free paths. These results were compared with the values computed by WinXCom program. The results of physical, structural, elastic and radiation shielding properties are related to modifications in the glass structure. There were significant changes in the number of non-bridging oxygen in the glass network due to the addition of WO_3 . Radiation shielding properties also depend on photon energies. The elastic property calculation using the Makishima-Mackenzie

model gave some elastic moduli similar to that obtained from the experiment, but the Abd El-Moneim-Alfifi approach provided inconsistent results.

CONTENTS

	PAGE
ACKNOWLEDGEMENTS	I
THAI ABSTRACT	II
ENGLISH ABSTRACT	III
CONTENTS	V
LIST OF TABLES	VII
LIST OF FIGURES	IX
LIST OF APPREVIATIONS	XII
CHAPTER 1 INTRODUCTION	
1.1 Importance and source of research	1
1.2 Objectives	4
1.3 Scope of research	4
1.4 Research site	5
1.5 Expected outcomes	5
CHAPTER 2 THEORY AND LITERATURE REVIEWS	
2.1 Basic knowledge about glass	6
2.2 Basic principle of density measurement and molar volume calculation	18
2.3 Basic principle of elastic properties and ultrasonic testing	20
2.4 Theory of elastic moduli from theoretical models	30
2.5 Gamma rays	32
2.6 Broad beam transmission geometry	42
2.7 WinXCom program	44
2.8 Related Research	45
CHAPTER 3 METHODOLOGY	
3.1 Scientific instruments	52
3.2 Scientific equipment	53
3.3 Chemical and materials	53
3.4 Programs used in research	54

CONTENTS (CONTINUED)

	PAGE
3.5 Methods	54
CHAPTER 4 RESULTS AND DISCUSSION	
4.1 The components of bagasse and cassava rhizome	65
4.2 The physical properties of glass samples	65
4.3 The homogeneity of glass samples	67
4.4 The structural properties of glass samples	68
4.5 The elastic properties of glass samples	73
4.6 Microhardness of glass samples	81
4.7 The radiation properties of glass samples	82
CHAPTER 5 CONCLUSION AND RECOMMENDATIONS	
5.1 Conclusion	89
5.2 Recommendations	91
REFERENCES	93
APPENDICES	
A Raw materials and chemicals for research	107
B Scientific equipment and instruments for research	110
C WinXCom program for research	116
D Publications and Conferences	119
E Experiences	122
VITAE	124

LIST OF TABLES

TABLE	PAGE
2.1 Radius ratios for typical glass-formers	11
2.2 Cross-sectional dependence of dominant photon interaction processes	38
3.1 The composition of barium-borate-bagasse-cassava rhizome-WO ₃ glass system	55
3.2 The related variables in theoretical elastic moduli calculation using Makishima-Mackenzie model	59
3.3 The related variables in theoretical bulk modulus calculation using Abd El Moneim-Alfifi's approaches	60
3.4 Chemical composition and density of concretes	63
4.1 EDS analysis results of dry bagasse and cassava rhizome	66
4.2 Structural units and observed peaks in different wave numbers	71
4.3 Elastic moduli and Poisson's ratio of barium-borate-bagasse-cassava rhizome-WO ₃ glass system from ultrasonic testing	75
4.4 Elastic moduli and Poisson's ratio of barium-borate-bagasse-cassava rhizome-WO ₃ glass system from Makishima-Mackenzie model	76
4.5 Bulk modulus of barium-borate-bagasse-cassava rhizome-WO ₃ glass system from Abd El-Moneim and Alfifi's approaches	80
4.6 Microhardness of barium-borate-bagasse-cassava rhizome-WO ₃ glass system and lead glass	82
4.7 The comparison of experimental (Ex) and theoretical (Th) mass attenuation coefficients of glass samples and standard radiation shielding concretes	87
4.8 The comparison of experimental (Ex) and theoretical (Th) linear attenuation coefficients of glass samples and standard radiation shielding concretes	87
4.9 The comparison of experimental (Ex) and theoretical (Th) mean free path of glass samples and standard radiation shielding concretes	88

LIST OF TABLES (CONTINUED)

TABLE		PAGE
4.10	The comparison of experimental (Ex) and theoretical (Th) half value layer of glass samples and standard radiation shielding concretes	88

LIST OF FIGURES

FIGURE	PAGE
2.1 Effect of temperature on the enthalpy of a glass forming melt	7
2.2 The disruption of silica structure by alkali oxide Na_2O	8
2.3 The reflection of the wave that incident the interface of the medium at angling with the normal line	23
2.4 Schematic diagram of the ultrasonic testing (UT) set-up, depicting the test screen and probe	24
2.5 Diagrammatic illustration of longitudinal modulus showing directions of load (F) and of expansion	26
2.6 Diagrammatic illustration of shear modulus showing directions of load (F) and of expansion	27
2.7 Diagrammatic illustration of bulk modulus showing directions of load (F) and of expansion	27
2.8 Diagrammatic illustration of Poisson's ratio showing directions of load (F) and of expansion	28
2.9 Diagrammatic illustration of Young' modulus showing directions of load (F) and of expansion	29
2.10 Diagrammatic illustration of microhardness showing directions of load (F) and of expansion	30
2.11 Radiation shielding materials for various types of radiation	33
2.12 Z-E diagram	35
2.13 Photoelectric effect	36
2.14 Compton effect	37
2.15 Pair production and Annihilation	39
2.16 Broad beam geometry	42
3.1 Schematic illustration of the density measuring of glass samples	56
3.2 Schematic illustration of the microhardness testing of glass samples	61
3.3 Broad beam transmission geometry	61
3.4 Research process diagram	64

LIST OF FIGURES (CONTINUED)

FIGURE	PAGE
4.1 Physical characteristics of barium-borate-bagasse-cassava rhizome- -WO ₃ glass system	67
4.2 Variation of density and molar volume of barium-borate-bagasse- cassava rhizome-WO ₃ glass system	68
4.3 X-ray mapping images of barium-borate-bagasse-cassava rhizome- WO ₃ glass system	69
4.4 XRD patterns of barium-borate-bagasse-cassava rhizome-WO ₃ glass System	70
4.5 FTIR spectra of barium-borate-bagasse-cassava rhizome-WO ₃ glass System	72
4.6 Variation of longitudinal and shear ultrasonic velocities of barium- borate-bagasse-cassava rhizome-WO ₃ glass system	74
4.7 The comparative of theoretical and experimental elastic moduli in barium- borate-bagasse-cassava rhizome-WO ₃ glass system on the basis of Makishima-Mackenzie's theory. The solid line is the 1:1 correlation line.	77
4.8 The comparative of theoretical (σ_M) and experimental Poisson's ratios (σ) in barium-borate-bagasse-cassava rhizome-WO ₃ glass system on the basis of Makishima-Mackenzie's theory. The solid line is the 1:1 correlation line	78
4.9 Variation of bulk modulus with the ratio between packing density and mean atomic volume in barium-borate-bagasse-cassava rhizome-WO ₃ glass system. The solid line represents the least-square fitting of the data	80
4.10 The comparative of theoretical and experimental Poisson's ratios in barium borate-bagasse-cassava rhizome-WO ₃ glass system on the basis of Abd El-Moneim and Alfifi's approaches	81
4.11 Variation of mass attenuation coefficient of barium-borate-bagasse- cassava rhizome-WO ₃ glass system	83
4.12 Variation of linear attenuation coefficient of barium-borate-bagasse- cassava rhizome-WO ₃ glass system	83

LIST OF FIGURES (CONTINUED)

FIGURE		PAGE
4.13	Variation of mean free path of barium-borate-bagasse-cassava rhizome-WO ₃ glass system	84
4.14	Variation of half value layer of barium-borate-bagasse-cassava rhizome-WO ₃ glass system	85

LIST OF APPREVIATIONS

APPREVIATION	UNIT DEFINITION	UNIT
ρ	Density	Gram per cubic centimetre (g/cm^3)
V_m	Molar volume	Cubic centimetre per mole (cm^3/mol)
v_s	Shear ultrasonic velocity	Metre per second (m/s)
v_L	Longitudinal ultrasonic velocity	Metre per second (m/s)
L	Longitudinal modulus	Gigapascal (GPa)
G	Shear modulus	Gigapascal (GPa)
K	Bulk modulus	Gigapascal (GPa)
σ	Poisson's ratio	none
E	Young's modulus	Gigapascal (GPa)
H	Microhardness	Gigapascal (GPa)
V_i	Packing factor of the i th component	Cubic centimetre per mole (cm^3/mol)
G_i	Dissociation energy per unit volume	Kilojoule per cubic metre (kJ/cm^3)
E_m	Makishima-Mackenzie Young's modulus	Gigapascal (GPa)
K_m	Makishima-Mackenzie bulk modulus	Gigapascal (GPa)
G_m	Makishima-Mackenzie shear modulus	Gigapascal (GPa)
L_m	Makishima-Mackenzie longitudinal modulus	Gigapascal (GPa)
σ_m	Makishima-Mackenzie Poisson's ratio	none

LIST OF APPREVIATIONS (CONTINUED)

APPREVIATION	UNIT DEFINITION	UNIT
\bar{V}	Mean atomic volume	Cubic centimetre per mole (cm^3/mol)
ψ	total number of atoms in glass formula unit	none
M	Molecular weight	Grams per mole (g/mol)
K_{Abd}	Abd El-Moneim and Alfifi bulk modulus	Gigapascal (GPa)
μ	Linear attenuation coefficient	Reciprocal centimetre (cm^{-1})
μ_{m}	Mass attenuation coefficient	Reciprocal centimetre (cm^{-1})
HVL	Half value layer	Centimetre (cm)
MFP	Mean free path	Centimetre (cm)
HV	Vickers hardness number	Newton per square millimetre (N/mm^2)
F	Test force	Newton (N)
d	Average of the two diagonals	Millimetre (mm)
N_{A}	Avogadro's number equal to $6.02214076 \times 10^{23}$	Reciprocal mole (mol^{-1})

CHAPTER 1

INTRODUCTION

1.1 Importance and source of research

The growth of the world's population and economic development in many areas has led to the need for enhanced agricultural production of both food and non-food products. The Food and Agricultural Organization of the United Nations (FAO) predicts that global food production will need to increase by more than 63% by 2050 compared to that in the 2005/2007 period. Of course, this increase in food production requires more agricultural crops. After food production, large quantities of agricultural waste are left and need to be well managed. If not, it can cause a serious issue to both public health and the environment worldwide [1]. In many agricultural countries like Thailand, there are many kinds of agricultural waste such as bagasse, cassava rhizome, corn cob, rice husk and others. Especially a large quantities of bagasse are left after the sugar production process from sugarcane. This bagasse is burned to generate electricity in the waste power plant, leaving significant amounts of bagasse ashes. These bagasse ashes are normally dumped in landfills as fertilizer for plants [2]. The leftover part of cassava after cassava starch production like Cassava rhizome also cannot be utilized for human or animal consumption. Due to the cassava rhizome are hard and do not have beneficial element. Therefore, it is often burned in the open air, causing air pollution. The smoke from burning will contain very small dust particles, i.e. PM_{2.5}, which can be harmful to human health as well as the environment [3,4]. Many researchers have realized the problems from traditional waste management and searched for new ways to create benefits from waste products. S.R. Teixeira et al. recycled bagasse ashes along with limestone and fluxing agent to produce a glass-ceramic material [5]. G. N. K. Reddy et al. partially replaced the cement in concrete with bagasse [6]. A. L. M. P. Leite et al. utilized the nanofibers from cassava root as reinforcement material in the development of biodegradable films [7]. N. Tippayawong et al. proposed the use of cassava rhizome as an alternative biomass fuel for power generation [8]. A large amount of this material is also interesting for use in alternative applications. Therefore,

these waste materials were analyzed in this study using the EDS technique, which found that the main components of bagasse and cassava rhizome were SiO_2 and CaO , respectively. Accordingly, these waste products could be used as raw materials for glass production. In general, SiO_2 acts as a glass network former and the CaO is network modifier in glass fabrication.

At present, the use of radiation and techniques in nuclear, medical, industrial, agricultural, energy, as well as other science and technology have brought many benefits to society. On the other hand, radiation can harm humans as well, if not strictly careful. Human received high dose of radiation may be die. We should consider is preventing danger from radiation sources outside the body, including the shortest working time, keep the distance from the source of radiation as much as possible and should provide radiation shielding materials to suit the properties of each type of radiation [9-10]. Gamma rays are high energy electromagnetic waves. Therefore, gamma radiation protection requires high density materials such as thick concrete or lead walls, depending on the energy of radiation [11]. Due to concrete has several limitations, many researchers have developed a glass material to be used instead of a concrete use as radiation shielding material. Glass is a material that is useful and can be used widely. Due to this glass material has transparency properties, resistant to corrosion, inert to chemical reactions and the composition of glass materials can be changed according to the purpose of applications [12]. Many researchers studied the use of glass materials in radiation field such as radiation shielding glass and radioactive waste sealing, etc [13].

In this research, a new novel glass system was fabricated with bagasse and cassava rhizome in the composition. The use of these waste materials, by replacing pure chemicals, can reduce the overall costs associated with glass material production. Y. Hao and J. Cao reported that glass containing CaO , B_2O_3 and SiO_2 glass had the advantages of being homogeneous and transparent, as well as having good stability and being easy to prepare [14]. Therefore, SiO_2 and CaO from pure chemicals in this research were replaced by SiO_2 from bagasse and CaO from cassava rhizome. SiO_2 from bagasse served as a glass network former together with B_2O_3 [15], while CaO from cassava rhizome acted as a network modifier [16]. This network modifier plays a role in reducing the melting temperature and water solubility of glass [17]. BaO is added

in this new type of glass materials since BaO is very strong and has a strong effect on the glass properties, such as phase formation and thermal stability [18,19]. Moreover, the primary glass composition will also be modified by WO₃. WO₃ is transition metal oxide, which can exist in glasses in four valences, the trivalent, tetravalent, pentavalent and hexavalent states. The percent of each state depends on the type and composition of the glass, condition of melting beside the concentration of the transition metal oxide. Extended studies of WO₃ doped glasses have indicated that the hexavalent states W⁶⁺ of the transition metal is the prevailing form in alkali borate and alkali silicate glasses while the lower valences (W⁵⁺, W⁴⁺, W³⁺) are predominant in the phosphate glasses. M. A. Ouis et al. found that after gamma irradiation (8×10^4 Gy) of ZnO-CdO-P₂O₅ glassy system, the two transition metal ions (MoO₃ and WO₃) reveal some shielding effects and WO₃-glasses are more effective than MoO₃-doped glasses [20]. A.M.A. Mostafa et al. described that the gamma ray absorption capability of the B₂O₃-P₂O₅-PbO-WO₃ glass system increased with increasing WO₃ content. This glass system was developed successfully to be used as gamma radiation properties [21]. S. Azianty and A.K. Yahya also found the enhancement of elastic moduli of ternary TeO₂-PbO-WO₃ glass system, where WO₃ > 5 mol%, can be attributed to an increase in the amount of bridging oxygen (BO) in the glass network. The formation of the BO leads to an increase in the rigidity and stiffness of the glass network [22]. In addition, WO₃ has the advantages of being environmentally friendly, simple and cost-effective in terms of the production process.

The novel glass system with bagasse and cassava rhizome along with BaO, B₂O₃ and WO₃ as compositions were prepared for potential use as a new radiation shielding material. As radiation exposure may degrade the properties of glass, many of the properties of this novel glass before exposure to radiation should be studied. Five different concentrations were used and its influence on the physical properties of this novel glass material (i.e. density measurement) was studied. The homogeneity of this novel glass was obtained by X-ray mapping technique. XRD and FTIR techniques were employed to investigate its structural properties. Elastic properties of the glass were tested by ultrasonic testing and compared to interesting theoretical model. Microhardness of the glass was also measured by using microhardness testing machine. Then, experimental radiation properties were measured using broad beam transmission method compare to the calculation by WinXCom program. The collected data can be

also used to further improve and develop the qualities of this glass material for radiation-shielding applications in the future.

1.2 Objectives

1.2.1 To study the composition of recycled bagasse and cassava rhizomes with Energy-dispersive X-ray spectroscopy technique

1.2.2 To prepare barium-borate-bagasse-cassava rhizome glass system with different WO_3 using melt-quenching technique

1.2.3 To study the physical properties of barium-borate-bagasse-cassava rhizome glass with different WO_3 by density measuring with the principle of Archimedes

1.2.4 To study the homogeneity of barium-borate-bagasse-cassava rhizome glass with different WO_3 using by X-ray mapping technique

1.2.5 To study the structural properties of barium-borate-bagasse-cassava rhizome with different WO_3 using Fourier-transform infrared spectroscopy technique and X-ray diffraction technique

1.2.6 To study the radiation properties of barium-borate-bagasse-cassava rhizome glass with different WO_3 both from the experiment by broad beam transmission method compare to the calculation by WinXCom program

1.2.7 To study the elastic properties of barium-borate-bagasse-cassava rhizome glass with different WO_3 using Ultrasonic contact technique compare to calculation using Makishima-Mackenzie model and Abd El-Moneim-Alfifi approaches

1.2.8 To study the microhardness of barium-borate-bagasse-cassava rhizome glass with different WO_3 using Microhardness testing machine

1.3 Scope of research

We analyzed the composition of recycled bagasse and cassava rhizomes by EDS technique. We determined amorphous nature of the barium-borate-bagasse-cassava rhizome glass with different WO_3 using X-ray diffraction techniques. Density of studied glasses was measured using to weigh balance system then also molar volume were calculated. The homogeneity of studied glasses was investigated using X-ray mapping technique. Study the radiation properties (mass attenuation coefficient, linear attenuation coefficient, half value layer and mean free path) of glass by broad beam

transmission method compared with the calculation by WinXCom program. We use the straight and angle beam probes to find the ultrasonic velocity in the glass material, that to calculate modulus values, Poisson's ratio and hardness. Theoretical modulus was calculated using Makishima-Mackenzie model and Abd El-Moneim-Alfifi approaches. Microhardness values were also measured with Microhardness testing machine.

1.4 Research site

1.4.1 Department of Physics, Faculty of Science, Ubon Ratchathani University, Ubon Ratchathani 34190, Thailand

1.4.2 Glass Technology Excellence Center, Department of Physics, Faculty of Science, Ubon Ratchathani University, Ubon Ratchathani 34190, Thailand

1.4.3 Scientific Equipment Center, Ubon Ratchathani University, Ubon Ratchathani, 34190, Thailand

1.4.4 Department of Industrial Engineering, Faculty of Engineering, Ubon Ratchathani University, Ubon Ratchathani, 34190, Thailand

1.4.5 Department of Nuclear Engineering, Faculty of Engineering, Chulalongkorn University, Bangkok, 10330, Thailand

1.4.6 National Metal and Materials Technology Center, 114 Thailand Science Park, Pathumthani, 12120, Thailand

1.5 Expected outcomes

The researchers had more knowledge and understand the glass melting process. Also, we can specify the ratio of raw materials and chemicals used to melt glass. We can identify the physical, structural, radiation properties and elastic properties of barium-borate-bagasse-cassava rhizome glass with different WO_3 . We can develop glass formulas to be suitable for gamma radiation shielding materials and corresponds work field. This knowledge helps to select materials that will be used in radiation applications such as we use agricultural waste as composition of the studied glass, this is to reduce waste and reduce environmental pollution. It also has advantages of saving production costs as well.

CHAPTER 2

THEORY AND LITERATURE REVIEWS

2.1 Basic knowledge about glass

2.1.1 General introduction of glass

Glass is a state of matter. It is a solid produced by cooling molten material so that the internal arrangement of atoms, or molecules, remains in a random or disordered state, similar to the arrangement in a liquid. Such a solid is said to be amorphous or glassy. Ordinary solids, by contrast, have regular crystalline structures. Many materials can be made to exist as glasses. Hard candies, for example, consist primarily of sugar in the glassy state. What the term "glass" means to most people, however, is a product made from silica (SiO_2). The common form of silica is sand, but it also occurs in nature in a crystalline form known as quartz. Pure silica can produce an excellent glass, but it is very high-melting (1,723 °C), and the melt is so extremely viscous that it is difficult to handle. All common glasses contain other ingredients that make the silica easier to melt and the hot liquid easier to shape [23].

Glass is an amorphous solid. The term is usually applied to inorganic solids and not to plastics or other organics. Glasses do not have crystalline internal structure. They usually are hard and brittle solids. Glass is a transparent material, particularly in the visible region of electromagnetic spectrum. The transparent and coloration have made the glasses best suitable for decorative and illumination purposes in the early days of their invention. Today glasses find applications in various fields viz., electrical transmission, optical instruments, laboratory glassware, domestic appliances, textiles, optical fibers, electrochemical devices, solid electrolytes, biological systems (bioactive glasses) etc. The isotropic properties of glasses have given an edge in variety of applications [24,25].

2.1.2 Definition of glass in science

Glass has been defined in several ways.

Glass is an inorganic product of fusion, which has been cooled to a solid state condition without crystallizing [26] - ASTM.

Glass is a non-crystalline solid that exhibits a glass transition temperature [27]. Above the glass transition temperature [T_g] glass exhibits properties of liquid and below T_g , it retains liquid structure in rigid form.

It is now known that glasses can be formed from almost any material either organic or inorganic if cooled rapidly by avoiding crystallization.

2.1.3 Glass forming

The formation of crystal, liquid and glass can be explained from the temperature volume relationship as shown in the figure 2.1. It is clear from the figure that slow cooling process leads to formation of crystal nuclei and crystallization takes place. If the cooling rate is fast, leaving no time to the formation of crystal nuclei, structure of super cooled liquid state turns to rigid and forms a glass [28].

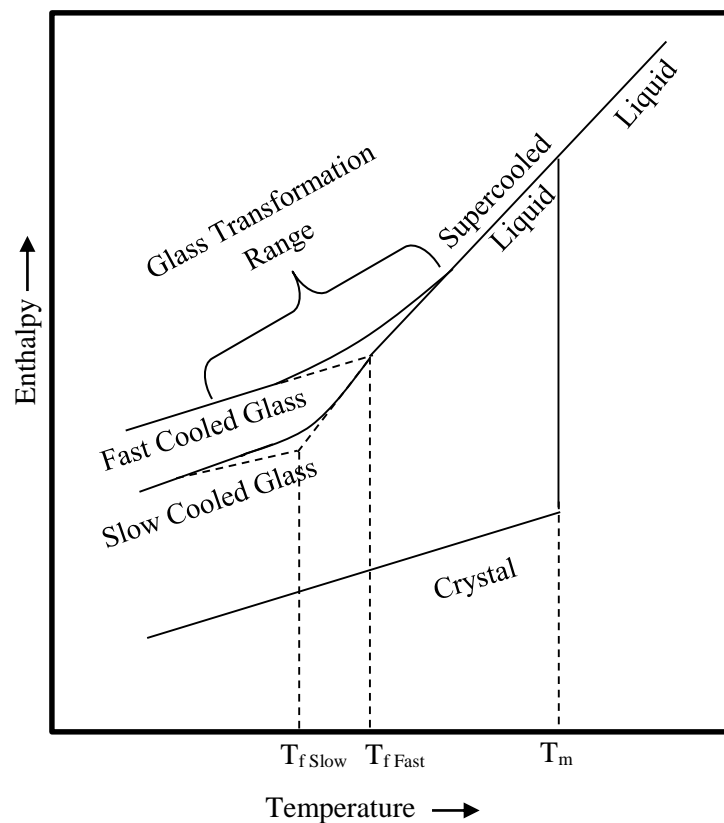


Figure 2.1 Effect of temperature on the enthalpy of a glass forming melt [36]

Some oxides easily form glasses. These substances which form glass are generally called “Glass formers” or “Glass network formers”. The Oxides SiO_2 , B_2O_3 ,

P_2O_5 , GeO_2 and As_2O_3 can form glass by their own. These oxides can also form glasses when mixed with other oxides in various proportions.

Some oxides such as Na_2O , Li_2O , K_2O , Bi_2O_3 , Al_2O_3 , V_2O_5 , PbO , TeO_2 , MoO_3 , WO_3 etc which cannot form glasses by themselves can disrupt the glass forming oxides network and extend the glass forming region. These oxides are called ‘glass-modifiers’ or ‘glass network modifiers’. Glass modifier oxides form glass when combined with appropriate quantity of second oxide. Hence glass modifier oxides are also known as conditional glass formers.

Some oxides such as Al_2O_3 , ZnO , TiO_3 , ZrO_2 , PbO , Sb_3O_2 etc are chemicals that can behave as network formers or modifiers depending on the glass composition. Glasses are naturally highly disordered, and require a carefully tuned balance of network formers, intermediates, and modifiers to prevent the formation of ordered crystallites within the material.

Figure 2.2 shows the disruption of silica (glass former) structure by alkali oxide Na_2O (glass modifier) and thereby formation of non-bridging oxygens (NBO).

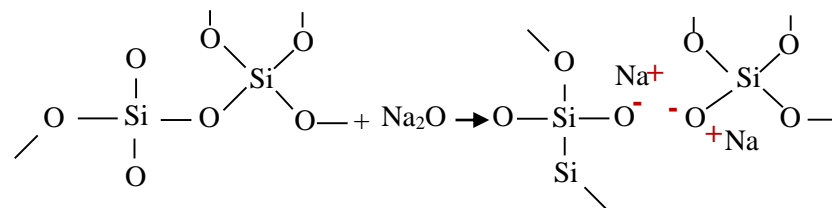


Figure 2.2 The disruption of silica structure by alkali oxide Na_2O

2.1.4 Type of glass

Glass is a unique and extremely versatile material that can be engineered to exhibit specific optical, thermal, chemical, and mechanical properties. As a result of its exceptional engineering properties is transparency, strength, workability and transmittance, glass has been heavily used in the many industries. Nowadays, there are many different types of glass, and scientists have classified glass for various purposes. Here, we will briefly feature of some important glass types and these types are based on chemical composition as follow [29]:

2.1.4.1 Soda-lime glass

This type of glass is the most common in daily life, and least expensive form of glass. Soda-lime glass accounts for about 90% of manufactured glass, used for window panes and glass containers (bottles and jars) for beverages, food, and some commodity items. It usually contains 60-75% silica, 12-18% soda, 5-12% lime. Resistance to high temperatures and sudden changes of temperature are not good and resistance to corrosive chemicals is only fair.

2.1.4.2 Lead glass

This type of glass has a high percentage of lead oxide (at least 20% of the batch). It is relatively soft, and its refractive index gives a brilliance that may be exploited by cutting. It is somewhat more expensive than soda-lime glass and is favored for electrical applications because of its excellent electrical insulating properties. Thermometer tubing and art glass are also made from lead-alkali glass, commonly called lead glass. This glass will not withstand high temperatures or sudden changes in temperature.

2.1.4.3 Borosilicate glass

This type of glass is any silicate glass having at least 5% of boric oxide in its composition. It has high resistance to temperature change and chemical corrosion. Not quite as convenient to fabricate as either lime or lead glass, and not as low in cost as lime, borosilicate's cost is moderate when measured against its usefulness. Pipelines, light bulbs, photochromic glasses, sealed-beam headlights, laboratory ware, and bake ware are examples of borosilicate products.

2.1.4.4 Aluminosilicate glass

This type of glass has aluminum oxide in its composition. It is similar to borosilicate glass but it has greater chemical durability and can withstand higher operating temperatures. Compared to borosilicate, aluminosilicates are more difficult to fabricate. When coated with an electrically conductive film, aluminosilicate glass is used as resistors for electronic circuitry.

2.1.4.5 Ninety-six percent silica glass

This type of glass is a borosilicate glass, melted and formed by conventional means, then processed to remove almost all the non-silicate elements from the piece. By reheating to 1200°C the resulting pores are consolidated. This glass is

resistant to heat shock up to 900°C. This glass is used as a substitute in optical components and spacecraft windows. It can withstand the heat of reentry into the earth's atmosphere, and is used as heat resisting coating applications on the exterior of the space shuttle. Other uses include laboratory ware and lighting components such as arc tubes in halogen lamp.

2.1.4.6 Fused silica glass

This type of glass is pure silicon dioxide in the non-crystalline state. It is very difficult to fabricate, so it is the most expensive of all glasses. It can sustain operating temperatures up to 1200°C for short periods. It finds use in situations such as semiconductor fabrication and laboratory equipment. It transmits ultraviolet better than other glasses, so is used to make lenses and optics for the ultraviolet spectrum. The low coefficient of thermal expansion of fused silica glass makes it a useful material for precision mirror substrates.

2.1.5 Theory of glass structures

2.1.5.1 Glass Structure According to Tammann (1903)

Tammann [30], the first investigator concerned with the constitution of glasses, regarded them as strongly undercooled liquids. To a certain degree this is in agreement with later interpretations using X-ray diffraction data. At that time the structures of liquid crystals and of liquids were not yet known. Tammann's model of the freezing-in of a structure quite similar to that of the liquid was quite general, but did represent a good start. Tammann also was the first to investigate low-melting-point model glasses, organic glasses obtained by rapid cooling of molten piperidine, salicin, phenolphthalein, sugars, etc. These investigations resulted in fundamental information about nucleation and crystallization of glasses.

2.1.5.2 Glass Formation According to Goldschmidt (1926)

Goldschmidt [30], who is considered the founder of modern crystal chemistry, was in a position to derive empirical rules for glass formation from his studies. Just as in the case of crystal structure, relations of ionic size were to play a decisive role. He postulated a ratio of from 0.2 to 0.4 of radius-of-cation (r_c) to radius-of-anion (r_a) as a condition of glass formation. This condition is fulfilled in the case of SiO_2 , B_2O_3 , P_2O_5 , GeO_2 and BeF_2 as shown in table 2.1.

Table 2.1 Radius ratios for typical glass-formers [30]

Compound	Radius ratio ($r_k : r_A$)
SiO ₂	$r_{\text{Si}}:r_{\text{O}} = 0.39 \text{ \AA} : 1.4 \text{ \AA} \approx 0.28$
B ₂ O ₃	$r_{\text{B}}:r_{\text{O}} = 0.20 \text{ \AA} : 1.4 \text{ \AA} \approx 0.15$
P ₂ O ₅	$r_{\text{P}}:r_{\text{O}} = 0.34 \text{ \AA} : 1.4 \text{ \AA} \approx 0.25$
GeO ₂	$r_{\text{Ge}}:r_{\text{O}} = 0.44 \text{ \AA} : 1.4 \text{ \AA} \approx 0.31$
BeF ₂	$r_{\text{Be}}:r_{\text{F}} = 0.34 \text{ \AA} : 1.36 \text{ \AA} \approx 0.25$

Later, a convincing confirmation of this prediction was obtained by the discovery of the formation of BeF₂ glass, which indeed satisfied these specific conditions. Moreover, the same laws and dependencies should be valid for the formation of a glass structure as for crystal chemistry. Predominantly qualitative interpretations of measurable glass properties were attempted at that time. Only at the beginning of the twenties and thirties of our century structure hypotheses appeared which became more or less successful bases for glass development and research. e.g. the dependence of packing density on the state of polarization and deformation of constituent ions.

2.1.5.3 The Zachariasen-Warren Network Theory (1932)

Before Zachariasen [31], the structure of a glass was believed to be comprised of nanocrystals (~20 Å size) given the broadening of the diffraction peaks. He noted similar mechanical properties (elastic modulus, etc.) between glasses and crystals and so expected similar structural energies. Glasses lack the periodic (long range) order of a crystal. Infinite unit cell (no repeating large scale structures). 3D network lacking symmetry and periodicity. Same average packing and properties in all directions which different from crystals (directions).

Zachariasen's Rules for Glass formation based on an empirical observation on oxides.

- 1) No oxygen atom may be linked to more than two cations
- 2) The cation coordination number CN is small: 3 or 4.
- 3) Oxygen polyhedra share corners, not edges or faces.
- 4) For 3D networks, at least three corners must be shared

In general, all four rules should be satisfied for glass formation to occur. Low coordination numbers, corner-sharing rules imply that glass formation is more likely with open, low density polyhedral structures. Having stated this, one identifies a certain number of compounds to be either good glass formers (i.e. satisfying the 4 rules) or bad glass formers (do not satisfying at least one of the rules). Example:

1) SiO_2 , GeO_2 are good glass formers (CN=4)

2) V_2O_5 (CN=5) is not a good glass former (breakdown of rule 2)

2.1.5.4 Dietzel (1942)

He examined direct Coulombic interactions. He defined r_c is radius of cation and r_a is radius of anion, let $a = (r_c + r_a)$ and z_c is cation charge. Then, Dietzel categorized cations using:

$$\text{Field strength (F.S.)} = \frac{z_c}{a^2} \quad (2.1)$$

High field strength cations refer to high cation-oxygen bond energy as follow; Glass formers have field strength cations > 1.3 , Glass modifiers < 0.4 and Intermediates $0.4 \leq \text{F.S.} \leq 1.3$. More factors are important than just bond strength as: Small cations with high charge are glass formers, Large cations with small charge are modifiers and Medium sized cations with medium charge are intermediates [32].

2.1.5.5 Sun (1947)

He considered a single bond strength approach and The reaction of dissociation energy (E_d) for a molecule shown as follows $A_nO_m \rightarrow nA + mO$.

$$\text{single bond (S.B.)} \sim \frac{E_d}{\text{CN}} \text{ (kcal)} \quad (2.2)$$

where CN is coordination number. Glass Formation is brought about by both connectivity of bridge bonds and strong Bonds between atoms (ions). Sun noted that rigid network, high viscosity has high S.B. strength oxides (> 80 kcal/mole) such as B_2O_3 , SiO_2 , GeO_2 , P_2O_5 etc. These oxides have a role of glass formers in glass structure. Low S. B. strength oxides (< 60 kcal/mole) such as Li_2O , Na_2O , K_2O , MgO , CaO etc.

from weak bonds to oxygen. These are representing as disrupt, modify, network. In addition, S.B. strength oxides (60-80 kcal/mol) such as TiO_2 , ZnO , PbO etc. are intermediates. It forms intermediate bonds to oxygen, can't form glasses on their own but aid with other oxides to form glasses. The Sun criteria relate to melt crystallization as followed [33]:

- 1) High bond strengths, difficult to break and reform into ordered lattice upon cooling
- 2) High bond strengths, high viscosity, so good glass formers
- 3) Low bond strengths, easy to break/reform into preferred crystal

2.1.5.6 Stanworth (1971)

He noted similar patterns with electronegativity/ion size. The obtained results from the research of J. E. Stanworth showed that [34]:

- 1) None of the oxides of atoms with radii $>1.5 \text{ \AA}$ are known to form glasses.
- 2) The atoms with radii $<1.3 \text{ \AA}$ and electronegativities from 1.8 to 2.1 (Ge, Si, As, P and B) form oxides which are the well-known conventional glass formers.
- 3) The atoms in the same electronegativity range (1.8 to 2.1) with radii slightly larger than those of the atoms of Sb, V, W, Mo and Te are known to form a glassy phase on splat quenching. Glass formation with these oxides in relatively slowly cooled melts requires the addition of other oxides (e.g. PbO or BaO) before the slight oversize can be accommodated.
- 4) None of the oxides with cations of electronegativity $< 1.8 \text{ \AA}$ form glasses; in this sense, the electronegativity criterion is dominant. However, atom size affects glass formation, in that the smallest atoms in this classification (Al and Ga) form complex glasses, i.e. aluminates and galliumates.
- 5) Pure oxides with cations of electronegativity $> 2.1 \text{ \AA}$ (Se, S, C and N) are not known to form glasses, but glasses can be formed in certain selenite, sulfate, carbonate, and nitrate systems.

2.1.5.7 Izumatani (1986)

Izumtani offers the table summarizes various ion properties as appear in the research of him (1986) [35]. All these empirical crystal chemical approaches describe which compounds are likely to form glasses; no predictions about how easily glass formation might be. We need to return to our kinetic description (nucleation and growth) for that information.

2.1.5.8 Shelby (1997)

Glasses have well-defined short range (nearest neighbor) bond arrangements. Precisely measured Coordination numbers and bond lengths. Fairly well determined bond angle distributions. Breadth of this distribution that is responsible for the loss of long-range order. Shelby defines the 'elements of structure'; what do we need to know to describe the atomic networks of glasses which dependent upon length scale [36]:

- 1) Coordination of network cations/glass formers
- 2) Bond angle distributions
- 3) Network connectivity
- 4) Network dimensionality
- 5) Intermediate range order
- 6) Morphology
- 7) Interstitial/Free volume

2.1.6 Glass composition

The making of glass involves three basic types of ingredients: glass forming oxide, intermediate oxide and glass modifying oxide. The most common glass, made in largest amounts by both ancient and modern glassmakers, is based on silica as the glass former, soda as the flux, and lime as the stabilizer. It is the glass used to make windows, bottles, jars, and lightbulbs. The details of oxide components added in to a glass batch are as follows [23,37]:

2.1.6.1 Glass forming oxide

Glass formers and network formers include oxides such as SiO_2 , B_2O_3 , GeO_2 , P_2O_5 , V_2O_5 and As_2O_3 which are indispensable in the formation of glass since they form the basis the random three dimensional network of glass.

Boron oxide, B_2O_3 , is a glass-forming oxide and by itself forms a subunit that is a flat triangle with the boron atom slightly out of the plane of the oxygen atoms. Boron oxide is an important addition to many types of commercial glass such as borosilicate and aluminoborosilicate glasses.

2.1.6.2 Intermediate oxide

Intermediates include Al_2O_3 , Sb_2O_3 , ZrO_2 , TiO_2 , PbO and ZnO , these oxides are added in high proportion for linking up with the basic glass network to retain structural continuity. Some oxides cannot form a glass network by themselves but can join into an existing network. These oxides are known as intermediate oxides.

For example, aluminum oxides, silica network as AlO_4 -tetrahedra replacing some of the SiO_4 groups. However, since the valence of Al is 3 instead of the necessary 4 for the tetrahedral, alkali cations must supply the necessary other electrons to produce electrical neutrality. Intermediate oxides are added to silica glass to obtain special properties. For example, aluminosilicate glasses can withstand higher temperature than common glasses. Depending on the composition of the glass, intermediate oxides may sometimes act as network modifiers as well as taking part in the network of the glass.

2.1.6.3 Glass modifying oxide

Modifiers include MgO , Li_2O , BaO , CaO , SrO , Na_2O and K_2O . The oxides are added to modify the properties of glass oxides that break up the glass network are known as network modifiers. Alkali oxides such as Na_2O and K_2O and alkaline earth oxides such as CaO and MgO are added to silica glass to lower its viscosity so that it can be worked and formed more easily. The oxygen atoms from these oxides enter the silica network at points joining the tetrahedra and break up the network, producing oxygen atoms with an unshared electron. The Na and K ions from the Na_2O and K_2O do not enter the network but remain as metal ions ionically bonded in the interstices of the network. By filling some of the interstices, these ions promote crystallization of the glass. Modifiers break up the silica network if the oxygen to silica ratio (O:Si) increases significantly when Na_2O is added, the sodium ions enter holes within the network, rather than becoming part of the network, however, the oxygen ion that enters with Na_2O does become part of the network. The effect of Na_2O on the silica

glass network. Sodium oxide is a modifier disrupting the glassy network and reducing the ability to form a glass.

The other addition in glass are the fluxes which lower the fusion temperature of the glass batch and render the molten glass workable at reasonable temperature, modification lower the melting point and viscosity of silica, making it possible to produce glass at lower temperature. Modifiers fluxes may reduce the resistance of glass to chemical attack, render it water soluble or make it subject to partial or complete devitrification. Devitrified glass is undesirable since the crystalline areas are externally weak and brittle, stabilizers are therefor, added to the glass batch overcome these problems. Adding CaO which reduces the solubility of the glass in water further modifies these glasses [38].

2.1.7 Raw materials used in the production of glass

The chemical composition of glass affects the properties of glass as follows [39]

2.1.7.1 Silicon dioxide (SiO_2)

The glass with a high content of SiO_2 will give the glass a strong structure, resistant to heat and chemicals. This glass is difficult to produce because it requires high melting temperatures and difficult to form due to its high viscosity.

2.1.7.2 Sodium oxide (Na_2O) or potassium oxide (K_2O)

Glass with high Na_2O or K_2O content will melt at low temperatures. This glass is fragile, easily broken and not resistant to chemicals. If the content of Na_2O or K_2O are very high, it can be dissolved in water.

2.1.7.3 Calcium oxide (CaO), Magnesium oxide (MgO) or Barium oxide (BaO)

CaO MgO or BaO will help to glass forming. They make the glass stabilize faster when it cools down and increased chemical resistance. Glass with a higher MgO content than CaO will cause the crystallization to be slow, resulting in beautiful crystal arrangement.

2.1.7.4 Aluminium oxide (Al_2O_3)

Glass with a high content of Al_2O_3 will make the glass more resistant to wear and corrosion.

2.1.7.5 Boron oxide (B_2O_3)

The glass with B_2O_3 as composition will be resistant to acid-alkali and resistant to heat. Because B_2O_3 will cause the thermal expansion coefficient to decrease. This type of glass is used in scientific equipment, and it can be used in a microwave oven.

2.1.7.6 Lead(II) oxide (PbO)

Glass with PbO has a clear glass surface due to its high refractive index. PbO glass is softening glass, being easy to cut. When knocked, the sound resonated.

2.1.7.7 Iron(III) oxide (Fe_2O_3)

The glass with Fe_2O_3 has properties to make the glass texture clear and green.

2.1.7.8 Other oxides

If you want the glass to be colorful, add substances other than the above reported ingredients are Chromium oxide (Cr_2O_3) for green tone, Cobalt oxide (CoO) for blue tone, Uranium (U) for yellow tone, Carbon-Sulfur-Iron (C-S-Fe) for amber tone, Nickle (Ni) for brown tone and Manganese (Mn) for purple tone.

2.1.8 Uses and benefit of glass

2.1.8.1 Uses of glass

The glass is an unlimited and innovative material that has various uses. It is an essential component of numerous products that we use in our day to day to life, most often without noticing it. We give certain uses of glass which are as under [40]:

- 1) Windows and doors
- 2) Reinforcement structures
- 3) Tableware (plate, cups, bowls, Jar packaging for food, Bottles)
- 4) Insulation
- 5) Conservatory
- 6) Renewable energy (solar energy glass, Wind turbines)
- 7) Interior design and furniture element (mirrors)
- 8) Applications and electronics element (cook top, oven doors)
- 9) Automotive and transport (aircraft, ships, windscreens)

- 10) Medical technology, optical glass, biotechnology, etc.
- 11) Fibre optic cables to carry information from phones, computer.
- 12) X-ray & Gamma-ray radiation protection

2.1.8.2 Benefits of glass

We try to provide certain benefits of using a glass which are as under [41]:

- 1) The glass is 100% recyclable and can be recycled endlessly without loss in its quality or purity.
- 2) Glass is available in different colors or colorless.
- 3) Glass is a unique transparent material which allows light to pass through it so that the objects behind the glass are visible clearly.
- 4) Glass has a smooth glossy surface, so it is dustproof and waterproof material.
- 5) Glass is UV stable since it is not affected by ultraviolet radiation and hence cracks, discoloration or disintegration will not occur.
- 6) Glass is corrosion resistant, and only under certain conditions, the glass is chemically attacked.
- 7) Glass is a transparent, hard material that can be easily moulded into desired shapes.
- 8) Glass is an excellent insulator. It does not readily conduct electricity.
- 9) Glass absorbs, refracts or transmits light. It can be made transparent or translucent, so it adds extraordinary beauty to the building.
- 10) The glass is excellent abrasion resistant material so it will resist surface wear caused by flat rubbing and direct contact with another material.
- 11) Glass is stable over a wide range of temperature.

2.2 Basic principle of density measurement and molar volume calculation

2.2.1 Density

Archimedes' principle [42], physical law of buoyancy, discovered by the ancient Greek mathematician and inventor Archimedes, stating that a body at rest in a fluid is acted upon by a force pushing upward called the buoyant force, which is equal

to the weight of the fluid that the body displaces. If the body is completely submerged, the volume of fluid displaced is equal to the volume of the body. If the body is only partially submerged, the volume of the fluid displaced is equal to the volume of the part of the body that is submerged.

Archimedes' principle is very useful for calculating the volume of an object that does not have a regular shape. The oddly shaped object can be submerged, and the volume of the fluid displaced is equal to the volume of the object. It can also be used in calculating the density or specific gravity of an object. For example, for an object denser than water, the object can be weighed in air and then weighed when submerged in water. When the object is submerged, it weighs less because of the buoyant force pushing upward. The object's specific gravity is then the object's weight in air divided by how much weight the object loses when placed in water.

The buoyancy force (B) is equal to the weight (W) of the fluid that a body in that fluid displaces. The weight W can be written in terms of the density (ρ) of the fluid as $W = \rho Vg$, where V is the volume of the fluid that has been displaced and g is 9.8 meters per second, the value of the acceleration from Earth's gravity.

In this research, the liquid used is n-Hexane, whose density is 0.661 g/cm³ using electronic balance of Denver Instrument, resolution 0.0001 g. The calculated values are given in the equation (2.3) [43]

$$\rho = \rho_l \left(\frac{W_a}{W_a - W_b} \right) \quad (2.3)$$

where ρ and ρ_l are the density of the glass sample and liquid, respectively. For W_a and W_b are the weight of the glass sample weighing in the air and liquid, respectively.

2.2.2 Molar volume

The Molar Volume [43], represented by V_m , is another way to view number density. The Molar Volume is the volume occupied by one mole of a substance which can be a chemical element or a chemical compound at Standard Temperature and Pressure (STP). It can be calculated by dividing Molar mass (M) by mass density (ρ). The Molar volume is directly proportional to molar mass and inversely proportional to density. The formula of molar volume is expressed as

$$V_m = \frac{M_w}{\rho} \quad (2.4)$$

where V_m is Molar volume, M_w is the molecular mass of glass sample and ρ is the density of glass sample.

2.3 Basic principle of elastic properties and ultrasonic testing

2.3.1 Elastic properties

In physics, elasticity is the ability of a body to resist a distorting influence and to return to its original size and shape when that influence or force is removed. Solid objects will deform when adequate forces are applied to them. If the material is elastic, the object will return to its initial shape and size when these forces are removed. Hooke's law states that the force should be proportional to the extension. The physical reasons for elastic behavior can be quite different for different materials. In metals, the atomic lattice changes size and shape when forces are applied (energy is added to the system). When forces are removed, the lattice goes back to the original lower energy state. For rubbers and other polymers, elasticity is caused by the stretching of polymer chains when forces are applied [44].

All solid objects are deformable under the applied external forces. Internal forces resist deformation. The resistance in crystals is greater than that in amorphous materials. However, the external forces can change size and shape of any solid. This change we will call deformation.

Measurement of elastic properties can be obtained by destructive testing (DT) or non-destructive testing (NDT). At present, the elastic properties testing is commonly used non-destructive testing. This method is used in industry to evaluate the integrity and properties of material or components without causing damage to the tested object. This research studies the elastic properties using Ultrasonic Testing [45] which is non-destructive testing.

2.3.2 Ultrasonic wave

Sound wave is a vibration that is transmitted through a medium, such as air, water, and metals. Ultrasonic wave is defined as “inaudible sound with high frequency for human” the frequency of which generally exceeds 20 kHz. These days, sound wave

which is not intended to be heard is also called ultrasonic wave. There are types of ultrasonic waves, longitudinal wave, transverse wave and surface wave, etc. In a solid, there simultaneously exist two types of elastic waves as follows [46]

2.3.2.1 Longitudinal wave

An elastic wave that has a displacement in the same direction of the propagation direction of the wave. The longitudinal sound wave velocity or called longitudinal velocity is constant in each type of material, for example the longitudinal velocity in steel is 5,920 m/s.

2.3.2.2 Transverse wave or shear wave

An elastic wave that has a displacement to the vertical direction of the propagation direction of the wave. The shear sound wave velocity or shear velocity is less than the longitudinal velocity. The shear velocity is constant in each material, for example the shear velocity of steel is equal to 3,250 m/s.

2.3.3 Ultrasonic properties

The properties of the ultrasonic wave are accordance with the properties of general sound wave. Among the properties of waves propagating in isotropic solid materials are wavelength (λ), frequency (f), and velocity (v). The wavelength is directly proportional to the velocity of the wave and inversely proportional to the frequency of the wave. This relationship is shown by the following equation (2.5). In ultrasonic testing, the shorter wavelength resulting from an increase in frequency will usually provide for the detection of smaller discontinuities [47].

$$\lambda = \frac{v}{f} \quad (2.5)$$

When sound waves arrive to the boundary between the different medium. The reflected and transmitted waves can occur in the following 2 cases.

2.3.3.1 The reflection of the wave when the incident wave perpendicular to the boundary between the two mediums

The ratio of the reflection waves and the transmission wave that move through the boundary depends on the sound properties called the acoustic

impedance of the two mediums. The acoustic impedance (Z) of a material is defined as the product of its density (ρ) and acoustic velocity (v) [48].

$$Z = \rho v \quad (2.6)$$

Acoustic impedance is important in the determination of acoustic transmission and reflection at the boundary of two materials having different acoustic impedances, the design of ultrasonic transducers and assessing absorption of sound in a medium.

Ultrasonic waves are reflected at boundaries where there is a difference in acoustic impedances (Z) of the materials on each side of the boundary. This difference in Z is commonly referred to as the impedance mismatch. The greater the impedance mismatch, the greater the percentage of energy that will be reflected at the interface or boundary between one medium and another.

The fraction of the incident wave intensity that is reflected can be derived because particle velocity and local particle pressures must be continuous across the boundary. When the acoustic impedances of the materials on both sides of the boundary are known, the fraction of the incident wave intensity that is reflected can be calculated with the equation below. The value produced is known as the reflection coefficient. Since the amount of reflected energy plus the transmitted energy must equal the total amount of incident energy, the transmission coefficient is calculated by simply subtracting the reflection coefficient from one.

$$R = \left(\frac{Z_2 - Z_1}{Z_2 + Z_1} \right)^2 \quad (2.7)$$

2.3.3.2 The reflection of the wave when the incident wave as oblique angle with the boundary between the two mediums

When an ultrasonic wave passes through an interface between two materials at an oblique angle, and the materials have different indices of refraction, both reflected and refracted waves are produced. Refraction takes place at an interface due

to the different velocities of the acoustic waves within the two materials. The velocity of sound in each material is determined by the material properties (elastic modulus and density) for that material.

Snell's Law describes the relationship between the angles and the velocities of the waves. Snell's law equates the ratio of material velocities v_1 and v_2 to the ratio of the sine's of incident (θ_1) and refracted (θ_2) angles, as shown in the following equation [49].

$$\frac{\sin\theta_1}{v_1} = \frac{\sin\theta_2}{v_2} \quad (2.8)$$

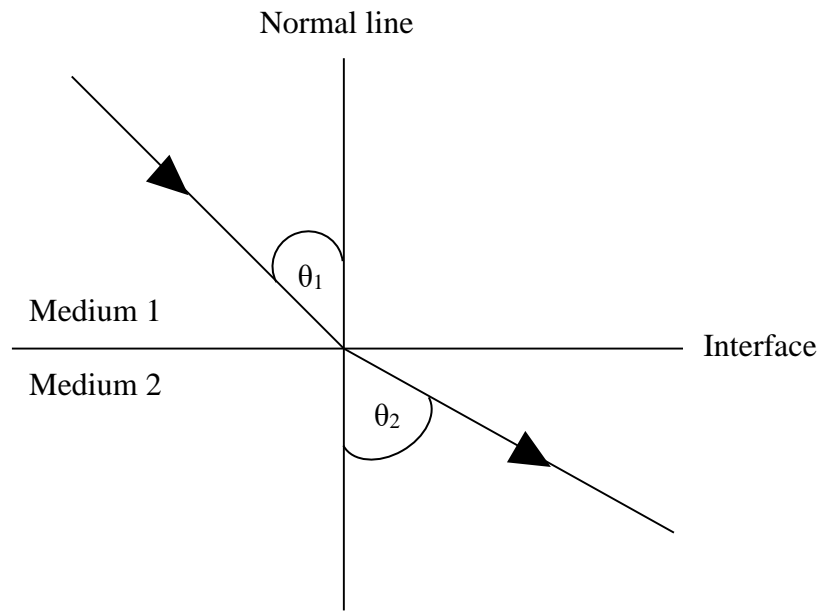


Figure 2.3 The reflection of the wave that incident the interface of the medium at angling with the normal line

2.3.4 Ultrasonic Testing (UT)

Ultrasonic Testing (UT) uses high frequency sound energy to conduct examinations and make measurements. Ultrasonic inspection can be used for flaw detection/evaluation, dimensional measurements, material characterization, and more. To illustrate the general inspection principle, a typical pulse/echo [50] inspection configuration as illustrated in figure 2.4.

A typical UT inspection system consists of several functional units, such as the pulser/receiver, transducer, and display devices. The principle of inspection by ultrasonic echo-pulse method is based on the fact that a pulser/receiver is an electronic device that can produce high voltage electrical pulses. Driven by the pulser, the transducer generates high frequency ultrasonic energy. The sound energy is introduced and propagates through the materials in the form of waves. When there is a discontinuity (such as a crack or a back surface) in the wave path, part of the energy will be reflected back from the flaw surface. The reflected wave signal is transformed into an electrical signal by the transducer and is displayed on a screen. The reflected signal strength is displayed versus the time from signal generation to when an echo was received. Signal travel time can be directly related to the distance that the signal traveled. From the signal, information about the reflector location, size, orientation and other features can sometimes be gained.

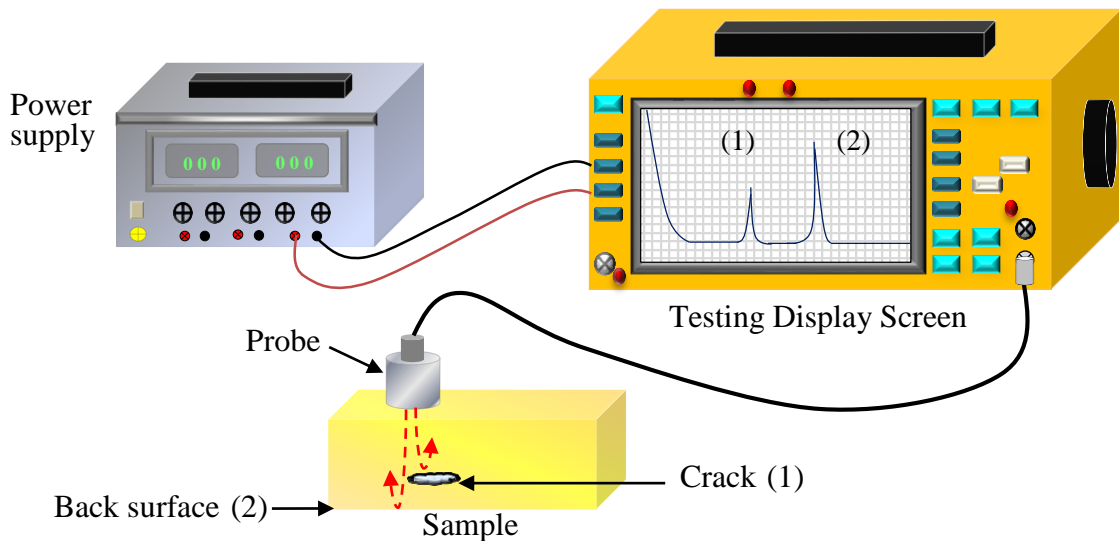


Figure 2.4 Schematic diagram of the ultrasonic testing (UT) set-up, depicting the test screen and probe

In the calculation of the ultrasonic velocity of the test material, it can be found from the equation (2.9) as follows

$$v_w = \frac{v_{ST} \times s_w}{s_{ST}} \quad (2.9)$$

where v_w is the ultrasonic velocity in the test material (m/s), v_{ST} is the ultrasonic velocity in the standard calibration block (m/s), s_w is the thickness of the test material measured by the vernier caliper (mm) and s_{ST} is the thickness of the test material obtained by an ultrasonic device (mm).

2.3.4.1 Advantages of ultrasonic testing [48]

- 1) It is sensitive to both surface and subsurface discontinuities.
- 2) The depth of penetration for flaw detection or measurement is superior to other NDT methods.
- 3) Only single-sided access is needed when the pulse-echo technique is used.
- 4) It is highly accurate in determining reflector position and estimating size and shape.
- 5) Minimal part preparation is required.
- 6) Electronic equipment provides instantaneous results.
- 7) Detailed images can be produced with automated systems.
- 8) It has other uses, such as thickness measurement, in addition to flaw detection.

2.3.4.2 Limitations of Ultrasonic testing [48]

- 1) Surface must be accessible to transmit ultrasound.
- 2) Skill and training is more extensive than with some other methods.
- 3) It normally requires a coupling medium to promote the transfer of sound energy into the test specimen.
- 4) Materials that are rough, irregular in shape, very small, exceptionally thin or not homogeneous are difficult to inspect.
- 5) Cast iron and other coarse grained materials are difficult to inspect due to low sound transmission and high signal noise.
- 6) Linear defects oriented parallel to the sound beam may go undetected.

2.3.5 Elastic moduli obtained from ultrasonic testing

When measuring the ultrasonic velocity both longitudinal and shear, elastic properties can be calculated as follows [51]:

Longitudinal modulus (L) numerical constant that describes the elastic properties of a solid undergoing tension or compression in the longitudinal direction. In other words, longitudinal modulus is a measure of the ability of a material to resist longitudinal deformations.

$$L = \rho v_L^2 \quad (2.10)$$

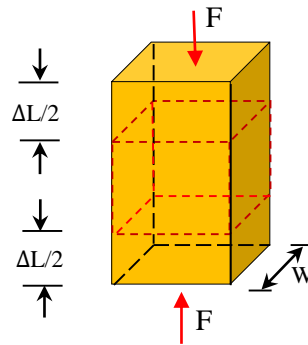


Figure 2.5 Diagrammatic illustration of longitudinal modulus showing directions of load (F) and of expansion

Shear modulus (G) is a measure of the ability of a material to resist transverse deformations. It is one of property for measuring the stiffness of materials. Which describes how the material's response to shear stress. The shear modulus is concerned with the deformation of a solid when it experiences a parallel force (Shear Force) to one of its surfaces while its opposite face experiences an opposing force.

$$G = \rho v_s^2 \quad (2.11)$$

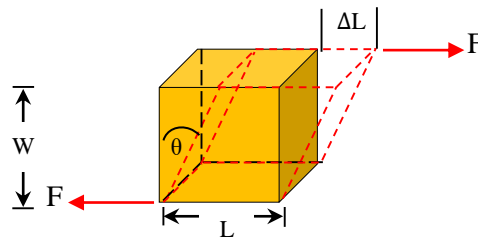


Figure 2.6 Diagrammatic illustration of shear modulus showing directions of load (F) and of expansion

Bulk modulus (K) is numerical constant that describes the elastic properties of a solid or fluid when it is under pressure on all surfaces. The applied pressure reduces the volume of a material, which returns to its original volume when the pressure is removed. The bulk modulus is a measure of the ability of a substance to withstand changes in volume when under compression on all sides. Bulk modulus is used to measure how incompressible a solid is. Besides, the more the value of K for a material, higher is its nature to be incompressible.

$$K = L - \left(\frac{4}{3}\right)G \quad (2.12)$$

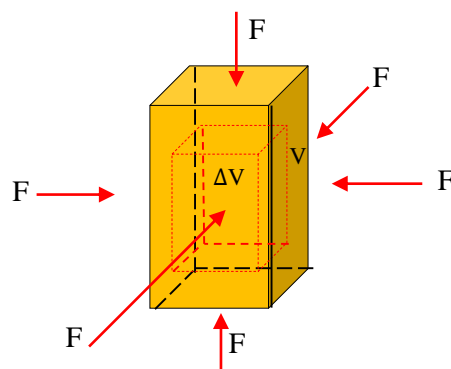


Figure 2.7 Diagrammatic illustration of bulk modulus showing directions of load (F) and of expansion

Poisson's ratio (σ) is the ratio of transverse contraction strain to longitudinal extension strain in the direction of stretching force. Tensile deformation is considered positive and compressive deformation is considered negative. When a material is stretched in one direction, it tends to compress in the direction perpendicular to that of force application and vice versa. The measure of this phenomenon is given in terms of Poisson's ratio. For example, a rubber band tends to become thinner when stretched. For most materials, the value of Poisson's ratio lies in the range, 0 to 0.5. Poisson ratio of glass material lies in the range, 0.18 to 0.3.

$$\sigma = \frac{L - 2G}{2(L - G)} \quad (2.13)$$

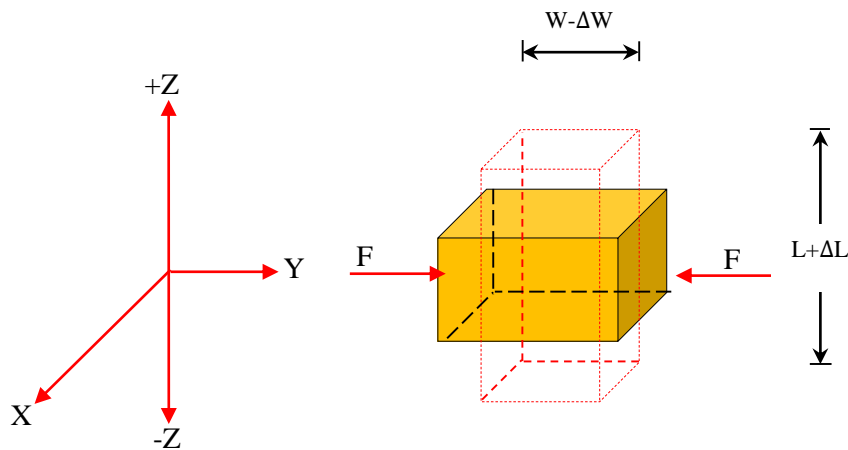


Figure 2.8 Diagrammatic illustration of Poisson's ratio showing directions of load (F) and of expansion

Young's modulus (E) is numerical constant that describes the elastic properties of a solid undergoing tension or compression in only one direction, as in the case of a metal rod that after being stretched or compressed lengthwise returns to its original length. Young's modulus is a measure of the ability of a material to withstand changes in length when under lengthwise tension or compression. Young's modulus is equal to the longitudinal stress divided by the strain. Rocks with low Young's modulus tend to be ductile and rocks with high Young's modulus tend to be brittle. Generally, brittle rocks have better completion quality and are better hydraulic fracturing targets

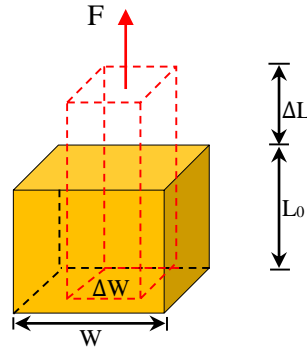


Figure 2.9 Diagrammatic illustration of Young' modulus showing directions of load (F) and of expansion

$$E = 2(1 + \sigma)G \quad (2.14)$$

Material hardness [52] is the property of the material which enables it to resist plastic deformation, usually by penetration or by indentation. The term of hardness is also referred to stiffness or temper, or to resistance to bending, scratching, abrasion, or cutting.

Microhardness (H) is the hardness of a material as determined by forcing an indenter such as a Vickers or Knoop indenter into the surface of the material under 15 to 1000 gf load; usually, the indentations are so small that they must be measured with a microscope. Capable of determining hardness of different microconstituents within a structure, or measuring steep hardness gradients such as those encountered in case hardening. Conversions from microhardness values to tensile strength and other hardness scales (e.g. Rockwell) are available for many metals and alloys. Micro-indenters work by pressing a tip into a sample and continuously measuring: applied load, penetration depth and cycle time.

$$H = \frac{(1 - 2\sigma)E}{6(1 + \sigma)} \quad (2.15)$$

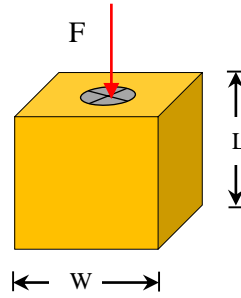


Figure 2.10 Diagrammatic illustration of microhardness showing directions of load (F) and of expansion

2.4 Theory of elastic moduli from theoretical models

2.4.1 Makishima-Mackenzie model

Makishima and Mackenzie [53,54] have reported a theoretical model for calculating the packing density (defined as the ratio between the minimum theoretical volume occupied by the ions and the corresponding ionic volume of the glass), dissociation energy per unit volume (defined as the volume density of binding energy), elastic moduli and Poisson's ratio of the glass. The same authors [53,54] have expressed these parameters for multi-component glasses in terms of the packing factor and dissociation energy per unit volume of the oxide constituent. The formula used to determine elastic moduli include: Makishima-Mackenzie Young's modulus (E_m), Makishima-Mackenzie bulk modulus (K_m), Makishima-Mackenzie shear modulus (G_m), Makishima-Mackenzie longitudinal modulus (L_m) and Makishima-Mackenzie Poisson's ratio (σ_m) in this model are given below [55-57];

$$V_t = \left(\frac{1}{V_m} \right) \sum_i V_i x_i = \sum_i \frac{\rho_i}{M_i} \sum_i V_i x_i \quad (2.16)$$

$$G_t = \sum_i x_i G_i \quad (2.17)$$

$$E_m = 8.36 V_t G_t \quad (2.18)$$

$$K_m = 10.0V_t^2G_t \quad (2.19)$$

$$G_m = 3K_m/(10.2V_t - 1) \quad (2.20)$$

$$L_m = K_m + 4G_m/3 \quad (2.21)$$

$$\sigma_m = 0.5 - (1/7.2V_t) \quad (2.22)$$

where G_i and V_i are the respective dissociation energy per unit volume and packing factor of the i th component. For i th component oxide in the form A_nO_m , the values of G_i and V_i can be estimated from the respective Eqs. (2.23) and (2.24);

$$G_i = \frac{\rho_i}{M_i} U_i \quad (2.23)$$

$$V_i = \frac{4}{3} \pi N_A (nR_A^3 + mR_O^3) \quad (2.24)$$

where R_A and R_O are the respective ionic radius of metal and oxygen, N_A is Avogadro's number and U_i is the dissociation energy per mole (molar dissociation energy) of the i th component.

2.4.2 Abd El-Moneim and Alfifi's approaches

Abd El-Moneim and Alfifi [58-60] suggested that the experimental bulk modulus (K_{Abd}) of glasses can be predicted in terms of the ratio between packing density and mean atomic volume according to the following semi-empirical formula;

$$K_{Abd} = Q(V_t/\bar{V})^\gamma \quad (2.25)$$

where γ & Q are two new constants. Values of γ & Q depend strongly upon the type of the glass network and its constitution.

The molar volume (V_m) and mean atomic volume of multi-component oxide glasses (\bar{V}) can be obtained from the molecular weights of the constituent components (M_w) and measured density as follows;

$$V_m = \frac{M_w}{\rho} \quad (2.26)$$

$$\bar{V} = \frac{V_m}{\psi} \quad (2.27)$$

$$M_w = \sum_i M_i x_i \quad (2.28)$$

where ρ and ψ are the respective glass density and total number of atoms in glass formula unit, whereas M_i and x_i are the respective molecular weight and molar fraction of the i th component.

2.5 Gamma rays

2.5.1 Basic knowledge about gamma rays

A gamma ray [61] is a packet of electromagnetic energy (photon) emitted by the nucleus of some radionuclides following radioactive decay. Gamma rays are a form of electromagnetic radiation (EMR). They are similar to X-rays, distinguished only by the fact that they are emitted from an excited nucleus. Electromagnetic radiation can be described in terms of a stream of photons, which are massless particles each travelling in a wave-like pattern and moving at the speed of light. Each photon contains a certain amount of energy, and all electromagnetic radiation consists of these photons. Gamma ray photons have the highest energy in the EMR spectrum and their waves have the shortest wavelength.

Scientists measure the energy of photons in electron volts (eV). X-ray photons have energies in the range 100 eV to 100,000 eV (or 100 keV). Gamma ray photons generally have energies greater than 100 keV. For comparison, ultraviolet radiation has energy that falls in the range from a few electron volts to about 100 eV

and does not have enough energy to be classified as ionizing radiation. The high energy of gamma rays enables them to pass through many kinds of materials, including human tissue. Very dense materials, such as lead, are commonly used as shielding to slow or stop gamma rays as shown in figure 2.11.

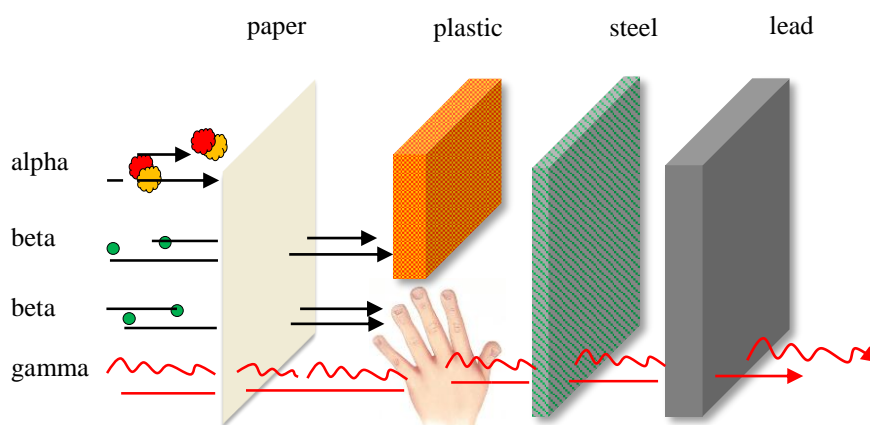


Figure 2.11 Radiation shielding materials for various types of radiation

The key difference between gamma rays and X-rays is how they are produced. Gamma rays originate from the settling process of an excited nucleus of a radionuclide after it undergoes radioactive decay whereas X-rays are produced when electrons strike a target or when electrons rearrange within an atom. Cosmic rays also include high-energy photons and these are also called gamma-rays whether or not they originated from nuclear decay or reaction. Gamma radiation is highly penetrating and interacts with matter through ionization via three processes; photoelectric effect, Compton scattering or pair production. Due to their high penetration power, the impact of gamma radiation can occur throughout a body, they are however less ionizing than alpha particles. Gamma radiation is considered an external hazard with regards to radiation protection. Similar to all exposure to ionizing radiation, high exposures can cause direct acute effects through immediate damage to cells. Low levels of exposure carry a stochastic health risk where the probability of cancer induction rises with increased exposure.

Gamma radiation is released from many of the radioisotopes found in the natural radiation decay series of uranium, thorium and actinium as well as being emitted by the naturally occurring radioisotopes potassium-40 and carbon-14. These are found

in all rocks and soil and even in our food and water. Artificial sources of gamma radiation are produced in fission in nuclear reactors, high energy physics experiments, nuclear explosions and accidents. Gamma emitting radionuclides are the most widely used radiation sources. The penetrating power of gamma rays has many applications. However, while gamma rays penetrate many materials, this does not make them radioactive. The three radionuclides that are by far the most useful are cobalt-60, caesium-137 and americium-241 [61].

2.5.1.1 Uses of Cobalt-60

The Cobalt-60 radiation source is used in various fields as follows

- 1) sterilization of medical equipment in hospitals
- 2) pasteurization, via irradiation, of certain foodstuffs
- 3) levelling or thickness gauges (i.e. food packaging, steel mills)
- 4) industrial radiography

2.5.1.2 Uses of Caesium-137

The Caesium-137 radiation source is used in various fields as follows

- 1) measurement and control of the flow of liquids in industrial processes
- 2) investigation of subterranean strata (i.e. oil, coal, gas and other)
- 3) measurement of soil moisture-density at construction sites
- 4) levelling gauges for packaging of food, drugs and other products

2.5.1.3 Uses of Americium-241

The Americium-241 radiation source is used in various fields as follows

- 1) smoke detectors for households
- 2) fluid levelling and density gauges
- 3) thickness gauges for thin materials (i.e. paper, foil, glass)
- 4) aircraft fuel gauges
- 5) when mixed with beryllium, americium-241 produces a $^{241}\text{AmBe}$ neutron source with uses in well logging, neutron radiography and tomography.

2.5.2 Interaction of gamma rays with matter

When Gamma rays interact with matter, these can be either absorbed completely or scattered either by an electron or a nucleus through number of processes. Many of these processes are quite infrequent and some have yet not been observed. In the energy domain 0.01 to 100 MeV, gamma rays interrelate with matter primarily through three processes namely; Photoelectric effect, Compton Effect and Pair production. The amount of particular type of interaction probably depends upon incident photon energy, scattering angle, nature of the target material (atomic number) and experimental conditions (figure 2.12) [62,63].

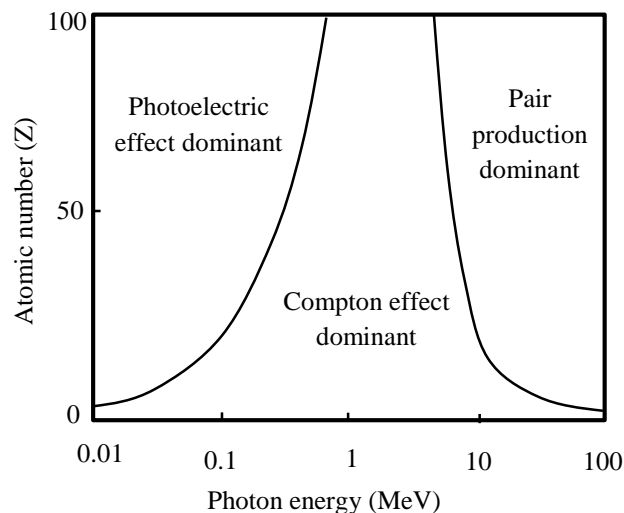


Figure 2.12 Z-E diagram

The predominant mode of interaction of gamma rays with matter depends on the energy of incident photons and the atomic number of the material with which they are interacting. At low energies and with high Z materials the photoelectric effect is main interaction process. At intermediate energies and in low Z materials, the Compton scattering is dominating. At very high energies pair production is the most dominant interaction process. The details of these interaction processes are discussed below:

2.5.2.1 Photoelectric effect

The photoelectric effect is process of absorption of gamma photon by an atom as shown in figure 2.13. It occurs when photon interacts with matter and

energy of the photon is transferred to one of the orbital electrons, usually K-shell electron which is nearest to the nucleus and results in ejection of electron from the atom. The ejection of electrons from a given shell creates a vacancy in that shell and leaves the atom in an excited state. An electron from the higher shells fills this vacancy and as a result characteristic X-ray of the shell is emitted with energy equal to the difference of binding energy of the shells.

The momentum of ejected electron is balanced by the recoil of nucleus. The ejected electron possesses energy (E_{Kin}) equal to the difference in energy of gamma photon ($h\nu$) and binding energy of the electron in its orbit (E_B) as shown in the equation (2.29) [62,64].

$$E_{\text{Kin}} = h\nu - E_B \quad (2.29)$$

About 80% of photoelectric interactions take place in K-shell, and remaining 20% of interactions take place in L shell and higher shells. The photoelectric effect is more pronounced in high atomic number absorbers and at low incident energies. The photoelectric cross-section varies discontinuously for photon energies equal to binding energy of the electrons in the atom.

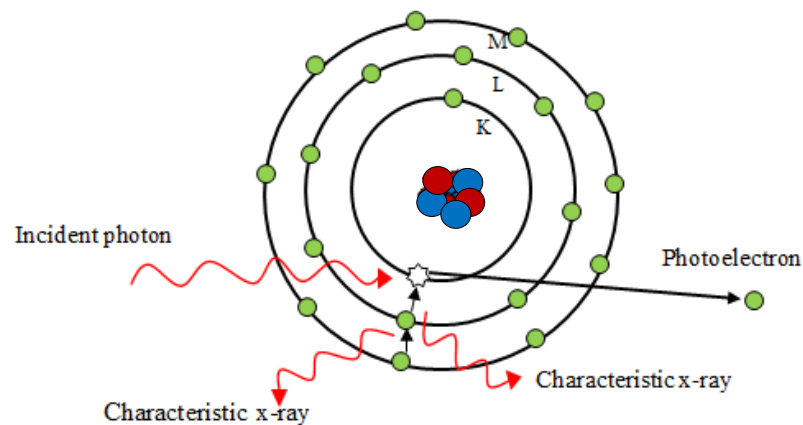


Figure 2.13 Photoelectric effect

2.5.2.2 Compton effect

Characteristic of the Compton effect (figure 2.14) [62,64] is that only part of its total amount of energy is transferred from the entering photon to an electron. The freed electron, which is called Compton electron (recoil electron), reaches a certain velocity that is dependent on the energy transferred to the electron. The rest of the energy continues as a photon of lower energy in another direction, and is therefore called a scattered photon. Because of the lower energy the scattered photon has a longer wavelength than the original.

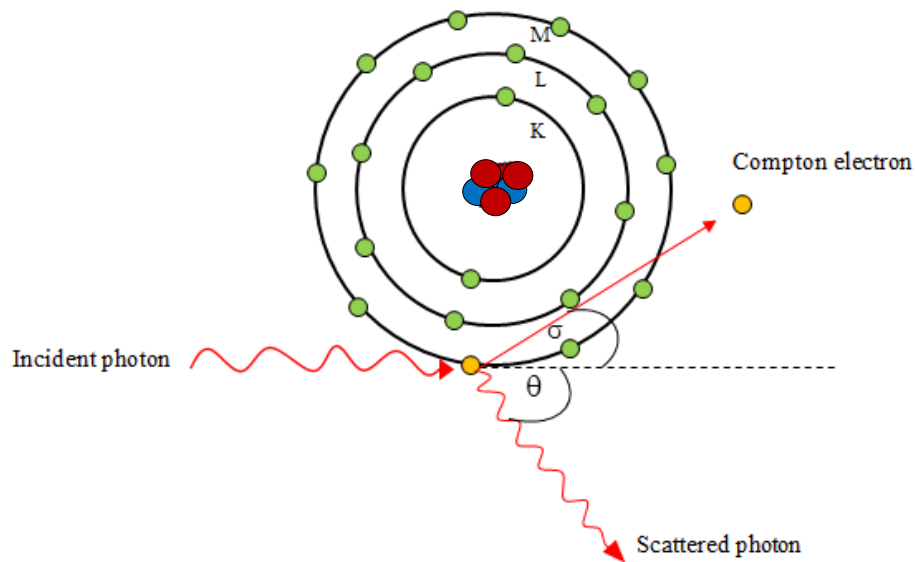


Figure 2.14 Compton effect

The Compton process occurs only then when the photon energy passes the limiting value of the photoelectric process. Since the impulse and the energy are divided among the Compton electron and the scattered photon, the law of preservation of impulse is complied with, and the process occurs with the electrons from the outer shells as well. For this reason, the atomic number (Z) of the material is less influential. The freed Compton electrons can, depending on the energy content, ionize other atoms along their routes. The scattered photon continues its way and continues to enter into Compton processes up until the energy is reduced to such an extent that a photoelectric process takes place. Only then the photon has disappeared.

Because the electron binding energy is very small compared to the gamma ray energy, the kinetic energy of electron is nearly equals to the energy lost by the gamma

$$E_e = E_\gamma - E' \quad (2.30)$$

where E_e is energy of scattered electrons, E_γ is energy of incident of gamma ray and E' is energy of scattered of gamma ray.

2.5.2.3 Pair production and Annihilation

With photon energies larger than 1.022 MeV pair production may occur as an alternative to the Compton process. When such a high energetic photon comes close to a nucleus, transformation of energy into mass can occur because of the electric field of the nucleus. With this the photon is converted into an electron and a positron with the same mass, but the reverse charge. If the photon energy is, for example, 2 MeV, $2 \times 0.511 = 1.022$ MeV goes to the electron-positron pair and the remainder (0.978 MeV) is divided as kinetic energy among the electron and the positron. In this process, in which the original photon disappears completely, the surplus of impulse is transferred to the nucleus [65].

Pair Annihilation [64,65] means the reverse process of pair production. In the pair annihilation, the electron and positron in the stationary state combine with each other and annihilate. Surely, the particles are disappeared and radiation energy will occur instead of two particles. For the momentum conservation, the most frequent process in pair annihilation is making two photons that have exactly opposite direction and the same amount of momentum.

Table 2.2 Cross-sectional dependence of dominant photon interaction processes
[62-65]

Interaction process	Cross-Section dependence	
	On Atomic number (Z)	On Photon energy (E)
Photoelectric process	Z^{4-5}	$E^{3.5}$
Compton Process	Z	$1/E$
Pair production process	Z^2	$\log_e E$

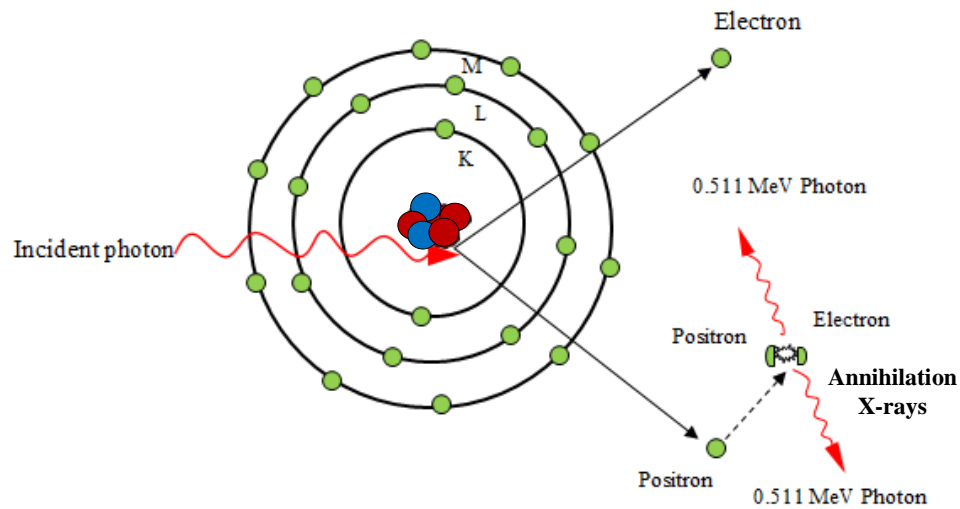


Figure 2.15 Pair production and Annihilation

The cross-sectional dependence of different dominant photon interaction processes on number of interacting material (Z) and energy of the incident radiation has been summarized in Table 2.2.

2.5.3 The fundamental law of gamma ray attenuation

Besides numerous applications of gamma rays in different fields, gamma rays are the most dangerous form of electromagnetic radiation emitted by nuclear explosion because they are highly trenchant, highly energetic ionizing radiation. The longer exposure of these highly penetrating radiations is hazardous to living cells, which can cause redness of skin, headache, vomiting and even death. Composite materials as gamma ray shielding materials has been analyzed in terms of measuring linear attenuation coefficient, mass attenuation coefficient, half value layer and mean free path.

2.5.3.1 Linear attenuation coefficient (μ)

The linear attenuation coefficient [66,67] describes the extent to which the intensity of an energy beam is reduced as it passes through a specific material. The linear attenuation coefficient gives information about the effectiveness of a given material per unit thickness, in promoting photon interactions. The large value of attenuation coefficient is more likely to the given thickness of material. The magnitude of attenuation coefficient varies with thickness of material and its density, while specific values of the attenuation coefficient will vary among materials for photons of

specified energy. The plots of attenuation coefficient versus photon energy are similar for different materials. In general, trends show high values of attenuation coefficient at low photon energies that decreases as photon energy increases goes through a rather minimum value, and then increases as energy continues to increase. The reason of these trends is that the linear attenuation coefficient is made up of three major components, each of which is depends upon different types of photon interaction. At lower energy, a process is called photoelectric effect is the dominant interaction mode that has strong energy dependence, decreasing approximately as the inverse cube of the energy. At intermediate energies the dominant interaction is Compton scattering, which shows a decreasing trends with increasing energy. Finally, at higher energies the dominant interaction is pair production, this shows increasing nature as energy increases. This process is occurred in the energy 1.022 MeV. Thus, at low energies photoelectric contribution decreases which causes in the attenuation coefficient as energy increases.

Linear attenuation coefficient (μ) cm^{-1} is determined by using a well collimated narrow beam of photon passing through a homogeneous absorber of thickness 't', the ratio of intensity of emerging beam from the source along the incident direction, to the intensity is given by the Beer Lambert law as given by Eq. (2.31)

$$I = I_0 e^{-\mu t} \quad (2.31)$$

where I_0 and I are the photon intensities that arrive to the material and leave from the material, respectively, and μ (cm^{-1}) stand for the linear attenuation coefficient.

2.5.3.2 Mass attenuation coefficient (μ_m)

Mass attenuation coefficient [66,67] is the most fundamental parameter to study the interaction of gamma radiations with matter. Mass attenuation coefficient (μ_m), measures the number of photons interacted (scattered/absorbed) with the interacting material. It depends on the incident photon energy and density of composite materials. The ratio of linear attenuation coefficient (μ) to the density (ρ) is called the mass attenuation coefficient (μ/ρ or μ_m) and has the dimension of area per unit mass (cm^2/gm). A narrow beam of mono-energetic photons with an incident intensity I_0 , penetrating a layer of material with mass thickness x and density ρ , emerges with intensity I given by the following relation,

$$\frac{I}{I_0} = \exp \left[- \left(\frac{\mu}{\rho} \right) x \right] \quad (2.32)$$

$$\frac{\mu}{\rho} = x^{-1} \ln \left(\frac{I_0}{I} \right) \quad (2.33)$$

From which the mass attenuation coefficient can be obtained from measured values of incident photon intensity I_0 , transmitted photon intensity I and thickness of the absorber t . The thickness of the absorber is defined as the mass per unit area, and it is obtained by multiplying thickness t and density of the absorber, i.e. $x = \rho t$.

2.5.3.3 Half value layer (HVL)

The half value thickness, or half value layer, is the thickness of the material that reduces the intensity of the beam to half its original magnitude. When the attenuator thickness is equivalent to the HVL, N/N_0 is equal to 0.5. Thus, it can be shown that [68,69]

$$\text{HVL} = \frac{\ln 2}{\mu} \quad (2.34)$$

This value is used clinically quite often in place of the linear attenuation coefficient.

2.5.3.4 Mean free path (MFP)

Mean free path [68,69] is the average distance a single particle travels through a given attenuating medium before interacting. It is also the depth to which a fraction $1/e$ (~37%) of a large homogeneous population of particles in a beam can penetrate. For example, a distance of three free mean paths, $3/\mu$, reduces the primary beam intensity to 5%. The mean free path is related to the HVL according to

$$\text{MFP} = \frac{\text{HVL}}{\ln 2} \quad (2.35)$$

The mean free path, or relaxation length, is the quantity

$$\text{MFP} = \frac{1}{\mu} \quad (2.36)$$

2.6 Broad beam transmission geometry

The measurement of photon attenuation in different materials is usually performed in a narrow beam geometry configuration. This is important for the detailed and precise measurement of attenuation coefficient of primary radiation in the absorber by preventing the scattered photons from reaching the detector [70]. However, the varieties of application fields such as gamma ray shielding, energy absorption studies, food and agriculture, industry, medicine, biology, transport, building, mining and forest industry involve attenuation measurements in a broad beam geometry configuration. Also, some limited work has been done in the measurement of attenuation coefficient employing a broad beam geometry configuration. Hence the study of attenuation of photons in broad beam geometry is considered relevant [71]. Broad beam geometry is a more realistic case. As we can see on the figure 2.16, when we have broad beam geometry, some scattered radiation reaches the detector. We have attenuated primary photons reaching the detector as well as scattered radiation reaching the detector.

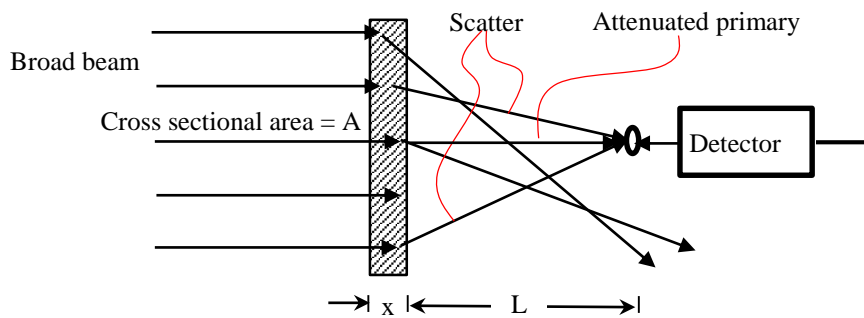


Figure 2.16 Broad beam geometry

A new method has been proposed by H. A. Jahagirdar et al. (1992a) [71] to measure the attenuation coefficient of 0.1236 MeV photons in various elements under a broad beam geometry set up. Also, H. A. Jahagirdar et al. (1992b) [72] have been used this method to determine narrow beam attenuation coefficients from a broad beam geometrical configuration for 0.32 MeV photons in different compounds of high Z

elements. After that, H. A. Jahagirdar et al. (1993) [73] extract the narrow beam attenuation coefficients from a broad beam measurement at 145.4 keV gamma rays in lead and in different compounds of high Z elements.

For the attenuator thickness of the order of one to two mean free path lengths, they assumed even for broad beam geometry an exponential law of attenuation of the type.

$$I_b = I_0 \exp \left[- \left(\frac{\mu_b}{\rho} \right) t \right] \quad (2.37)$$

where I_b is the intensity of transmitted through an absorber of mass per unit area t which includes primary and scattered photons, but not other secondary radiation. I_0 is the incident intensity and μ_b/ρ is the broad beam attenuation coefficient of the absorber.

Secondary radiations composed of characteristic x-rays which are excluded from the transmitted intensity as they correspond to absorption of photons in the target. The relation (2.37) may be expressed as [72]:

$$T = I_b/I_0 = \exp \left[- \left(\frac{\mu_b}{\rho} \right) t \right]$$

$$\ln T = - \left(\frac{\mu_b}{\rho} \right) t$$

or

$$\frac{\mu_b}{\rho} = - \frac{\ln T}{t} \quad (2.38)$$

It is well known that, μ_b/ρ , the broad beam attenuation coefficient, is not a characteristic constant (unlike the narrow beam attenuation coefficient μ/ρ) but is a function of thickness of the attenuator. From equation (2.38) it can be seen that as t increases, T decreases and hence μ_b/ρ decreases but slowly because of the term $\ln T$. Their work indicates that it is possible to extract narrow beam attenuation coefficients from the broad beam geometrical configuration. Thus they conclude from their investigation as follows [72,73]: (1) In the limited region of transmission, it is possible

to obtain the narrow beam attenuation coefficients under the broad beam geometry configuration. (2) The attenuation coefficients derived from this method agree fairly well with the narrow beam attenuation coefficients and hence the mixture rule is also valid for situations approximating their experimental materials and configuration.

It is interesting to note that even in our broad beam geometry configuration, if the transmission is in the range 50% to 20%, the experimental u/p values agree well with theoretical values.

2.7 WinXCom program

The information on absorption of X-rays and gamma rays are needed for many engineering, scientific and medical applications. Hubbell and Seltzer (1995) [74] published the attenuation coefficient of elements and compounds in the energy range 1 keV to 20 MeV using theoretical calculations through the mixture rule. This attenuation coefficient can be used to calculate effective atomic numbers. Berger and Hubbell (1987) [75] developed XCOM software for ease of operation in processing mass attenuation coefficients or photon interaction cross sections for any element, compound or mixture at energies from 1 keV to 100 GeV in DOS version. This program was compiled in the National Institute of Standards and Technology (NIST) database. Later, Gerward et al. (2001) [76] transformed this program to the Windows version, called WinXCom. The WinXCom runs under the Windows operating system and provides an interface that comfort defining, redefining and saving item in a substance definition list. Once a substance has been defined, it can be used for defining compounds or mixtures. It is even possible to define mixtures of already defined compounds or mixtures. The substance definition list comes with a predefined list of the first hundred elements in the periodic table ($Z=1-100$).

The processing of WinXCom program based on mixture rule. As the materials are composed of various elements, it is assumed that the contribution of elements of the compound to the total photon interaction is yielding the well-known mixture rule that represents the total mass attenuation coefficient of any compound as the sum of appropriately weighted proportion of the individual atoms, which is calculated by [77],

$$\left(\frac{\mu}{\rho}\right)_c = \sum w_i \left(\frac{\mu}{\rho}\right)_i \quad (2.39)$$

where, $(\mu/\rho)_c$ is the photon mass attenuation coefficient for the compound, $(\mu/\rho)_i$ is the photon mass attenuation coefficient for the individual elements in the compound and w_i is the fractional weight of the elements in the compound.

WinXCom can generate cross-sections or attenuation coefficients on a standard energy grid, spaced approximately logarithmically, or on a grid specified by the user, or for a mix of both grids. The program provides total cross-sections and attenuation coefficients as well as partial cross-sections for incoherent and coherent scattering, photoelectric absorption and pair production. For compounds, the quantities calculated are partial and total mass attenuation coefficients. Total attenuation coefficients without the contribution from coherent scattering are also given, since they are often used in gamma ray transport calculations. WinXCom makes it possible to export the table of cross-sectional or mass-attenuation data to a predefined Microsoft Excel template. In this way, graphical display and further data treatment is made easy [78].

2.8 Related Research

As mentioned in the introduction that many agricultural countries like Thailand, there are many kinds of agricultural waste such as bagasse, cassava rhizome, corn cob, rice husk and others. Many methods of managing these agricultural wastes may cause health and environmental problems. Researchers have realized the problems from traditional waste management and searched for new ways to create benefits from waste products. In 2011, A.E. Souza et al. (2011) [79] studied about reuse of sugarcane bagasse ash (SCBA) to produce ceramic materials. SCBA is a residue resulting from the burning of bagasse in boilers in the sugarcane/alcohol industry. SCBA has a very high silica concentration. In their research, the properties of sintered ceramic bodies were evaluated based on the concentration of SCBA, which replaced non-plastic material. The results reported show that the reuse of SCBA in the ceramic industry is feasible. Therefore, the ash (SCBA) may be used as an additive to produce ceramic materials that meet the standards Brazilians. Hence, this process can lower the volume of solid residues disposed on the environment and to increase the lifetime of the

reserves of raw materials. Three year later, S.R. Teixeira et al. (2014) [5] estimated cost of producing glass-ceramic materials from sugarcane bagasse ash. The most significant glass-ceramic for building applications has wollastonite as the main crystal phase. They report on the use of SCBA to produce glass-ceramics with silicates as the major crystalline phases. In their study, it was shown that sugarcane bagasse ash (45-40 wt%), along with limestone (45-50 wt%) and fluxing agent (K_2CO_3 , 10 wt%), can be recycled to produce glass-ceramic material with wollastonite as the main phase. The glass-ceramic material was obtained at relatively low crystallization temperatures. These temperatures lead to lower production costs due to lower consumption of energy and time, and the material obtained can be of great value in the construction industry. In the same year, G. N. K. Reddy et al. (2014) [6] have ideas about development partial replacement materials of cement in concrete with sugarcane bagasse ash and studied its behavior in aggressive environments. Every one ton of cement manufacture releases half ton of carbon dioxide, so there is an immediate need to control the usage of cement. On the hand materials wastes such as sugar cane bagasse ash is difficult to dispose which in return is environmental hazard. The bagasse ash imparts high early strength to concrete and also reduce the permeability of concrete. The silica present in the bagasse ash reacts with components of cement during hydration and imparts additional properties such as chloride resistance, corrosion resistance etc. The result also showed that SCBA concrete performed better when compared to ordinary concrete up to 10% replacement of sugar cane bagasse ash due to presence of high amount of silica in SCBA. Therefore, the use of bagasse ash in concrete not only reduces the environmental pollution but also enhances the properties of concrete and also reduces the cost.

In 2017, the research of A. L. M. P. Leite et al. (2017) [7] aimed to obtain and characterize nanofibers from cassava bagasse and peelings, which are waste originating from cassava starch extraction. Their work, a methodology to isolate nanofibers from cassava bagasse and peelings, inexpensive byproducts of starch production, was developed. The nanofibers obtained in their study had diameters between 2.33 - 5.37 nm and high crystallinity ratio. It was proved that nanofibers with very good properties can be also isolated from the cassava peelings to be used as reinforcement material in the development of biodegradable films reducing the solid waste generated from cassava starch processing. The same year, Thai researchers offered work on cassava

rhizomes as well. N. Tippayawong et al. (2017) [8] showed cassava waste consists mainly of rhizome. Around four million tons of the agro-residue is available annually. It has great potential to be used for energy and power generation. In their work, cassava rhizome was converted into biochar in an alternative carbonizer based on semi-continuous, externally heated, retort type, pyrolysis gas burning concept. The reactor capacity was 35-50 kg/h, suitable for local entrepreneurs. Tests with cassava rhizome showed that good quality charcoal can be produced in shorter time with much lower atmospheric pollutants, compared with traditional kilns. The carbonization system was demonstrated to perform well in terms of temperature evolution, biochar yields and characteristics.

These research shows that recycling bagasse ash and cassava rhizome have many advantages such as good potential to be a component of the material type glass-ceramics and concrete, very good way to manage waste, reduce the environmental pollution and also reduces the cost production. The interesting properties of bagasse ash and cassava rhizomes make the researchers interested in studying and utilizing them in the development of radiation shielding glass materials. After the researchers analyzed the composition of bagasse and cassava rhizome using EDS technique, it was found that the main components of bagasse and cassava rhizome were SiO_2 and CaO , respectively. Accordingly, these waste products are possible to use as raw materials for glass production. Therefore, the researcher studied the glass system related to these substances and compiled interesting research as follows:

Beginning in 2004, Y. B. Saddeek (2004) [80] interested in elastic and physical properties of some borate glasses. The structure of the glass system $(75 - x)\text{B}_2\text{O}_3 - x\text{Bi}_2\text{O}_3 - 25\text{Li}_2\text{O}$, where $x = 5, 10, 15$, and 20 mol% was investigated by using pulse-echo technique. Elastic properties of the glass system have been calculated from the measured densities as well as longitudinal and shear ultrasonic velocities. Estimated parameters based on Makishima-Mackenzie theory and bond compression model were calculated in order to analyses the experimental elastic moduli. Ultrasonic technique plays a significant role in understanding the structural characteristics of glass network. The measurement of ultrasonic parameters such as velocity and attenuation as a function of composition, temperature, and frequency is of great interest in glass. These ultrasonic parameters besides density and molar volume are sensitive and informative

about the changes occurred in the structure of glass network. Therefore, any change in the lattice due to modifier doping can be directly noted.

Two years later borate glass is still of continuing interest, E. S. Lim et al. (2006) [18] studied effect of BaO content on the sintering and physical properties of BaO-B₂O₃-SiO₂ glasses. Their glass system was chosen as a candidate composition for the application to Pb-free low temperature sinterable glass. The study of them examined the effect of BaO/B₂O₃. Since BaO played the role of network modifier, the glass transition temperature and crystallization temperature decreased as the BaO content increased. After that in 2008, S. Singh et al. (2008) [81] reported about radiation shielding properties of Barium-borate-flyash glasses. The attenuation coefficients of their glasses have been measured for gamma ray photon energies of 356, 662, 1173 and 1332 keV using narrow beam transmission geometry. The attenuation coefficients were then used to obtain the values of mean free path (MFP), effective atomic number and electron density. Good agreements have been observed between experimental and theoretical values of these parameters. From the studies of the obtained results it is reported here that from the shielding point of view their glasses are better shields to gamma radiations in comparison to the standard radiation shielding concretes and also to the ordinary barium-borate glasses. These research is interesting about the borosilicate glass system and the role of BaO. BaO played the role of network modifier. Radiation shielding properties of glass can be improved by BaO and flyash. Therefore, the works are a good way for the development of radiation shielding glass materials from bagasse and cassava rhizomes.

In 2016, Y. Hao and J. Cao (2016) [14] reported structure and luminescence of Dy³⁺ doped CaO-B₂O₃-SiO₂ glasses prepared by melt quenching technique. The presence of various stretching and bending vibrations of different borate and silicate groups were identified from FTIR spectral measurements. The optical absorption and luminescence spectra were also measured. The researcher prepared the CaO-B₂O₃-SiO₂ glass system by melt quenching technique. It is possible to prepare glass from cassava rhizomes and bagasse; whose main components are similar to the glass system of them. FTIR spectral measurements are interesting for identified various stretching and bending vibrations of some bond in the network of studied glass.

During the same, K. Kaur et al. (2016) [82] studied structural properties of $\text{Bi}_2\text{O}_3\text{-B}_2\text{O}_3\text{-SiO}_2\text{-Na}_2\text{O}$ glasses for gamma ray shielding applications. Their glass samples have been prepared using melt quenching technique. Cs-137 source has been used for experimental measurements of mass attenuation coefficient of gamma rays at 662 keV. Mass attenuation coefficient of their glass samples has been compared with standard nuclear radiation shield “barite concrete”. It has been concluded that bismuth containing glass samples can be potential candidates for gamma ray shielding applications. Glasses must have appreciable elastic moduli values for their practical utility as gamma ray shields which are related to coordination number and non-bridging oxygens. Structural properties of their glass system have been estimated from the detailed analysis of Optical, Raman and FTIR spectra. Their reported investigations can contribute to the development of transparent gamma ray shields. A year later, B.O. El-bashir et al. (2017) [83] have been carrying out to characterize the structural, elastic and shielding properties of novel ternary $\text{BaO-Bi}_2\text{O}_3\text{-P}_2\text{O}_5$ glasses. Their glass series were prepared by conventional melt-quenching technique and the variation in density, molar volume, X-ray diffraction and ultrasonic velocities has also been studied and correlated with the structural modifications in the glasses. The shielding parameters, effective atomic numbers, half value layers, and exposure buildup factor values have been computed using WinXCom program and G-P fitting method. The variations of shielding parameters, density, ultrasonic velocity and the calculated elastic moduli are found to be composition dependent and discussed in terms of Bi_2O_3 modifiers. Their results indicate that the increment in the content of Bi_2O_3 improves the gamma ray shielding characteristics of the selected glasses and potentially used as gamma ray shielding material. These two studies are good guidelines for examining the radiation shielding properties of the glass systems investigated. The shielding parameters have been computed using WinXCom program. The increment in the content of heavy metal oxides improves the gamma ray shielding characteristics of the selected glasses and potentially used as gamma ray shielding material. In addition, X-ray diffraction technique can be used to confirm amorphous nature of glass.

Many research found that the improvement of gamma ray shielding properties can be produce by adding heavy metal oxide substances. The researchers interest to study WO_3 , it has the advantages of being environmentally friendly, simple and cost-effective

in terms of the production process. Since 2012, H.A. ElBatal et al. (2012) [84] studied optical and FTIR spectral properties of tungsten ions in a host lead borate glass with composition PbO 55%, B_2O_3 45% (wt%). The same spectral properties were re-measured after subjecting the samples to successive gamma irradiation. The studied host lead borate glass has been found to show obvious shielding behavior towards successive gamma irradiation as revealed by the constancy of optical absorption spectral curves. The main conclusion reached is that the lead borate glass is a good shielding material and is even enhanced by the addition of WO_3 (1-15%). After that in 2017, A.M.A. Mostafa et al. (2017) [21] prepared WO_3 based glass system in composition $(100-x)[0.1\text{B}_2\text{O}_3-0.4\text{P}_2\text{O}_5-0.5\text{PbO}]-x\text{WO}_3$ where $x = 10, 20, 30, 40, 50$ and 60 mol% for gamma ray shielding properties. The emitted gamma ray has been detected by 3×3 inch NaI (Tl) scintillation detector. The obtained results indicate that the values of the mass attenuation coefficient, effective atomic number and electron density of the glass samples increase with the increasing of WO_3 . The values of the Poisson's ratio, half value layer and Mean free path of the investigated glasses were found to decrease with the increasing of WO_3 concentration. The mass attenuation coefficient results have been observed a perfect agreement with the XCOM values for all the glass samples. On that, they have succeeded in improving the investigated glass system to be better gamma radiation shielding materials in term of their volume needed for shield design with advantage of visible light transparent. Hence, this study could be useful in potential applications of shielding of gamma ray. Both studies suggest that increasing the concentration of WO_3 gives glass material a better gamma ray shielding potential.

Apart from calculating the elastic moduli with the information of the ultrasonic velocities and the density of the glass samples. There is still an interesting elastic moduli theory that were studied in 2019 as follow: A. A. El-Moneim (2019) [57] predicted the elastic properties and glass transition temperature under the substitution of AlF_3 by ZnO in ternary fluoro-zinc-tellurite $\text{AlF}_3\text{-ZnO-TeO}_2$ glasses. Prediction has been carried out on the basis of Makishima-Mackenzie's theory and Rocherulle et al. model. Both Makishima-Mackenzie's and Rocherulle et al. models are valid for all the studied glass systems. The agreement between the theoretical and experimental elastic moduli and Poisson's ratio is excellent for majority of the samples. The same year, A. A. El-Moneim and R. El-Mallawany (2019) [60] analyze and predicted elastic properties of

quaternary tellurite $x\text{Ag}_2\text{O}-(35-x)(0.5\text{V}_2\text{O}_5-0.5\text{MoO}_3)-65\text{TeO}_2$ and $x\text{WO}_3-(75-x)\text{B}_2\text{O}_3-10\text{MgO}-15\text{TeO}_2$ glass systems. This has been achieved on the basis of Makishima-Mackenzie's theory, Rocherulle et al. model and Abd El-Moneim and Alfifi's approaches. It has been found that, both Makishima-Mackenzie's theory and Abd El-Moneim and Alfifi's approaches can be applied successfully to predict the compositional changes in elastic moduli of $\text{WO}_3\text{-B}_2\text{O}_3\text{-MgO-TeO}_2$ glasses. In case of $\text{Ag}_2\text{O-V}_2\text{O}_5\text{-MoO}_3\text{-TeO}_2$ glasses, the best correlation between theoretical and experimental elastic moduli can be achieved if the effect of the basic structural units TeO_4 , TeO_3 , VO_4 , VO_5 , MoO_4 and MoO_6 is taken into account. In compared to Makishima-Mackenzie's theory, Rocherulle et al. model appears to be more applicable for predicting Poisson's ratio. Moreover, the compositional changes in bulk modulus are predictable from the molar volume. In this research, the researchers chose to use the analysis of elastic moduli theory with credible include Makishima-Mackenzie's theory and Abd El-Moneim and Alfifi's approaches.

CHAPTER 3

METHODOLOGY

3.1 Scientific instruments

3.1.1 Scanning electron microscopy, HITACHI brand, S-3400N model, Type II with EDAX element analyzer device, Genesis model

3.1.2 Electric furnace: temperature of 1,800 °C, built by Glass Technology Excellent Center (GTEC), Department of Physics, Faculty of Science, Ubon Ratchathani University

3.1.3 Electric oven: temperature of 1,000 °C, built by Glass Technology Excellent Center (GTEC), Department of Physics, Faculty of Science, Ubon Ratchathani University

3.1.4 Density measurement system, built by Glass Technology Excellent Center (GTEC), Department of Physics, Faculty of Science, Ubon Ratchathani University

3.1.5 Glass grinding and polishing machine built by Glass Technology Excellent Center (GTEC), Department of Physics, Faculty of Science, Ubon Ratchathani University

3.1.6 X-ray analytical microscope of energy dispersive X-ray fluorescence spectrometer, HORIBA Scientific brand, XGT-5200 WR model

3.1.7 Fourier transform infrared spectrometer (FTIR), Perkin Elmer brand, Spectrum RXI model

3.1.8 Microhardness testing machine, Mitutoyo company, Mitsubishi brand, MVK-H1 model

3.1.9 X-ray Diffractometer, Phillips PANalytical brand, X'Pert Highscore model

3.1.10 Electrical balance, Denver Instrument company with accuracy 0.0001

3.1.11 Cutting machine, Benetec limited brand, labcut 1010 model

3.1.12 Ultrasonic flaw detector, SONATEST brand, Sitescan 230 model with cable probe

3.1.13 Hydraulic press, SPECAC company

3.1.14 The detector type NaI (Tl), ORTEC brand, a division of AMETEK model

- 3.1.15 Multichannel analyzer machine, ORTEC company
- 3.1.16 Probe model: SLG4-10 for longitudinal velocity
- 3.1.17 Probe model: SA04-45 for shear velocity
- 3.1.18 Vernier caliper with accuracy 0.05 mm., Pro'skit company
- 3.1.19 Digital weight indicator and load Cell, Linear brand, Star-I model

3.2 Scientific equipment

- 3.2.1 Alumina crucible
- 3.2.2 Stainless steel molds
- 3.2.3 Silicon carbide papers
- 3.2.4 Beaker 250 ml
- 3.2.5 Ultrasonic calibration block V1 and V2
- 3.2.6 Lead sheets, Copper clads and lead containers for shielding radiation
- 3.2.7 Radioactive isotopes of type Cs-137, Co-57 and Am-241 of Department of Nuclear Engineering, Faculty of Engineering, Chulalongkorn University
- 3.2.8 lead glass (standard shielding), Kongsak X-ray Medical Industry CO., LTD. company

3.3 Chemical and materials

- 3.3.1 Barium carbonate, Ajax Finechem Pty Ltd company, Purity of 95.0 %
- 3.3.2 Dihydrogen borate, Fisher scientific company, Purity of 100.0 %
- 3.3.3 Tungsten trioxide, Fisher scientific company, Purity of 95.0 %
- 3.3.4 n-hexane, Carlo Erba company, Purity of 95.0 %
- 3.3.5 Magnaflux Ultragel II is used as a couplant for ultrasonic testing
- 3.3.6 Potassium bromide, S.P.Y. SCIENCE TECH. LDT. company, AR. Grade
- 3.3.7 Bagasse powder from Khon Kaen Sugar Industry Public Company Limited, 43 Moo 10, Nampong-Kranuan Rd., Nampong, Khon Kaen 40140, Thailand
- 3.3.8 Cassava rhizome powder from Cassava plantation, Sueang Khao, Si Rattana District, Si Sa Ket 33240, Thailand

3.4 Programs used in research

3.4.1 WinXCom computer software

3.4.2 Maestro-8099 program

3.4.3 Microsoft Excel 2016

3.5 Methods

3.5.1 Analysis of components of bagasse and cassava rhizome

Bagasse, collected from the power plant and leftover part of cassava rhizome after product processing in Northeast region of Thailand, were recycled in this research. Bagasse were calcined in an electrical furnace at 600 °C for 1 hour and cassava rhizome were calcined at 1,000 °C in the same amount of time. After that, they were grinded until it become a fine powder, named “BG powder” and “CR powder”, respectively. Then BG and CR powders were annealed for avoid some moisture using electric oven at temperature of 100 °C for 30 minutes. Energy dispersive X-ray spectroscopy or EDS analysis was used for composition analysis of these waste materials. EDS systems (EDAX element analyzer device, Genesis model) are integrated into either an SEM instrument (HITACHI Brand, S-3400N Model, Type II). EDS systems include a sensitive x-ray detector called “silicon drift detectors” and software to collect and analyze energy spectra. An EDS detector contains a crystal that absorbs the energy of incoming x-rays by ionization, yielding free electrons in the crystal that become conductive and produce an electrical charge bias. The x-ray absorption thus converts the energy of individual x-rays into electrical voltages of proportional size; the electrical pulses correspond to the characteristic x-rays of the element.

3.5.2 Glass Preparation

The glass samples were prepared in rectangular shapes from the 30 BaO - (50-x) B₂O₃ - 10 BG - 10 CR - x WO₃ glass system (BG and CR stand for bagasse and cassava rhizome, respectively and x = 0, 2, 4, 6 and 8 wt %) by the melt-quenching technique. The compositions of glass samples are shown in table 3.1. High purity grade of raw materials of BaCO₃ (for BaO), H₂BO₃ (for B₂O₃) and WO₃ were used. The prepared BG and CR powders like the same of the topic (3.5.1) were used as the composition of glass samples. Then BG and CR powders were annealed for avoid some moisture. Appropriate amounts of BaCO₃, H₂BO₃, WO₃, BG and CR powders were

weighed using an electronic balance with the accuracy of the order of 0.0001 g. Each batch of about 50 g in alumina crucible was melted in an electrical furnace at 1250 °C for 1 hour to ensure homogeneity. The melted glass was then poured into warmed stainless steel molds and annealed in electric oven around 580°C for 2 hours followed by slow cooling to room temperature in order to remove internal stress of glass sample. Finally, the glass samples were cut and then polished using different silicon carbide grades for elastic properties investigation. Measurement of glass thickness was carried out using Vernier caliper with accuracy 0.05 mm.

Table 3.1 The composition of barium-borate-bagasse-cassava rhizome-WO₃ glass system

Glass sample code	The concentration of chemical and raw materials in wt%				
	BaO	B ₂ O ₃	BG	CR	WO ₃
B1	30	50	10	10	0
B2	30	48	10	10	2
B3	30	46	10	10	4
B4	30	44	10	10	6
B5	30	42	10	10	8

3.5.3 Density and molar volume measurements

The density of glass samples (ρ) was measured based on the principle of Archimedes using n-hexane as immersion liquid and the relation (2.3) was applied. The schematic of the density measuring system of glass samples is shown in figure 3.1. The meanings of the symbols in this figure are as follows: ρ_b is the density of the n-hexane, W_a and W_b are weights of the glass sample in air and the n-hexane, respectively. In order to gain accurate values, the measurement was repeated three times. The estimated error of this measurement was about ± 0.0016 g/cm³. The formula (2.4) was chosen to calculate the molar volume (V_m) of the glass samples [38].

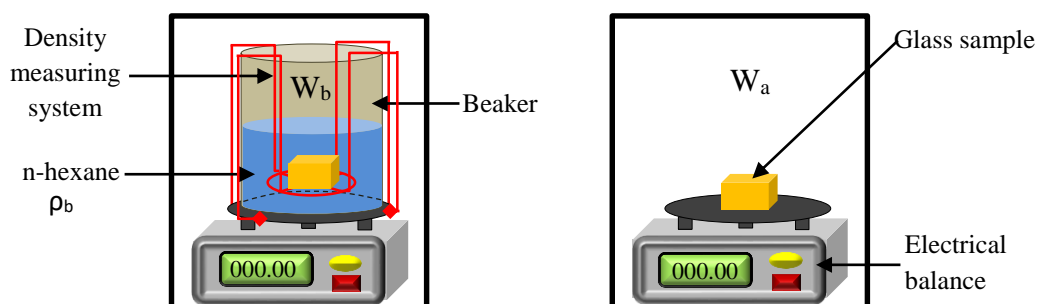


Figure 3.1 Schematic illustration of the density measuring of glass samples

3.5.4 Measuring the homogeneity of glass samples

The homogeneity of the glass sample was obtained by X-ray mapping technique using X-ray analytical microscope of energy dispersive X-ray fluorescence spectrometer or EDXRF spectrometer (HORIBA Scientific brand, XGT-5200 WR model). EDXRF spectrometer includes X-ray sources are made of rhodium (Rh), X-ray tube (voltage 50 kV, current 1.0 mA, diameter 1.2 mm) and silicon drift detector (SDD). The processing used live time 192 s. The measurement process is as follows: Place the sample in the sample holder, Load the sample holder into the XGT-5200WR, Multiple point analysis of a printed circuit board, Measurement and displaying the results, Determining compositions and collecting the results.

In EDXRF spectrometer, the X-ray tube acting as a source irradiates a sample directly, and the fluorescence coming from the sample is measured with a SDD. This detector is able to measure the different energies of the characteristic radiation coming directly from the sample. The detector can separate the radiation from the sample into the radiation from the different elements present in the sample. This separation is called energy dispersion. Elemental X-ray maps are produced by recording the number of X-ray photons of a specified energy generated from each point over a fixed counting time, while the electron beam is rastered over a rectangular area. An image is generated by converting the number of X-ray photons of specified energy detected at each point into a brightness value for a pixel on the screen or digital image. The raw data for the image is a matrix of integers corresponding to the number of X-rays counted at each point and these are mapped to a single-band image with 0-255

levels. The image can be displayed as a grayscale image or assigned false colors based on a look-up table.

3.5.5 XRD studies

X-ray diffraction (XRD) is a powerful nondestructive technique for structural characterizing of materials. X-ray diffraction peaks are produced by constructive interference of a monochromatic beam of X-rays scattered at specific angles from each set of lattice planes in a sample. The peak intensities are determined by the atomic positions within the lattice planes. Consequently, the X-ray diffraction pattern is the fingerprint of periodic atomic arrangements in a given material.

The amorphous structural study of glass samples was undertaken by X-ray diffractometer (Phillips PANalytical brand, X'Pert Highscore model) with Cu target and Ni filter. The diffractometer uses Cu K α radiations of wavelength 1.54 Å and operating at 40 kV, 15 mA in the range of 2θ from 10° to 80° with step width of 0.02° and scan speed of 4°/min at room temperature. An X-ray powder diffraction pattern is a plot of the intensity of X-rays scattered at different angles by a sample. The gas filled proportional detector used to measure the number of diffracted X-rays in this diffractometer. The detector moves in a circle around the sample. The detector position is recorded as the angle 2θ . The detector records the number of X-rays observed at each angle 2θ . The X-ray intensity is recorded as counts and the X-ray diffraction pattern was obtained. In case, XRD data did not show any crystallization peak and the XRD pattern as broad halo band, inferring the amorphous structure of the glass samples.

3.5.6 FTIR measurements

Fourier Transform-Infrared Spectroscopy (FTIR) measures the absorption of infrared radiation by the sample material versus wavelength. The infrared absorption bands identify molecular components and structures. When a material is irradiated with infrared radiation, absorbed IR radiation usually excites molecules into a higher vibrational state. The wavelength of light absorbed by a particular molecule is a function of the energy difference between the at-rest and excited vibrational states. The wavelengths that are absorbed by the sample are characteristic of its molecular structure.

The structural properties of the glass samples were investigated by FTIR spectrometer (Perkin Elmer brand, Spectrum RXI model) at room temperature.

Sample powder was mixed with potassium bromide (KBr) in 1:100 ratios so that grinded until fine mixture was obtained and that mixture was pressed using a hydraulic press. Then thin transparent pellets of approximate thickness 1 mm were obtained and these pellets were used for data analysis. The spectrum was taken in the range of 400 cm^{-1} to 2000 cm^{-1} . The FTIR spectrometer uses an interferometer to modulate the wavelength from a broadband infrared source. A detector measures the intensity of transmitted or reflected light as a function of its wavelength. The signal obtained from the detector is an interferogram, which must be analyzed with a computer using Fourier transforms to obtain a single-beam infrared spectrum. The FTIR spectra are presented as plots of intensity versus wavenumber (in cm^{-1}). Wavenumber is the reciprocal of the wavelength. The intensity can be plotted as the percentage of light transmittance or absorbance at each wavenumber.

3.5.7 Elastic properties study

3.5.7.1 Ultrasonic velocity measurements

The ultrasonic velocities were obtained by the ultrasonic contact technique with an ultrasonic flaw detector (SONATEST brand, Sitescan 230 model). Ultragel II was used as ultrasonic couplant due to that has many benefit such as highest corrosion protection, slow drying for longer inspection time, provides good transducer couplant and reduces surface noise. The 4 MHz resonant frequency of ultrasonic waves were generated from a ceramic transducer (Probe model: SLG4-10 for longitudinal velocity and SA04-45 for shear velocity), that can act as transmitter-receiver at the same time. The velocity was therefore, calculated by dividing the round trip distance by the elapsed time according to the relation (2.9). The measurements were repeated three times to check the reproducibility of the data. Each measurement uses a load cell to control the pressure to steady. The estimated errors in velocity measurements were ± 2 and $\pm 1\text{ ms}^{-1}$ for v_L and v_S , respectively.

Elastic moduli such as longitudinal modulus (L), shear modulus (G), Young' modulus (E), bulk modulus (K), Poisson's ratio (σ) and Microhardness (H) of the $30\text{BaO} - (50-x)\text{B}_2\text{O}_3 - 10\text{BG} - 10\text{CR} - x\text{WO}_3$ glass system have been determined from the measured ultrasonic velocities and density using the relations (2.10) to (2.15).

3.5.7.2 Calculation using Makishima-Mackenzie model

Theoretical elastic moduli based on Makishima-Mackenzie model obtained using the relation (2.16) to (2.22). The dissociation energy per unit volume (G_i) and packing factor (V_i) of the i^{th} component can be estimated from the equations (2.23) and (2.24), respectively. The related variables used to calculate the theoretical elastic moduli followed Makishima-Mackenzie model for the studied glasses are shown in table 3.2. The obtained results were compared with the experimental elastic moduli from ultrasonic testing in the topic (3.5.7.1).

3.5.7.3 Calculation using Abd El Moneim-Alfifi's approaches

Theoretical bulk modulus of glass samples can be predicted based on the approach of Abd El Moneim and Alfifi that according to the semi-empirical formula (2.25). The molar volume (V_m) and mean atomic volume of multi-component oxide glasses (\bar{V}) can be obtained from the equation (2.26) to (2.28). Any variables used to calculate the theoretical bulk modulus followed Abd El Moneim-Alfifi's approaches for the studied glasses are shown in table 3.3. Also, the obtained results were compared with the experimental bulk modulus from ultrasonic testing in the topic (3.5.7.1).

Table 3.2 The related variables in theoretical elastic moduli calculation using Makishima-Mackenzie model

Related variables	Chemical composition of the studied glasses				
	BaO	B ₂ O ₃	CaO (CR)	SiO ₂ (BG)	WO ₃
V_i	13.1283	21.28943	10.6591	14.2410	21.3105
G_i (kcal/cm ³)	9.70	18.60	15.50	15.40	16.20
R_A (cm)	1.35×10^{-8}	4.7×10^{-9}	1.14×10^{-8}	5.40×10^{-9}	6.00×10^{-9}
R_O (cm)	1.40×10^{-8}	1.40×10^{-8}	1.40×10^{-8}	1.40×10^{-8}	1.40×10^{-8}
M_i (g/mol)	153.33	69.62	56.08	60.08	231.84

Table 3.3 The related variables in theoretical bulk modulus calculation using Abd El Moneim-Alfifi's approaches

Glass sample code	Related variables				
	ψ	γ	Q	V_t	V_m (cm ³ /mol)
B1	3.60	1.6042	3725	0.5314	36.1076
B2	3.58	1.6042	3725	0.5199	36.7667
B3	3.56	1.6042	3725	0.5116	37.2367
B4	3.54	1.6042	3725	0.5025	37.7882
B5	3.52	1.6042	3725	0.4922	38.4626

3.5.8 Microhardness testing

Microhardness values of glass samples and lead glass were tested using a microhardness testing machine (Mitsubishi brand, MVK-H1 model). The microhardness testing machine consists of a Vicker indenter made of a pyramid-shaped diamond that can be controlled to a load of 10 - 1000 gf. To perform the Vickers test, the glass sample is placed on a test stage. The indenter is pressed into the sample by an accurately controlled test force of 100 gf and maintained for 10 s. After the dwell time is complete, the indenter is removed leaving an indent in the sample that appears square shaped on the surface. The size of the indent is determined optically by measuring the two diagonals of the square indent. The Vickers hardness number (HV) is a function of the test force (F) divided by the surface area of the indent as the relation (3.1). The average of the two diagonals (d) (3.2) is used in the formula (3.1) to calculate the Vickers hardness. The operation of applying and removing the load is controlled automatically.

$$HV = 0.102 \times \frac{2 \times F \times \sin \frac{136^\circ}{2}}{d^2} = 0.1891 \times \frac{F}{d^2} \quad (3.1)$$

$$d = \frac{d_1 + d_2}{2} \quad (3.2)$$

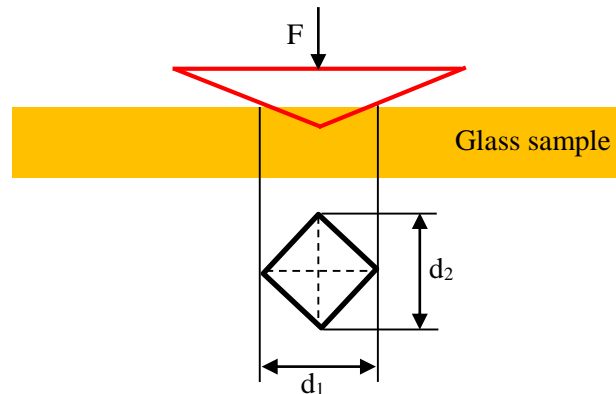


Figure 3.2 Schematic illustration of the microhardness testing of glass samples

3.5.9 Gamma ray shielding parameters

3.5.9.1 Broad beam transmission experiment

The radiation shielding parameters of the glass samples were measured at three photon energies comprising of 662 keV gamma photons emitted from Cs-137 point source, 122 keV emitted from Co-57 point source, and 60 keV emitted from Am-241 point source under appropriate geometrical conditions using a NaI (TI) scintillation detector (ORTEC brand, a division of AMETEK model).

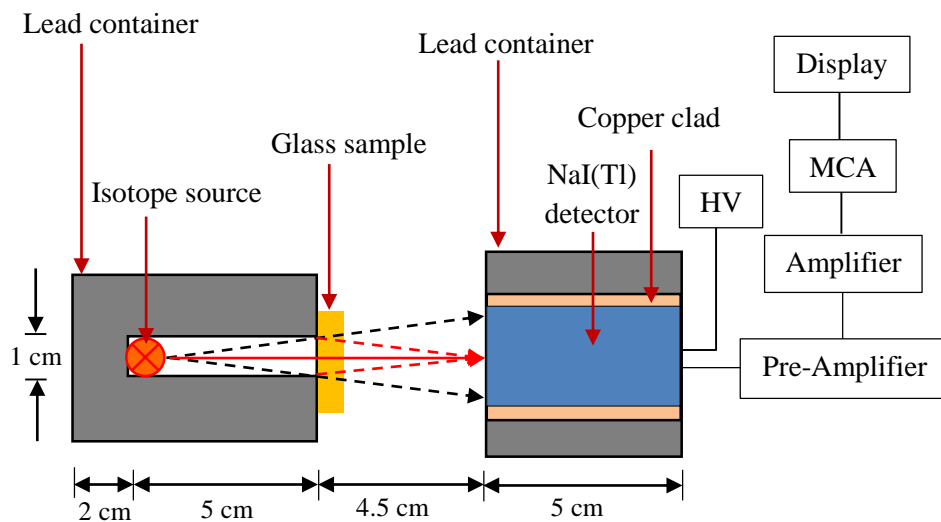


Figure 3.3 Broad beam transmission geometry

The experimental setup of broad beam transmission geometry is shown in figure 3.3. The initial photon (I_0) and the transmitted photon intensities (I) were processed with the Maestro-8099 program. The Beer-Lambert law can illustrate the attenuation of gamma radiations for glass samples as given by equation (2.31). The Half Value Layer (HVL) and mean free path (MFP) can be estimated from the relation (2.34) and (2.36), respectively.

3.5.9.2 Calculation by using WinXCom program

WinXCom computer program can be used as an authentic tool to evaluate the gamma ray shielding parameters. It has been verified that WinXCom program gives the results agree with experimental results. In this work, it is speculated that it is possible to obtain authentic data of mass attenuation coefficients (μ_m) of studied glass samples, barite concrete and ferrite concrete using WinXCom program in the wide energy range. The weight fraction data of each condition were entered in the program, the chemical composition of concretes are shown in table 3.4. We obtain the μ_m of the studied glass samples and different concretes by the mixture rule as given by the relation (2.37). The data of μ_m were exported to Microsoft Excel template. We chose the μ_m data of studied energies such as 60, 122 and 662 keV for linear attenuation coefficient calculation. Then, half value layer (HVL) and mean free path (MFP) parameters are evaluated from mass attenuation coefficients as followed equations (2.34) and (2.36), respectively. The all calculated values were compared with the experimental results in topic (3.5.9.1).

Table 3.4 Chemical composition and density of concretes [115]

Weight fraction elements	Concretes	
	Barite	Ferrite
H	0.0083	0.0280
B	0.0115	-
C	-	-
O	0.3475	0.4554
Na	-	-
K	-	-
Mg	0.0022	0.0019
Al	0.0044	0.0038
Si	0.0148	0.0128
S	0.0997	0.0007
Ca	0.0834	0.0595
Fe	0.0047	0.4378
Ba	0.4237	-
Density (g/cm ³)	3.5000	4.5000

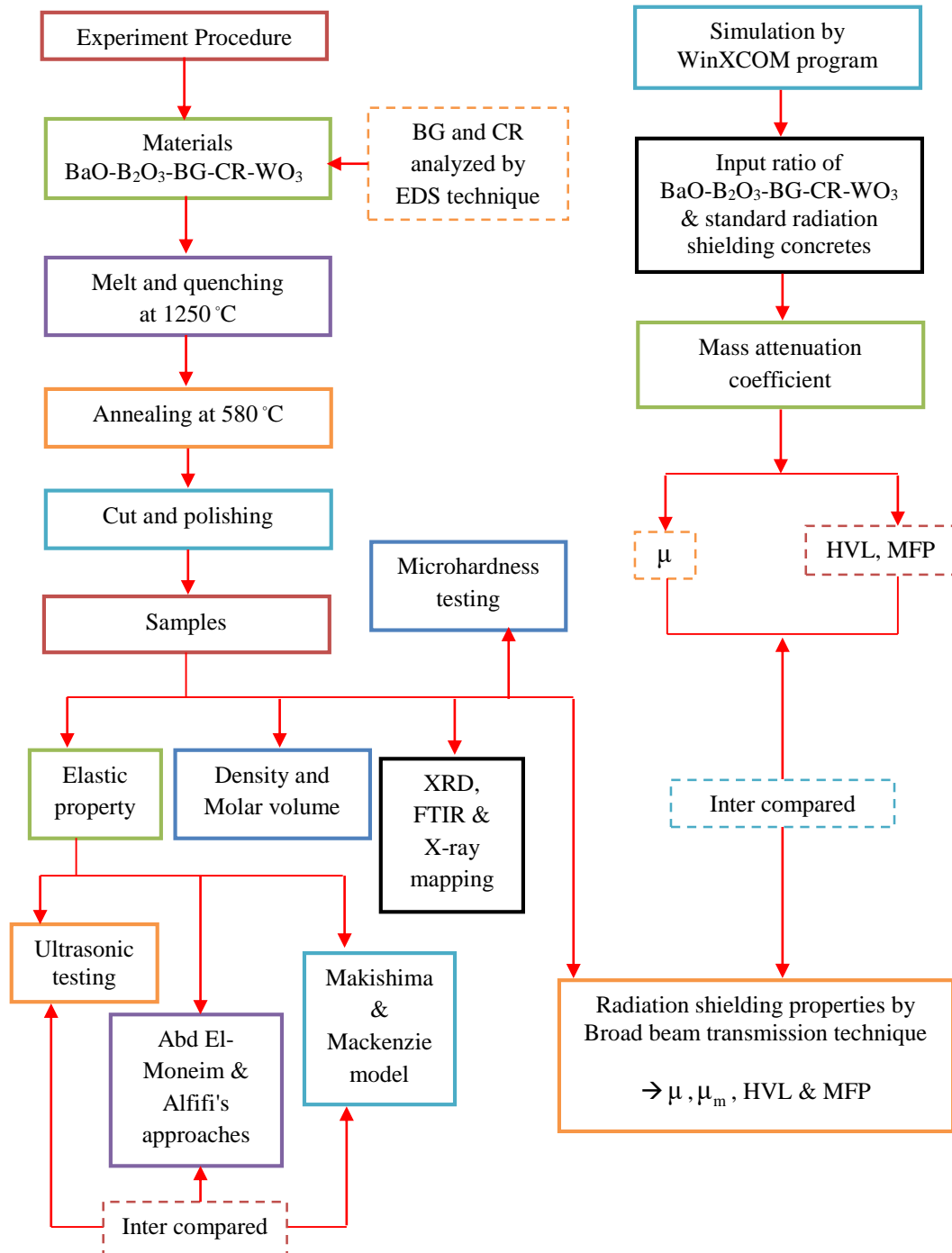


Figure 3.4 Research process diagram

CHAPTER 4

RESULTS AND DISCUSSION

4.1 The components of bagasse and cassava rhizome

The collected data from EDS technique are shown in table 4.1. It is found that the main composition of bagasse and cassava rhizome is Si and Ca, respectively. The prominent element of Bagasse is Si with 24.31 wt% and a little appear of Fe and Al with 4.20 and 3.11 wt%, respectively. While cassava rhizomes contain Ca, Si, K and Mg of 9.17, 8.67, 8.55 and 6.76 wt%, respectively. Si has a role of network former; it can form the interconnected backbone glass network. Ca, K and Mg have a potential as network modifier of glass structure. These network modifiers are ions to alter the glass network, they were compensated by non-bridging oxygen (NBO) in oxide glasses and usually reduce glass network connectivity. Therefore, Ca, K and Mg can be decreasing the softening point of glass from 1600 °C to 730 °C on average. Al is intermediates or conditional glass formers, do not form glasses by themselves, but act like glass formers when combined with others. Other composition like Fe has properties to reduce the melting point, makes the glass clear and also make glass has a green-yellow tone. From these information, bagasse and cassava rhizomes have potential as composition for glass production [33,85-87].

4.2 The physical properties of glass samples

4.2.1 Observable external characteristics

The color that can be observed from the glass samples appears as a yellow tone and transparent as shown in figure 4.1. The glass samples are more dark yellow with the increasing of WO_3 concentration from 0 - 8 wt%. These situations are the result of the properties of the change chemical compositions in this glass system. In general, pure borosilicate glass is colorless, and the metal impurities in the glass impart color. Color is formed when the electrons in the outer orbit of an atom interact with visible light, absorb or reflect certain spectrum which eye perceives as a color. Each person will have a different perception of the color based on his genetics [88]. Fe_2O_3 has

properties to makes the glass clear and has a green - yellow tone as well as K_2O . Especially, at elevated temperatures the color of the WO_3 changes from pale lemon-yellow to dark yellow and finally deep orange [89,90]. Other composition of this glass such as SiO_2 , CaO , BaO , MgO , and Al_2O_3 are colorless, so the color of WO_3 has a most of directly influence on the glass sample.

Table 4.1 EDS analysis results of dry bagasse and cassava rhizome

Composition elements	Concentration of composition elements (wt%)	
	bagasse	cassava rhizome
O	59.00	60.82
Na	0.18	-
Mg	0.84	6.76
Al	3.11	0.87
Si	24.31	8.67
P	0.29	2.45
S	0.14	1.01
Cl	-	0.73
K	2.85	8.55
Ca	3.29	9.17
Ti	0.24	0.13
Mn	0.17	0.21
Fe	4.20	0.47
Cu	0.75	0.07
Zn	0.63	0.08

4.2.2 Density and molar volume

The trend of density and molar volume changes followed WO_3 concentration are presented in figure 4.2. When WO_3 content was added into the studied glass system, the density of the glass samples increased because of the substitution of higher molecular weight of WO_3 ($M_w = 231.84$ g/mol) for lower molecular weight of B_2O_3 ($M_w = 69.617$ g/mol) and SiO_2 ($M_w = 60.08$ g/mol) [91], which are the major network

former in the structures of the studied glass. For this reason, the density of the glass increased further when adding to the concentration of WO_3 . The molar volume is defined as the volume occupied by the unit mass of the glass, Molar volume can be used as a parameter to identify an open structure [43]. From figure 4.2, the molar volume of glass samples with WO_3 from 0 to 8 wt% is also observed due to this concentration range, the glass structures may have the vacancy sites that allow the atoms to be inserted. The increase trend of molar volume with the increasing of WO_3 concentration, because of the vacancy site is fulfilled and the greater size of the ionic radii of the tungsten ion ($\text{W}^{6+} = 60 \text{ pm}$) than that of the boron ion ($\text{B}^{3+} = 23 \text{ pm}$) and silicon ion ($\text{Si}^{4+} = 26 \text{ pm}$) [92]. In addition, the formation of non-bridging oxygen may be related to the enlargement of the glass structure causing an increase in the molar volume of glass samples.

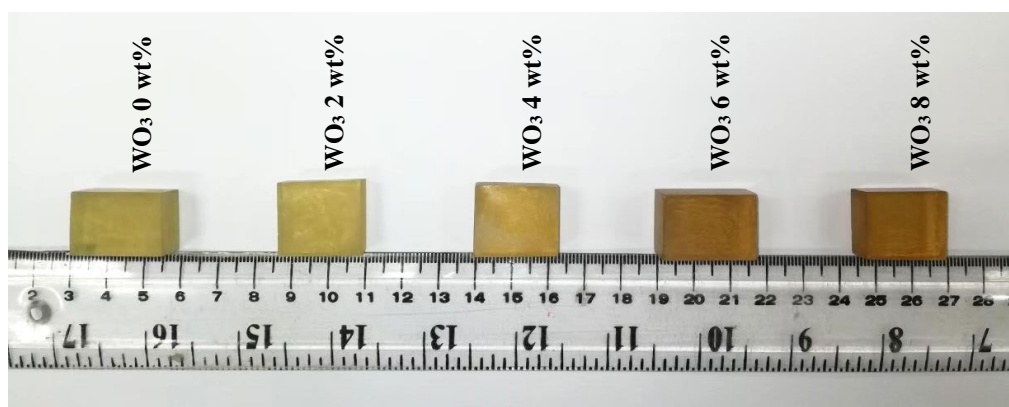


Figure 4.1 Physical characteristics of barium-borate-bagasse-cassava rhizome- WO_3 glass system

4.3 The homogeneity of glass samples

In order to verify the homogeneity of glass samples, we carried out a detailed study on elements distribution and chemical compositions by EDXRF. As shown by X-ray mapping results in figure 4.3, It is evident that the glass sample surface is covered by different elements of various dot densities, pointing to the homogeneous distribution of chemical compositions within the composite glasses. The dot density in X-ray maps is affected by concentration and atomic number of the elements [93]. Based on the chemical composition analysis, the concentration of Ca and Si ions is lower than that

of other elements (Ba, B and W). Furthermore, with respect to the Ca and Si ions have lower atomic numbers. That is why the Ca and Si ions present lower dot density as compared to other elements [94]. Moreover, it was also observed that the dot density increases with increasing of WO_3 concentration. The reasons for not showing the result of boron composition due to the range of detectable elements varies according to instrument configuration and set up, EDXRF covers all elements from sodium (Na) to uranium (U). Limits of detection depend upon the specific element and the sample matrix, but as a general rule, heavier elements will have better detection limits. However, the steadily distribution of the dot densities can be confirming the homogeneous of chemical compositions in all glass samples.

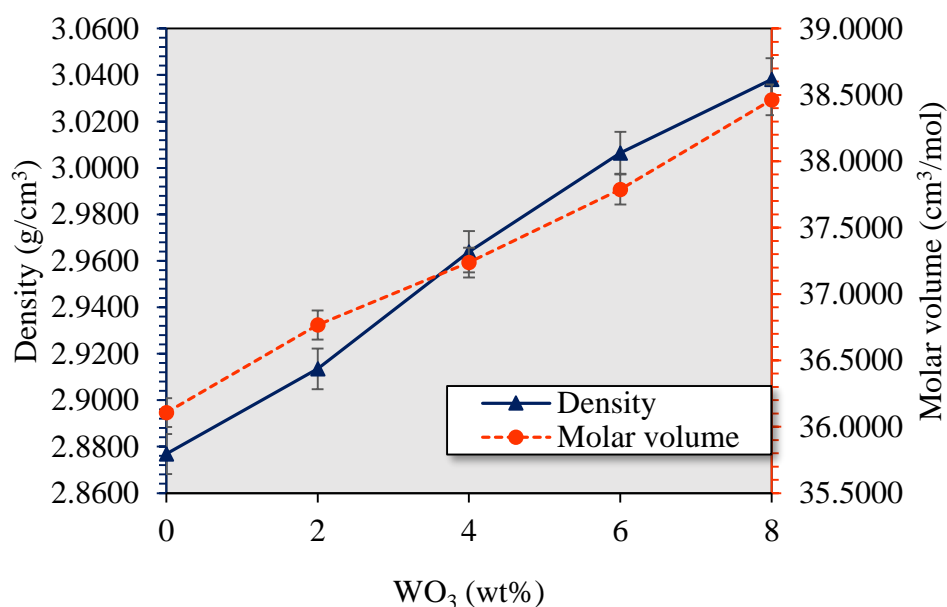


Figure 4.2 Variation of density and molar volume of barium-borate-bagasse-cassava rhizome- WO_3 glass system

4.4 The structural properties of glass samples

4.4.1 XRD studies

An X-ray diffraction pattern of the glass samples with different of WO_3 (0, 2, 4, 6 and 8 wt%) was demonstrated in figure 4.4. It is clear that the spectrum confirmed the amorphous nature of all the glass samples, there is no sharp crystalline peak only a broad halo around $20\text{-}35^\circ$. An amorphous is a solid that lacks the long-

range order, it is characteristic of non-crystalline solid. Glass is an amorphous solid that exhibits a glass transition; transition from supercooled liquid to amorphous solid (glass) [95].

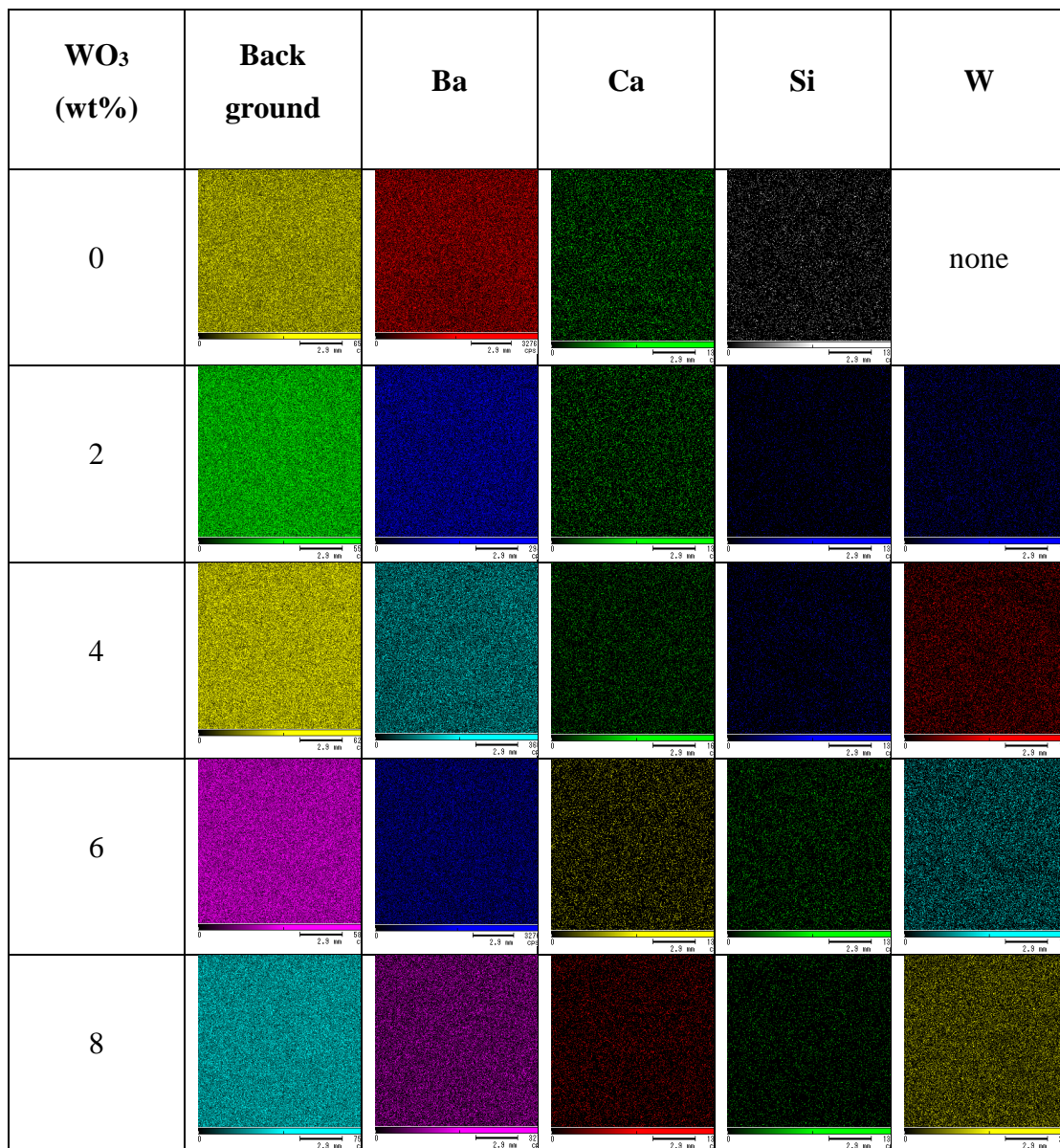


Figure 4.3 X-ray mapping images of barium-borate-bagasse-cassava rhizome-WO₃ glass system

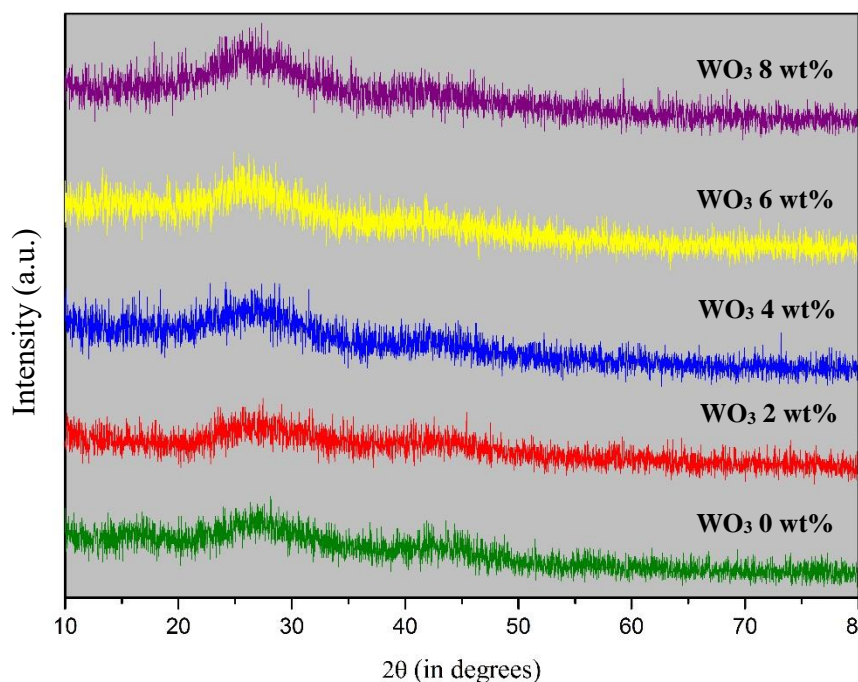


Figure 4.4 XRD patterns of barium-borate-bagasse-cassava rhizome- WO_3 glass system

4.4.2 FTIR studies

FTIR spectroscopy is an important tool for understanding the structure and dynamics of amorphous materials. It is also used to assign the observed absorption peaks to the proper vibration of the atoms in geometric grouping. The spectra of many solids variables can affect the absorption peaks, and the assignment of vibration peaks of the atoms is very difficult. Usually, the method of repeated occurrence is followed in analyzing the IR spectrum of solid materials [96,97]. Interaction of IR radiation with a normal mode of vibration only occurs when the electric field of radiation oscillates with same frequency as instant dipoles caused by atomic vibrations. A normal vibration is therefore, IR active only if a change in the dipole moment of the vibration occurs and is a one photon process, as only photon is absorbed [98]. The spectrum of a sample is compared with the spectrum of a large number of compounds containing a common atom group or groups. Certain absorption peaks are common to certain groups and are assigned the vibration characteristics of these atom groups. Borate glasses have been the subject of numerous infrared studies because of their structural peculiarities [99].

Table 4.2 Structural units and observed peaks in different wave numbers

Wave number (cm^{-1})	Structural units	Reference
431-447	Si-O-Si and O-Si-O bending modes of bridging oxygen (Q_4) overlapped with B-O-B linkages	[100]
549-561	In-plane bending of boron-oxygen triangles	[101]
690-700	Bending vibrations of B-O-B linkages of BO_3 Si-O-Si and O-Si-O symmetrical stretching of BOs between tetrahedral	[101,102] [100]
983-1006	BO bond stretching of BO_4 units	[101,103]
1211-1230	BO stretching vibrations of $(\text{BO}_3)_3$ -units in meta, orthoborate chains	[101,102]
1351-1359	Vibration of boron oxygen rings	[102,103]
1618-1646	Due to OH bending mode of vibration	[104]

FTIR transmittance spectrum of the glass samples are shown in figure 4.5. The spectral features of this glass system summarized in table 4.2. FTIR spectra of prepared glass samples give clear different absorption band can be classified into three main IR regions. Region-I is observed around 700 cm^{-1} because of the bending of B-O-B linkage in the borate networks. The region I contains the strong band occurred in the range $690\text{-}700 \text{ cm}^{-1}$ found due to the symmetrical stretching vibrations of the Si-O-Si and O-Si-O bonds of tetrahedral BOs structural units. The characteristic absorption band (806 cm^{-1}) of the boroxol ring in borate matrix is absent in the present FTIR spectra indicate that the formation of boroxol rings do not occur in the glass system under study [96]. The total alkali oxide content in these glasses is 50 wt%, which converts $[\text{BO}_3]$ into $[\text{BO}_4]$ units without formation of non-bridging oxygen ions in the borate matrix. It is worth noting that the characteristic vibration of $431\text{-}447 \text{ cm}^{-1}$ band observed in initial borate glass samples and nearly disappeared as WO_3 concentration increases indicating the formation of $[\text{BO}_4]$ units that reveals the role of tungsten oxide as network modifier. Similarly, $549\text{-}561 \text{ cm}^{-1}$ the stretching vibration of tetrahedral

[BO₄] units was not observed, but in-plane bending of boron-oxygen triangles occurred. This situation may refer WO₃ concentration increases can the conversion of borate triangles into [BO₄] units only partially and also WO₃ adding may cause the formation of non-bridging oxygen increased.

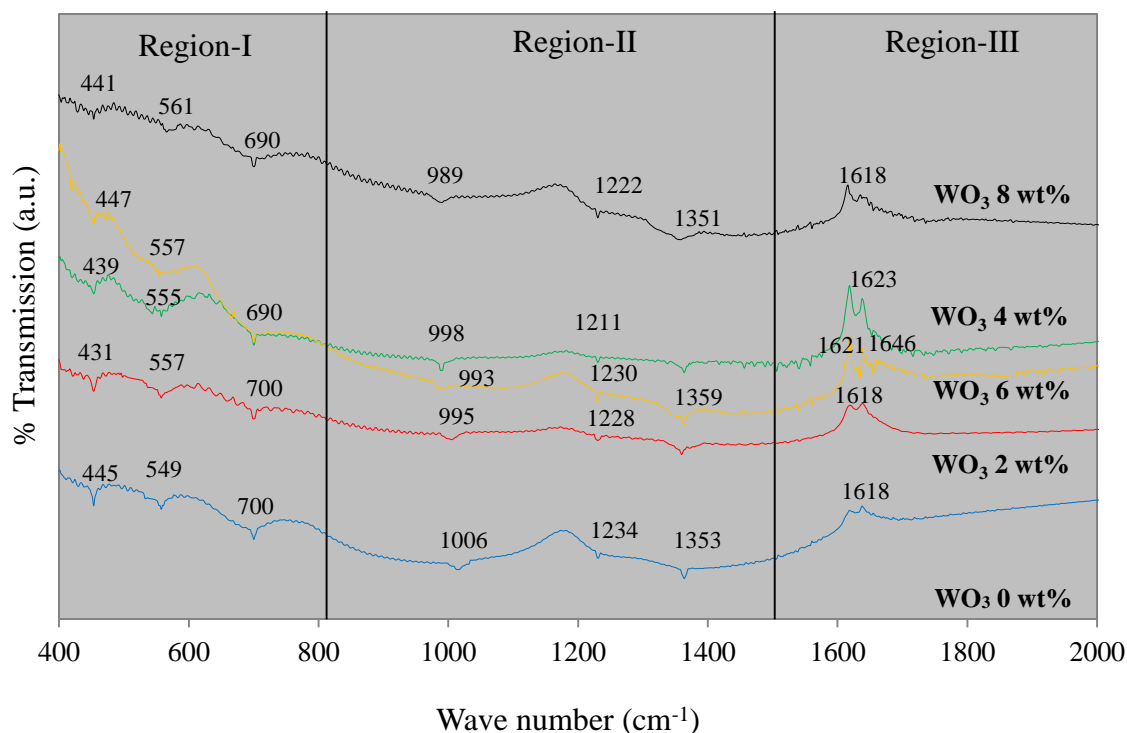


Figure 4.5 FTIR spectra of barium-borate-bagasse-cassava rhizome-WO₃ glass System

Region-II includes the absorption band in between 989 and 1359 cm⁻¹ obtained due to the B-O bond stretching vibration of the tetrahedral BO₄ structural units. The absorption bands at wave numbers about 983 to 1006 cm⁻¹ are appertaining to BO bond stretching of BO₄ units. The deeper absorption peak than others at wave number about 998 cm⁻¹ on green spectrum line are related to the glass sample with WO₃ 4 wt%. These may effect to more number of bridging oxygen which corresponds to an increasing of ν_L . The addition of 6 wt% WO₃ has effect on borate network. The absorption bands around 1230 cm⁻¹ are attributed to BO stretching vibrations of (BO₃)₃-units in meta, orthoborate chains. Therefore, W⁶⁺ ions deed as a network participator in the bank of [BO₃] units. Absorption band around 1359 cm⁻¹ found from glass sample

with 6 wt% of WO_3 is due to the vibration of boron oxygen rings, pointed to more number of bridging oxygen which corresponds to an increment of v_s . In addition, the absorption bands around 1600 cm^{-1} are attributed to hydroxyl or water groups as appear in region-III.

4.5 The elastic properties of glass samples

4.5.1 ultrasonic velocities

It was found that the ultrasonic velocities of the prepared glass samples varied with WO_3 concentration, as shown in figure 4.6. This means the WO_3 concentration in the studied glasses has an influence on the glass network. Both v_L and v_s of the glass samples tend to decrease. However, an increase of v_L at 4 wt% of WO_3 is noticeable, possibly due to the behavior of BO bond in this glass network. Also, the unexpected increase of v_s at 6 wt% of WO_3 is described in the FTIR discussion section. The influence of WO_3 adding on glass structure is consistent with the research of G. P. Singh et al. [105]. The increase in the ultrasonic velocities can be attributed to the increase in the rigidity of the glass. This is due to the presence of the metal ions, W^{6+} ions which are involved in the glass network as network modifiers by breaking up bonds and fill the interstitial position within the glass network. Besides, the increase in ultrasonic velocities can be due to the introduction of coordination defects known as dangling bonds. During this process, some of the network bonds B-O-B can be broken and replaced by ionic bonds between metal ions and singly bonded oxygen atoms. It is suggested that the presence of metal ions leads to modification of the structure of the glass resulting in an increase in the linkages of the glass samples [106]. However, the decrease observed in both the ultrasonic velocities might be due to the addition of WO_3 with longer W-O bond length (1.70 to 1.75 Å) [107] at the expense of B_2O_3 with shorter B-O bond length (1.28 to 1.43 Å) [108]. This result of increase in bond length as causes a decrease in the obtained ultrasonic velocities. In general, the decrease in ultrasonic velocities is related to the increase in the number of non-bridging oxygen and consequently the decrease in the connectivity of the glass network. Here, W^{6+} ion may effect to the main bonds of the network cause to the new bonds with different average bond length and energy. The decrease in ultrasonic velocities of the glasses reveals that

the addition of WO_3 content to the glass network impedes the movement for ultrasonic wave inside the glass network [109].

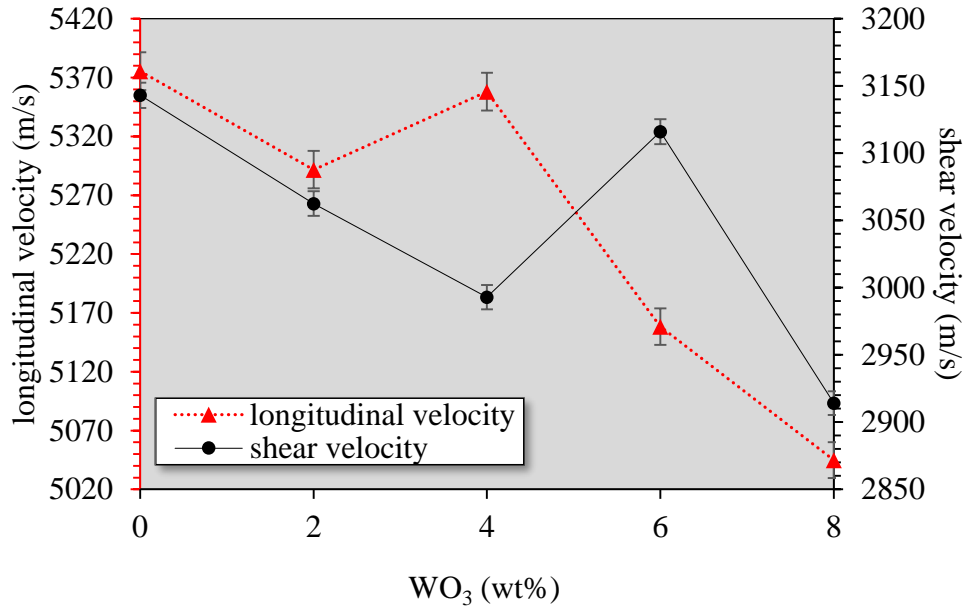


Figure 4.6 Variation of longitudinal and shear ultrasonic velocities of barium-borate-bagasse-cassava rhizome- WO_3 glass system

4.5.2 elastic moduli calculated from ultrasonic velocities

The elastic moduli (L, G, K, and E) of the prepared glass samples are shown in table 4.3. The addition of WO_3 content (0-8 wt%) to the glass system caused the longitudinal moduli to decrease from 83.1292 to 77.3222 GPa, the shear moduli decreases from 28.4213 to 25.8011 GPa, the bulk moduli decrease from 45.2092 to 38.7523 GPa and the Young's moduli decreases from 73.0170 to 68.6532 GPa.

The elastic moduli of the glass samples have a tendency to decrease with more adding WO_3 content. This can be explained by a decrease of the rigidity and strength of the glass samples when adding WO_3 [110]. The trends of elastic moduli are corresponding to the variation of ultrasonic velocity with WO_3 content. The values of L and K agree with v_L where the highest value is observed at 4 wt% of WO_3 . The values of G and E agree with v_s , where the highest value is observed at 6 wt% of WO_3 . The distinct increase of velocities for both concentrations shows that the insertion of tungsten ion to the network structure causes the alteration of coordination and formation

of bridging oxygen, which can be observed from the FTIR data [111]. The increasing of WO_3 at 4 and 6 wt% in the glass network is attributed to the formation of non-bridging oxygen to bridging oxygen. In this study, the structural unit of BO_3 are transformed to BO_4 [100]. The decline trend of glass elastic moduli between 0 to 8 wt% content of WO_3 as resulted from the number of non-bridging oxygen groups increases with more open structure. This suggests that WO_3 acts as network modifier, it can break glass network to discontinuity form as resulted the decrease in the rigidity of network structure [110]. The non-bridging oxygen will loosen the structure of glass network hence will reduce the ultrasonic velocities. The clear values of longitudinal, shear, bulk and Young's moduli, it is indicating effect in volume of compression, expansion and resistance to deformation [54,112]. The application of studied glasses could choose the glass samples according to the purpose of use by taking into account the resistance to the force acting differently.

Table 4.3 Elastic moduli and Poisson's ratio of barium-borate-bagasse-cassava rhizome- WO_3 glass system from ultrasonic testing

WO_3 (wt%)	$L \pm 0.0034$ (GPa)	$G \pm 0.0025$ (GPa)	$K \pm 0.0042$ (GPa)	$E \pm 0.0051$ (GPa)	σ ± 0.002
0	83.1292	28.4213	45.2092	73.0170	0.240
2	81.5861	27.3270	43.8770	71.8560	0.248
4	85.0874	26.5502	47.3460	69.3672	0.273
6	79.9981	29.1932	40.7181	74.8894	0.215
8	77.3222	25.8011	38.7523	68.6532	0.249

According to Rajendaan et al. [113] the changes in the cross-link density will affect the Poisson's ratio and whereby a Poisson's ratio of between 0.1 and 0.2 indicates a high cross-link density in the glass network structure. On the other hand, 0.3-0.5 shows the structure has low cross-link density. The value of Poisson's ratio obtained in this network shows an increasing and decreasing trend with a narrow change from 0.215 to 0.273 against the wt% of WO_3 . It can be concluded that the studied glasses have high cross-link density. Therefore, a higher Poisson's ratio may come about the changes of bonds from covalent bond to ionic bond. However, at 6 wt% of

WO₃ the Poisson's ratio value seems to decrease. According to Higazy and Bridge [114] the decrease in Poisson's ratio is attributed to the increase in the crosslink density of the glass system while Rajendran [113] also revealed that decrease in Poisson's ratio is attributed to the increase in network linkage.

Table 4.4 Elastic moduli and Poisson's ratio of barium-borate-bagasse-cassava rhizome-WO₃ glass system from Makishima-Mackenzie model

WO ₃ (wt%)	V _t	G _t	L _M (GPa)	G _M (GPa)	K _M (GPa)	E _M (GPa)	σ _M
0	0.5312	15.300	53.502	29.324	43.210	67.974	0.238
2	0.5191	15.252	52.072	28.745	41.236	66.299	0.232
4	0.5110	15.204	51.001	28.301	39.797	65.029	0.228
6	0.5021	15.156	49.863	27.829	38.270	63.670	0.223
8	0.4924	15.108	48.612	27.310	36.597	62.163	0.217

4.5.3 Elastic moduli calculated from Makishima-Mackenzie model

According to Makishima-Mackenzie's theory [53,54], the packing density and dissociation energy per unit volume are the key factors affecting the elastic properties of glasses. This is due to the fact that, changes in the packing density and/or dissociation energy per unit volume reflect the structural changes that can take place in the glass network. The gradual decrease in the packing density and/or dissociation energy per unit volume contributes to a weakening in the glass structure, which consequently decreases the elastic moduli and Poisson's ratio. The calculated values of packing density, dissociation energy per unit volume, theoretical elastic moduli and Poisson's ratio on the basis of Makishima-Mackenzie model for barium-borate-bagasse-cassava rhizome-WO₃ glass system, are listed in table 4.4. As expected, all the calculated compositional parameters and elastic properties depend strongly on composition of the glass.

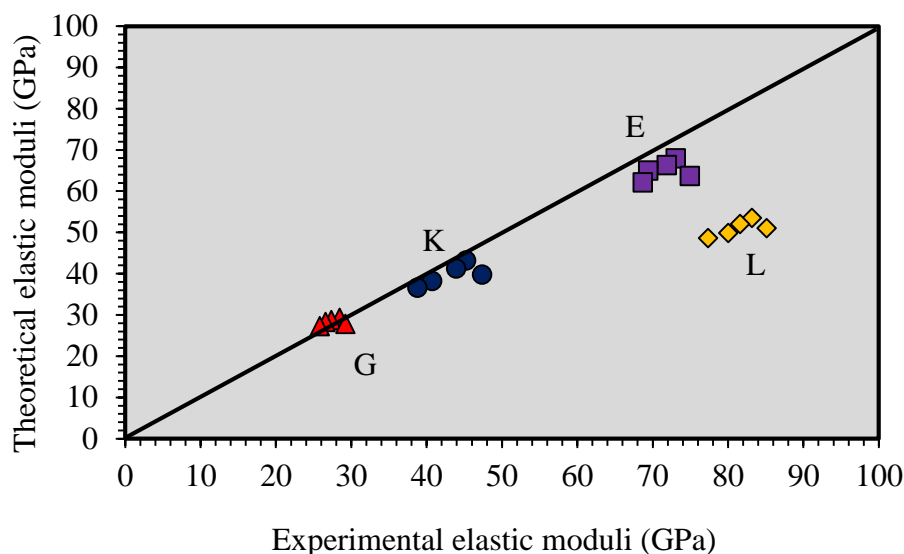


Figure 4.7 The comparative of theoretical and experimental elastic moduli in barium-borate-bagasse-cassava rhizome- WO_3 glass system on the basis of Makishima-Mackenzie's theory. The solid line is the 1:1 correlation line.

Figure 4.7 illustrates the relationship between the theoretical and experimental elastic moduli of the prepared glass systems. The straight line in this figure is the line of 1:1 correlation. The figure shows clearly that the glass systems under investigation, the comparative between theoretical and experimental values of elastic moduli (G, E and K) is excellent. Majority of the glass samples have experimental values of elastic moduli much greater than the corresponding theoretical values. For longitudinal modulus, the agreement is unsatisfactory as shown in figure 4.7. The divergence between the theoretical and experimental values has been attributed to the anomalous behavior between the experimental elastic moduli and calculated dissociation energy per unit volume of the glass. The variation of the experimental longitudinal modulus related to creating and breaking bonds in glass structures, these can be described by the results of longitudinal ultrasonic velocity and FTIR spectra. The theoretical longitudinal modulus related to the changes in the packing density and/or dissociation energy per unit volume reflects the atom packing changes that refer to the rigidity of the glass network. The basis of the theoretical longitudinal modulus that calculated from the theoretical shear and bulk moduli while the experimental

longitudinal modulus calculated from density and longitudinal ultrasonic velocity only, these may be the reason that the theoretical and experimental values are different [111].

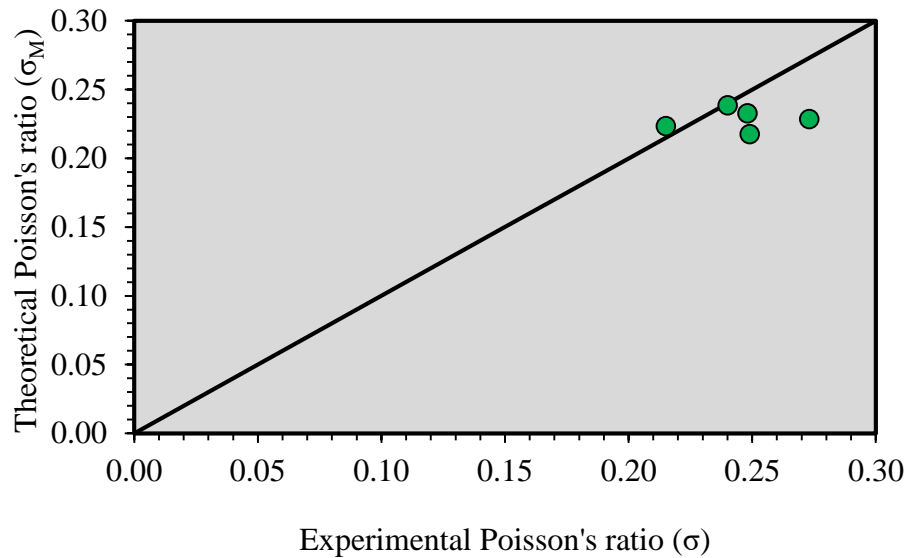


Figure 4.8 The comparative of theoretical (σ_M) and experimental Poisson's ratios (σ) in barium-borate-bagasse-cassava rhizome- WO_3 glass system on the basis of Makishima-Mackenzie's theory. The solid line is the 1:1 correlation line

Figure 4.8 shows the relation between theoretical and experimental Poisson's ratio of glass samples. One interesting observation in this figure is that, although the agreement between theoretical and experimental values of Poisson's ratio is satisfactory for most of the studied glasses, it is unsatisfactory for some glass samples such as B3 (WO_3 4 wt%) and B5 (WO_3 6 wt%). The reason that the both glass samples are different due to the addition of 4 wt% WO_3 cause to WO_3 bonds overlapping with BO bond and the changes of bonds from covalent bond to ionic bond (describe in topic 4.4.2). The FTIR spectra indicate that the W^{6+} ions deend as a network participator in the bank of $[\text{BO}_3]$ units. The vibration of boron oxygen rings of the glass sample with 6 wt% WO_3 pointed to more number of bridging oxygen, that related to the increase in the crosslink density of the glass system. These results reveal that the experimental longitudinal modulus and Poisson's ratio of studied glasses is not predictable from the

data of packing density and/or dissociation energy per unit volume, which have been calculated from Makishima-Mackenzie model.

4.5.4 Bulk modulus calculated from Abd El-Moneim and Alfifi's approaches

The semi-empirical formula (2.25) suggested that, a plot of K versus (V_t/V) ratio would give a forward proportionality. The data of K versus (V_t/V) have been presented in figure 4.9. The power regression performed K and V_t/V yields the semi-empirical (2.25) equation for this glass system;

$$K = 3725.3(V_t/V)^{1.6042} \quad (4.1)$$

with correlation coefficient of 0.575, $Q = 3725.3$ and $\gamma = 1.6042$. Although some data of K versus (V_t/V) ratio would give a forward proportionality, but some the data of the ratio (V_t/V) are quite dispersed and do not shows a clear correlation with K . It can be clearly observed that glass sample with 4 wt% WO_3 is dispersed from others. The experimental bulk modulus of this glass sample is higher than another samples. This is due to W^{6+} have some role in glass network (see topic 4.4.2). This behavior is against the semi-empirical formula (2.25) and suggests that the bulk modulus of these glasses are not predictable from the ratio (V_t/V) . Even though, the bulk modulus on the basis of Abd El-Moneim and Alfifi's approaches (table 4.5) shows a decreasing trend similar to the Makishima-Mackenzie model, the obtained values are not nearly similar. In addition, the agreement of both theoretical and experimental bulk moduli is unsatisfactory as shown in figure 4.10. The solid line is 1:1 correlation line between theoretical and experimental bulk moduli. The divergence between the theoretical and experimental values has been attributed to the anomalous behavior of the experimental elastic moduli, W^{6+} has effect to the change of some bond in glass network. These related to the ability of glass samples to withstand changes in volume when under compression on all sides. Moreover, the basic theory for theoretical bulk modulus calculation from mean atomic volume and packing density of the glass [58-60], may also cause the different of both theoretical and experimental bulk moduli.

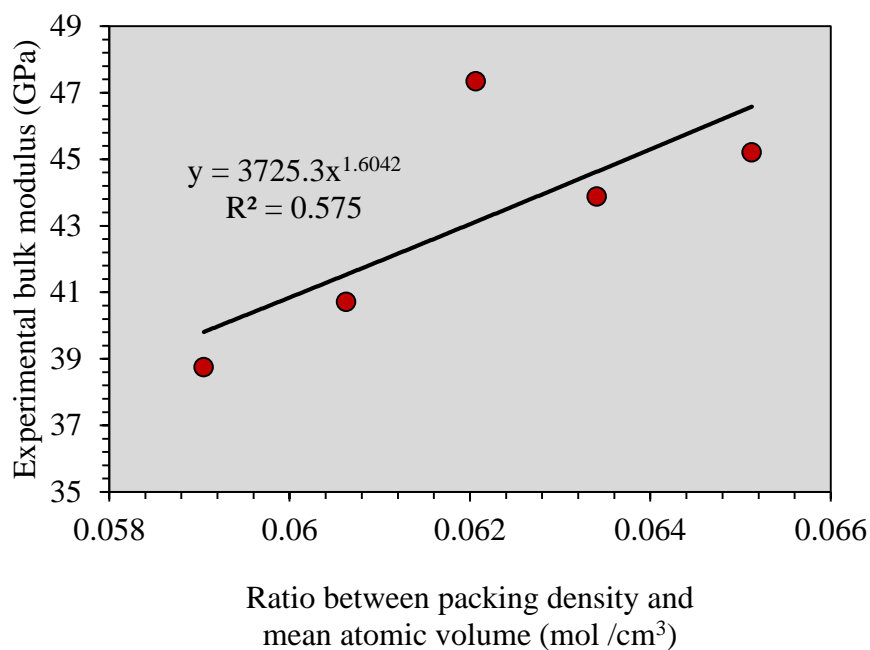


Figure 4.9 Variation of bulk modulus with the ratio between packing density and mean atomic volume in barium-borate-bagasse-cassava rhizome-WO₃ glass system. The solid line represents the least-square fitting of the data

Table 4.5 Bulk modulus of barium-borate-bagasse-cassava rhizome-WO₃ glass system from Abd El-Moneim and Alfifi's approaches

WO ₃ (wt%)	V _t	\bar{V} (cm ³ /mol)	Density ±0.0016 (g/cm ³)	V _m ±0.0016 (cm ³ /mol)	K _{Abd} (GPa)
0	0.5312	10.0291	2.8762	36.1071	33.4513
2	0.5191	10.2702	2.9133	36.7662	31.0984
4	0.5110	10.4592	2.9630	37.2363	29.4233
6	0.5021	10.6743	3.0062	37.7884	27.6692
8	0.4924	10.9262	3.0384	38.4622	25.7782

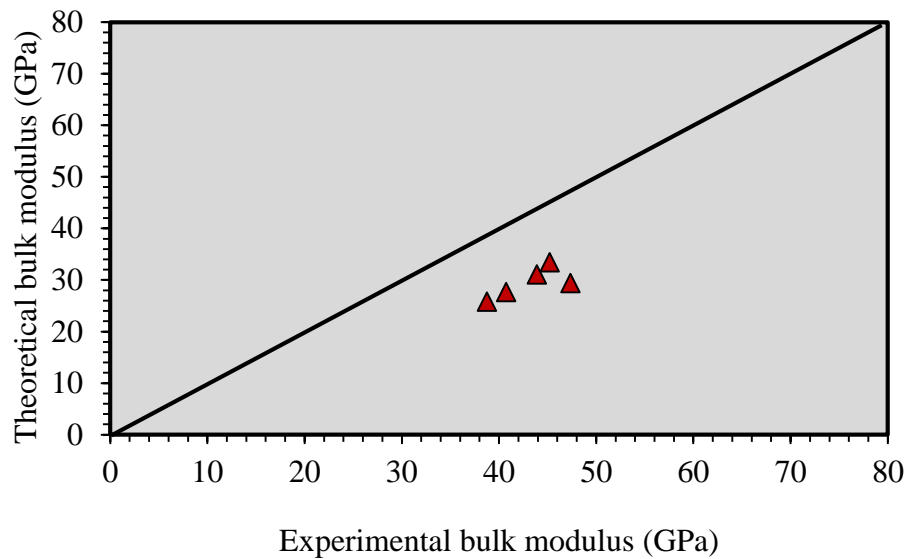


Figure 4.10 The comparative of theoretical and experimental Poisson's ratios in barium-borate-bagasse-cassava rhizome- WO_3 glass system on the basis of Abd El-Moneim and Alfifi's approaches

4.6 Microhardness of glass samples

Microhardness expresses the pressure required to eliminate the free volume and deformation of the glass network [52]. The microhardness of the prepared glass samples in this work shows a decreasing pattern from 5.343 to 4.190 GPa and from 5.103 to 4.123 GPa for measuring by using microhardness testing and ultrasonic testing, respectively, as the concentration of WO_3 increases from 0 to 4 wt%. Such pattern is observed probably due to the influence of WO_3 cause to formation of bridging atoms from structural unit BO_3 to BO_4 [100] and this modifier cause more the glass network with formation of non-bridging oxygen. These structural changes cause an increase in compactness of the glass system.

The microhardness values of all glass samples from microhardness testing and ultrasonic testing were compared with lead glass, which is standard shielding lead glass, are shown in table 4.6. The result shows that the microhardness of this glass system varied with WO_3 content. The microhardness acquired from microhardness testing and from ultrasonic testing of this glass system have an accordant trend. All glass samples with different of WO_3 exhibited a higher microhardness values than the lead glass. Moreover, the microhardness value of the glass sample with 6 wt% of WO_3 (B4) is

higher than the glass samples with other WO_3 concentrations. The highest microhardness is related to the amount of bridging oxygen occurring in the structure, which can be supported by ultrasonic velocities and FTIR data. These increasing trends imply an increase in the rigidity of the glass system.

Table 4.6 Microhardness of barium-borate-bagasse-cassava rhizome- WO_3 glass system and lead glass

Glass sample code	H of glass samples (GPa)		H of lead glass ± 0.02 (GPa) (standard radiation shielding)
	microhardness testing ± 0.04	ultrasonic testing ± 0.0011	
B1	5.34	5.1033	3.65
B2	4.52	4.8361	
B3	4.19	4.1233	
B4	5.74	5.8552	
B5	4.35	4.5981	

4.7 The radiation properties of glass samples

4.7.1 The attenuation coefficients of glass samples

The mass attenuation coefficients of prepared glass samples were measured and calculated at photon energies of 60, 122 and 662 keV, the results are shown in figure 4.11. It is found that the mass attenuation coefficients tend to decrease as the photon energy increases. It is also found that the same photon energy, this value tends to increase with increasing of WO_3 concentration. B5 glass sample (WO_3 8 wt%) is the best photon energy attenuator for all studied photon energies. The mass attenuation coefficients of all glass samples at 60 keV are highest when compared with another studied photon energy. Therefore, this glass system is more suitable for related work applying at the photon energy of 60 keV than 122 and 662 keV. The mass attenuation coefficients measured from experiment are consistent with that calculated (theory) by WinXCom program. The linear attenuation coefficients in figure 4.12 also show the same behavior as the mass attenuation coefficient.

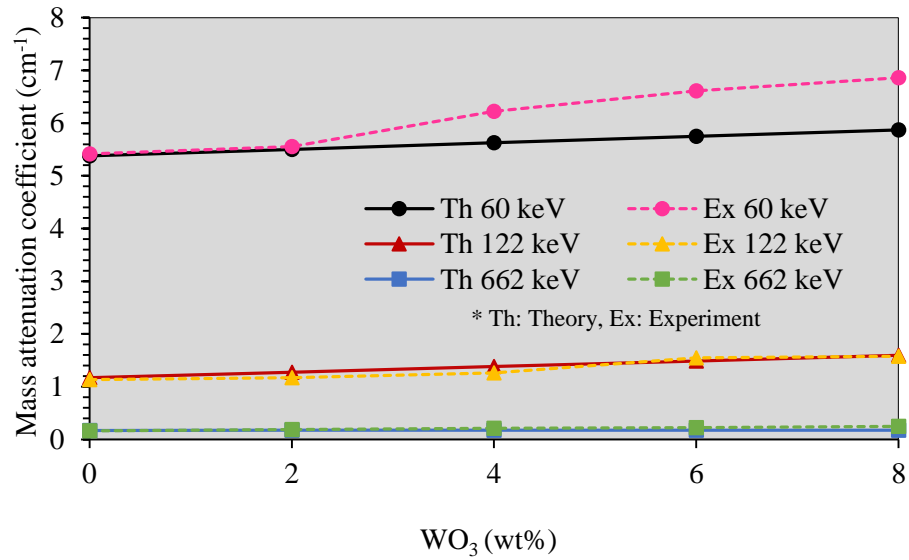


Figure 4.11 Variation of mass attenuation coefficient of barium-borate-bagasse-cassava rhizome- WO₃ glass system

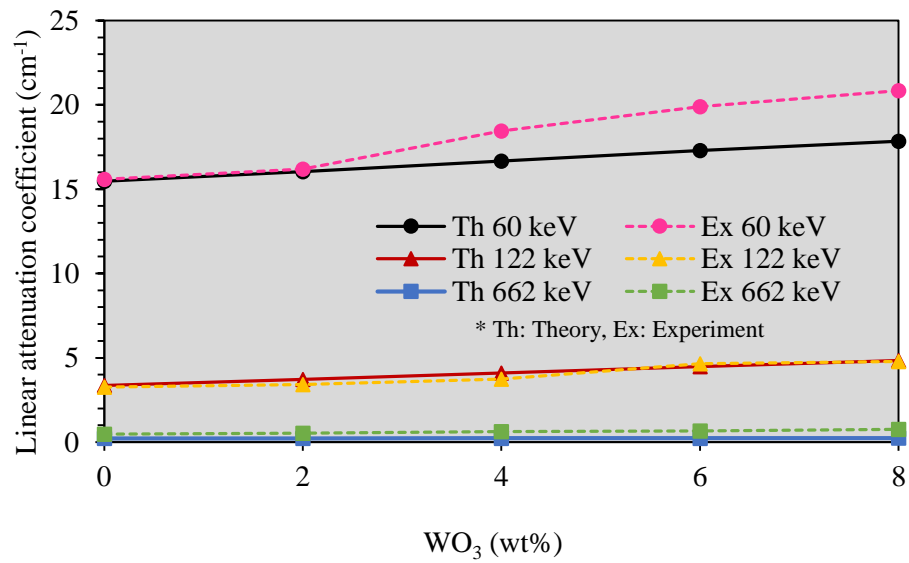


Figure 4.12 Variation of linear attenuation coefficient of barium-borate-bagasse-cassava rhizome- WO₃ glass system

4.7.2 The mean free path of glass samples

The mean free path (MFP) refers to the average distance between two consecutive interactions of photons [68,69]. The MFP values of this glass system in figure 4.13 tend to increase as the photon energy increases. At the same photon energy,

MFP values tend to decrease with increasing of WO_3 concentration. B5 glass sample (WO_3 8 wt%) possess the high possibility of a photon interacting with a target per unit path length for all studied photon energy [68]. The best value of MFP is observed at photon energy of 60 keV. Consequently, this glass system is more suitable for related work applying at the photon energy of 60 keV than 122 and 662 keV. In addition, a good agreement of MFP values between the experimental and theoretical (WinXCom program) is also observed in terms of the declined trend.

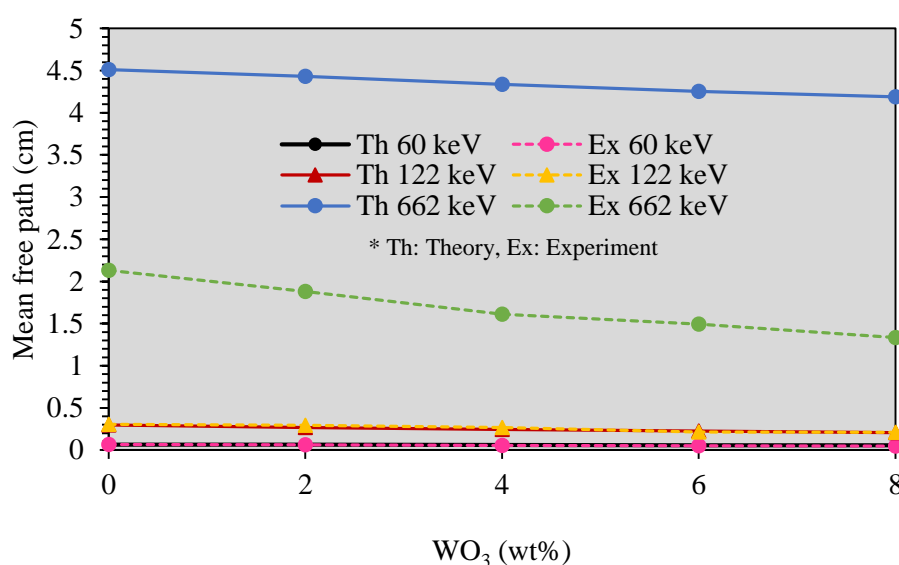


Figure 4.13 Variation of mean free path of barium-borate-bagasse-cassava rhizome- WO_3 glass system

4.7.3 The half value layer of glass samples

The gamma ray shielding capability of material can be acquired by other parameters such as the half value layer (HVL, 50% photon attenuation thickness) [68,69]. From figure 4.14, it is also found that the HVL have the same behavior as the MFP. Therefore, the use of this glass material for radiation shielding application is optimal at photon energy of 60 keV with requirement of low minimum thickness. For higher photon energy, the minimum required thickness increase. In addition, increasing the concentration of WO_3 improves the ability to prevent the transmission of photon energy because B5 glass sample (WO_3 8 wt%) has the smallest HVL values for all studied energy.

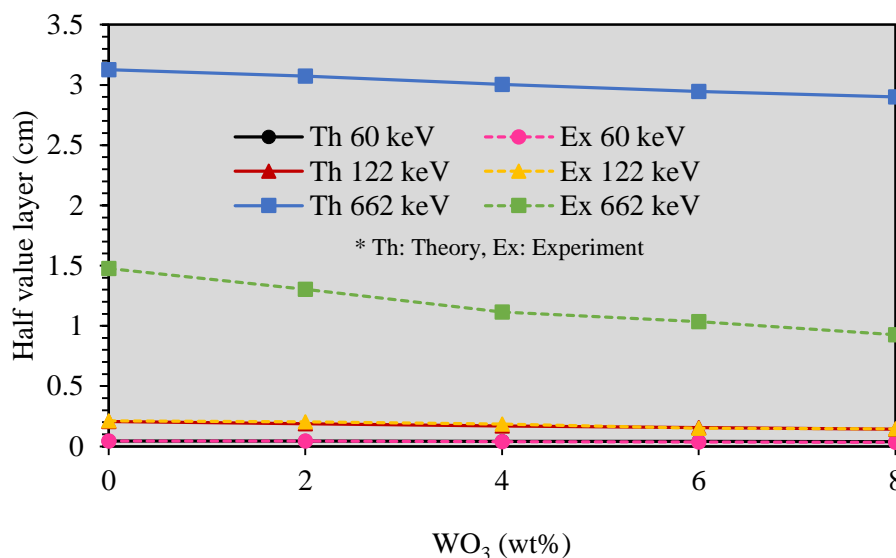


Figure 4.14 Variation of half value layer of barium-borate-bagasse-cassava rhizome-WO₃ glass system

It is worth noting that at 662 keV photon energy, the gamma ray attenuation coefficients (figure 4.11 and 4.12) have a lower value than other studied photon energy. The more pronounced is the MFP and HVL (figure 4.13 and 4.14), the theoretical MFP and HVL values are significantly more than the experimental values. These difference occurred because of the photoelectric effect is process of absorption of gamma photon by an atom. It is more pronounced in high atomic number absorbers and at low incident energies. This process dominates at low energies (50-500 keV). At intermediate energies (50 keV-5 MeV) and in low Z materials, the Compton scattering is dominating. When this glass system obtained a higher gamma photon (662 keV), Compton process occurs only then when the photon energy passes the limiting value of the photoelectric process. Since the impulse and the energy are divided among the Compton electron and the scattered photon. For this reason, the atomic number (Z) of the material is less influential. The freed Compton electrons can, depending on the energy content, ionize other atoms along their routes. The scattered photon continues its way and continues to enter into Compton processes up until the energy is reduced to such an extent that a photoelectric process takes place. Only then the photon has disappeared. Because the electron binding energy is very small compared to the gamma ray energy [62-64].

One main cause of different experimental and theoretical values may be due to the theoretical basis of the WinXCom program, which is processing from the mixture rule which involve the atomic weight fractions and the cross-section values of pure elements or compounds in this composited glass. This radiation experiment other related variables may also affect different values such as the thickness similar or good plane characteristics of every glass sample and the amount of substance, composition before and after glass melting should be nearly equivalent. Due to it has an effect on data of weight fraction of glass composition for processing in the WinXCom program. From the discussion, it can be concluded that WinXCom program can be used to predict the radiation properties of the studied glass system for 60 and 122 keV photon energies.

Moreover, it was likewise found that the values of μ_m and u parameters obtained from the experiment and WinXCom of the glass samples are much higher than standard radiation shielding concretes (barite and ferrite concretes) at the same photon energies are shown in table 4.7 and 4.8. This result indicates that the studied glass system has better shielding properties in terms of mass substance than standard radiation shielding concretes [115]. HVL and MFP values have also been compared with both of standard radiation shielding concretes at the same photon energy are shown in table 4.9 and 4.10. It was found that the HVL and MFP values of the studied glasses is lower than both of standard radiation shielding concretes at energies of 60 and 122 keV, while WinXCom values of this glass system higher than both concretes for energies of 662 keV. Therefore, the HVL and MFP parameters as well as the shielding properties depend on the energies of radioisotope source and WO_3 concentrations [116].

Table 4.7 The comparison of experimental (Ex) and theoretical (Th) mass attenuation coefficients of glass samples and standard radiation shielding concretes

WO₃ (wt%)	μ_m at 60 keV (cm⁻¹)		μ_m at 122 keV (cm⁻¹)		μ_m at 662 keV (cm⁻¹)	
	Th	Ex ± 0.0018	Th	Ex ± 0.0020	Th	Ex ± 0.0023
0	5.3788	5.4134	1.1693	1.1338	0.1695	0.1631
2	5.5022	5.5535	1.2753	1.1706	0.1703	0.1826
4	5.6255	6.2239	1.3813	1.2586	0.1712	0.2095
6	5.7488	6.6136	1.4874	1.5441	0.1721	0.2225
8	5.8721	6.8606	1.5934	1.5744	0.1730	0.2465
Barite concrete	3.7835		0.7624		0.0788	
Ferrite concrete	0.6687		0.2198		0.0782	

Table 4.8 The comparison of experimental (Ex) and theoretical (Th) linear attenuation coefficients of glass samples and standard radiation shielding concretes

WO₃ (wt%)	μ at 60 keV (cm⁻¹)		μ at 122 keV (cm⁻¹)		μ at 662 keV (cm⁻¹)	
	Th	Ex ± 0.0018	Th	Ex ± 0.0020	Th	Ex ± 0.0023
0	15.4741	15.5734	3.3638	3.2618	0.2216	0.4692
2	16.0307	16.1804	3.7156	3.4107	0.2256	0.5321
4	16.6733	18.4470	4.0941	3.7303	0.2306	0.6209
6	17.2837	19.8835	4.4718	4.6423	0.2351	0.6690
8	17.8403	20.8433	4.8410	4.7832	0.2388	0.7489
Barite concrete	13.2423		2.6685		0.2758	
Ferrite concrete	3.0089		0.9892		0.3518	

Table 4.9 The comparison of experimental (Ex) and theoretical (Th) mean free path of glass samples and standard radiation shielding concretes

WO ₃ (wt%)	MFP at 60 keV (cm)		MFP at 122 keV (cm)		MFP at 662 keV (cm)	
	Th	Ex ± 0.0018	Th	Ex ± 0.0020	Th	Ex ± 0.0023
0	0.0646	0.0642	0.2973	0.3066	4.5128	2.1315
2	0.0624	0.0618	0.2691	0.2932	4.4331	1.8793
4	0.0599	0.0542	0.2443	0.2681	4.3356	1.6105
6	0.0579	0.0503	0.2236	0.2154	4.2524	1.4947
8	0.0561	0.0479	0.2066	0.2091	4.1868	1.3353
Barite concrete	0.0755		0.3747		3.6253	
Ferrite concrete	0.3323		1.0109		2.8424	

Table 4.10 The comparison of experimental (Ex) and theoretical (Th) half value layer of glass samples and standard radiation shielding concretes

WO ₃ (wt%)	HVL at 60 keV (cm)		HVL at 122 keV (cm)		HVL at 662 keV (cm)	
	Th	Ex ± 0.0018	Th	Ex ± 0.0020	Th	Ex ± 0.0023
0	0.0448	0.0445	0.2060	0.2125	3.1274	1.4771
2	0.0433	0.0428	0.1865	0.2032	3.0722	1.3023
4	0.0416	0.0376	0.1693	0.1858	3.0046	1.1161
6	0.0401	0.0349	0.1550	0.1493	2.9469	1.0359
8	0.0388	0.0332	0.1432	0.1449	2.9015	0.9254
Barite concrete	0.0523		0.2597		2.5123	
Ferrite concrete	0.2303		0.7006		1.9698	

CHAPTER 5

CONCLUSION AND RECOMMENDATIONS

5.1 Conclusion

From the analysis it was found out that the main composition of bagasse and cassava rhizome is Si and Ca, respectively. Both raw materials can be used as the composition of glass producing in the $30\text{BaO} - (50-x)\text{B}_2\text{O}_3 - 10\text{BG} - 10\text{CR} - x\text{WO}_3$ system, successfully prepared using melt-quenching technique. All glass samples are a transparent yellow tone, the increasing of WO_3 concentration lead to the glass samples are more dark yellow. The density and molar volume of glass samples trends to increase when WO_3 content was added, the reason of the substitution of higher molecular weight and the greater size of the ionic radii of WO_3 , respectively. From the investigation by X-ray mapping technique, the chemical compositions of all glass samples are homogeneous. Also, the XRD pattern confirmed the amorphous nature of studied glass system.

Both v_L and v_S of this glass system tend to decrease with the increasing of WO_3 concentration. However, an increase of v_L at 4 wt% and v_S at 6 wt% of WO_3 has effect on borate network. These pointed to more number of bridging oxygen which were supported data from FTIR spectra. The elastic moduli of all glass samples have a tendency to decrease with more adding WO_3 content, corresponding to the variation of ultrasonic velocities. This suggests that WO_3 acts as network modifier, it can break glass network to discontinuity form as resulted the decrease in the rigidity of network structure. The application of studied glasses could select the glass samples according to the purpose of used by taking into the resistance of the force acting on samples. The Poisson's ratio obtained in this work shows a narrow change trend of increasing and decreasing and the studied glasses have high cross-link density.

The comparative study between theoretical and experimental values of elastic moduli (G, E and K) is excellent. Majority of the glass samples have experimental values of elastic moduli much greater than the corresponding theoretical values. For longitudinal modulus, this value is not corresponding. The divergence between the

theoretical and experimental values has been attributed to the anomalous behavior between the experimental elastic moduli and calculated dissociation energy per unit volume of the glass. Although the agreement between theoretical and experimental values of Poisson's ratio is satisfactory for studied glasses, it is not corresponding for B3 (WO_3 4 wt%) and B5 (WO_3 6 wt%) glass samples. The experimental longitudinal modulus and Poisson's ratio of studied glasses is not predictable from Makishima-Mackenzie model. The bulk modulus of these glasses are not predictable from the Abd El-Moneim and Alfifi's approaches. Even though, the bulk modulus on the basis of Abd El-Moneim and Alfifi's approaches shows a decreasing trend similar to the Makishima-Mackenzie model, the obtained values are not nearly similar. In addition, the agreement of both theoretical and experimental bulk moduli is not correspond. The microhardness of the glass samples acquired from microhardness testing and from ultrasonic testing have an accordant trend. All the glass samples with different of WO_3 exhibited a higher microhardness values than the standard radiation shielding lead glass. Moreover, the microhardness value of the glass sample with 6 wt% of WO_3 (B4) is higher than other studied glass samples. These increasing trends imply an increase in the rigidity of the glass system.

For radiation shielding properties, it was found that the mass attenuation coefficient and linear attenuation coefficient tend to decrease as the photon energy increases (60, 122 and 662 keV). Therefore, this glass system is more suitable for related work applying at the photon energy of 60 keV than 122 and 662 keV. It is also found that the same photon energy, these values tend to increase with increasing of WO_3 concentration. B5 glass sample (WO_3 8 wt%) is the best photon energy attenuator for all studied photon energies. The experimental and theoretical (WinXCom program) radiation attenuation coefficients are consistent.

The MFP values of this glass system tend to increase as the photon energy increases. Consequently, this glass system is more suitable for related work applying at the photon energy of 60 keV than 122 and 662 keV. At the same photon energy, MFP values tend to decrease with increasing of WO_3 concentration. B5 glass sample (WO_3 8 wt%) possess the high possibility of a photon interacting with a target per unit path length for all studied photon energy. In addition, a good agreement of MFP values between the experimental and theoretical is also observed in terms of the declined trend.

It is also found that the HVL have the same behavior as the MFP. Therefore, the use of this glass material for radiation shielding application is optimal at photon energy of 60 keV with requirement of low minimum thickness. For higher photon energy, the minimum required thickness increase. In addition, increasing the concentration of WO_3 improves the ability to prevent the transmission of photon energy because B5 glass sample (WO_3 8 wt%) has the smallest HVL values for all studied energy. Although the studied experimental and theoretical radiation parameters tend to be consistent, there is a clear observation that the experimental values are significantly different from the theoretical values. This may be due to the theoretical basis of the WinXCom program and some caution in the broad beam transmission geometry. WinXCom program can be used to predict the radiation properties of the studied glass system for 60 and 122 keV photon energies. Their high values of mass and linear attenuation coefficient and low value of HVL and MFP in comparison to standard radiation shielding concretes for 60 and 122 keV photon energies indicate that the volume required for shield design will be less than concretes. However, the application of cassava rhizome and bagasse as the composition in this glass production has many advantages such as reducing environmental pollution from agricultural waste and reducing the cost of glass production, etc.

5.2 Recommendations

Various properties of glass samples should be studied with more new techniques or methods to provide clearer results, which will be useful for wider application of glass samples such as:

In the field of radiation, other additional parameters should be studied such as buildup factor. Gamma ray measurement is an important issue in nuclear technology, since it is widely used in industry, medicine, agriculture and education research. Gamma ray is also needed to build radiation protection, which is very useful for human health. The buildup factor is a correction factor that considers the influence of the scattered radiation plus any secondary particles in the medium during shielding calculations. If we want to account for the buildup of secondary radiation, then we have to include the buildup factor. The buildup factor is then a multiplicative factor which accounts for the response to the uncollided photons so as to include the contribution of

the scattered photons. Thus, the buildup factor can be obtained as a ratio of the total dose to the response for uncollided dose.

Another interesting technique is differential scanning calorimetry (DSC) can be used to measure a number of characteristic properties of a sample. Using this technique, it is possible to observe fusion and crystallization events as well as glass transition temperatures (T_g). DSC can also be used to study oxidation, as well as other chemical reactions.

REFERENCES

REFERENCES

- [1] Green, A. **Agricultural waste and pollution**. Hertfordshire: University of Hertfordshire, 2019.
- [2] Moodley, P. and Kana, E. B. G. “Comparative study of three optimized acid-based pretreatments for sugar recovery from sugarcane leaf waste: A sustainable feedstock for biohydrogen production”, **Engineering Science and Technology, an International Journal**. 21(1): 107-116; February, 2018.
- [3] Office of Agricultural Economics. **Agricultural economic report: 1st Quarter 2019**. Bangkok: Ministry of Agriculture and Cooperatives, 2019.
- [4] Karagulian, F. and et al. “Contributions to cities' ambient particulate matter (PM): A systematic review of local source contributions at global level”, **Atmospheric Environment**. 120: 475-483; November, 2015.
- [5] Teixeira, S. R. and et al. “Valorization of sugarcane bagasse ash: Producing glass-ceramic materials”, **Journal of Environmental Management**. 134: 15-19; February, 2014.
- [6] Reddy, G. N. K., Vardhan, G. H. and Reddy, S. V. B. “Partial replacement of cement in concrete with sugarcane bagasse ash and its behavior in aggressive environments”, **IOSR Journal of Mechanical and Civil Engineering**. 12(6): 29-35; December, 2016.
- [7] Leite, A. L. M. P., Zanon, C. D. and Menegalli, F. C. “Isolation and characterization of cellulose nanofibers from cassava root bagasse and peelings”, **Carbohydrate Polymers**. 157: 962-970; February, 2017.
- [8] Tippayawong, N. and et al. “Biochar production from cassava rhizome in a semi-continuous carbonization system”, **Energy Procedia**. 141: 109-113; December, 2017.
- [9] International Atomic Energy Agency. **Radiation, People and the Environment**. Austria: IAEA, 2004.
- [10] Donya, M. and et al. (2014). “Radiation in medicine: Origins, risks and aspirations”, **Global Cardiology Science and Practice**.
www.ncbi.nlm.nih.gov. March 22, 2020.

REFERENCES (CONTINUED)

- [11] Erramli, H. and El Asri, J. (2019). “Gamma Rays: Applications in Environmental Gamma Dosimetry and Determination Samples Gamma-Activities Induced by Neutrons”, **Use of Gamma Radiation Techniques in Peaceful Applications**. www.intechopen.com. May 12, 2020.
- [12] SCHOTT AG Research and Development. (2014). “Application of specialty glass in select fields”, **Technical Glasses Physical and Technical Properties**. www.schott.com. May 15, 2020.
- [13] Erdem, M. and et al. “A novel shielding material prepared from solid waste containing lead for gamma ray”, **Radiation Physics and Chemistry**. 79(9): 917-922; September, 2010.
- [14] Hao, Y. and Cao, J. “Structure and luminescence of Dy³⁺ doped CaO-B₂O₃-SiO₂ glasses”, **Physica B: Condensed Matter**. 493: 68-71; July, 2016.
- [15] Gautam, C., Yadav, A. K. and Singh, A. K. “A review on infrared spectroscopy of borate glasses with effects of different additives”, **International Scholarly Research Network Ceramics**. 2012: 1-17; November, 2012.
- [16] Maniu, D. and et al. “Raman study on B₂O₃-CaO glasses”, **Journal of Molecular Structure**. 651-653: 485-488; June, 2003.
- [17] Thonglem, S. and et al. “Effects of CaO on Properties of P₂O₅-CaO-Na₂O Glasses and Glass Ceramics”, **Journal of Metals, Materials and Minerals**. 20(3): 173-177; September, 2010.
- [18] Lim, E. S. and et al. “Effect of BaO content on sintering and physical properties of BaO-B₂O₃-SiO₂ glasses”, **Journal of Non-Crystalline Solids**. 352(8): 821-826; June, 2006.
- [19] Zhu, H. and et al. “Crystallization behavior and properties of BaO-CaO-B₂O₃-SiO₂ glasses and glass-ceramics for LTCC applications”, **Ceramics International**. 44(9): 10147-10153; June, 2018.
- [20] Ouis, M. A., Azooz, M. A. and ElBatal, H. A. “Optical and infrared spectral investigations of cadmium zinc phosphate glasses doped with WO₃ or MoO₃ before and after subjecting to gamma irradiation”, **Journal of Non-Crystalline Solids**. 494: 31-39; August, 2018.

REFERENCES (CONTINUED)

- [21] Mostafa, A. M. A., Issa, S. A. M. and Sayyed, M. I. “Gamma ray shielding properties of PbO-B₂O₃-P₂O₅ doped with WO₃”, **Journal of Alloys and Compounds**. 708: 294-300; June, 2017.
- [22] Azianty, S. and Yahya, A. K. “Enhancement of elastic properties by WO₃ partial replacement of TeO₂ in ternary (80-x) TeO₂-20PbO-xWO₃ glass system”, **Journal of Non-Crystalline Solids**. 378: 234-240; October, 2013.
- [23] Kolb, K. E. “Glass”, **Chemistry Explained**.
<http://www.chemistryexplained.com>. May 13, 2020.
- [24] Helmenstine, A. M. (2019). “Glass Definition in Science”, **Science**.
<https://www.thoughtco.com>. May 13, 2020.
- [25] Pfaender, H. G. **Schott Guide to Glass**. London: Chapman & Hall, 1996.
- [26] Chakravorty, D. “Inorganic Glasses”, In **Modern Aspects of Solid State Chemistry**. Rao C.N.R. Editor. p. 391-423. New York: Plenum Press, 1970.
- [27] Zanutto, E. D. and Mauro, J. C. “The glassy state of matter: Its definition and ultimate fate”, **Journal of Non-Crystalline Solids**. 471: 490-495; September, 2017.
- [28] Uhlmann, D. “Kinetics of glass formation and devitrification behavior”, **Journal de Physique Colloques**. 43(C9): C9-175-C9-190; December, 1982.
- [29] Corning Museum of Glass. (2011). “Type of glass”, **All About Glass**.
<https://www.cmog.org>. May 15, 2020.
- [30] Vogel, W. **Classical Theories of Glass Structure**. Berlin: Springer, 1994.
- [31] Zachariasen, W. H. “The atomic arrangement in glass”, **Journal of the American Chemical Society**. 54(10): 3841-3851; October, 1932.
- [32] Dietzel, A. “Structure and properties of glass”, **Glass technology Berlin**. 22: 41-50, 1948.
- [33] Sun, K. H. “Fundamental condition of glass formation”, **Journal of the American Ceramic Society**. 30: 277-281; September, 1947.

REFERENCES (CONTINUED)

- [34] Stanworth, J. E. “Tellurite glasses”, **Journal of the Society of Glass Technology**. 36: 217-241, 1952.
- [35] Izumatani, T. S. **Optical Glass**. New York: American Institute of Physics, 1986.
- [36] Sherby, J. E. **Introduction to glass science and technology**. Tyne and Wear: Athenaeum Press Ltd, 1997.
- [37] Hasan, S. (2018). “Structure of glass”, **Lecture of glass**. <https://uomustansiriyah.edu.iq>. May 20, 2020.
- [38] Grayson, K. (2019). “Glass structure and composition”, **Glass 101: Using Glass Modifiers to Change Glass Characteristics**. <https://mo-sci.com>. May 22, 2020.
- [39] Sanguanpak, S. “Raw materials for glass melting”, **Glass science and technology information services**. <http://www2.mtec.or.th>. May 22, 2020.
- [40] Overath, J. (2012). “Applications”, **The world of glass**. <https://www.glassallianceeurope.eu>. May 23, 2020.
- [41] Gharpedia. “uses and benefits of glass”, **What is Glass & How it is Made?**. <https://gharpedia.com>. May 23, 2020.
- [42] The Editors of Encyclopaedia Britannica. “Archimedes’ principle”, **Physics**. www.britannica.com. May 25, 2020.
- [43] Nuanlaong Srakaew. **Mechanical properties of borosilicate glass added with Ti, Ba, Pb and Bi**. Bachelor’s Thesis: Ubon Ratchathani University, 2007.
- [44] Khunaset, M., Puipairote, S. and Kapkraikaew, W. **Ultrasonic Imaging System**. Bachelor’s Thesis: Khon Kaen University, 2005.
- [45] Raewat Laopaiboon. **Selected Topic in Material Science 1**. Faculty of Science: Ubon Ratchathani University, 2013.
- [46] SONOTEC Co., Ltd. “What is ultrasonic wave?”, **Sonotec Ultrasonic hand-tools**. <https://www.sonotec.com>. May 27, 2020.
- [47] Liu, Y. **Aerospace structure and materials**. United States of America: Bentham, 2016.

REFERENCES (CONTINUED)

- [48] NDT resources center. (2001). “Ultrasound”, **NDT Course Material**.
<https://www.nde-ed.org>. May 27, 2020.
- [49] El-reedy, M. A. **Assessment, Evaluation, and Repair of concrete, steel, and offshore structures**. Boca Raton: CRC Press, 2018.
- [50] Gaafar, M. S. and et al. “Structural studies and mechanical properties of some borate glasses doped with different alkali and cobalt oxides”, **Current Applied Physics**. 13(1): 152-158; January, 2013.
- [51] Bootjomchai, C. and et al. “Structural investigation of borosilicate recycled-barium-bismuth glasses under the influence of gamma-irradiation through ultrasonic and FTIR studies”, **Nuclear Engineering and Design**. 248: 28-34; July, 2012.
- [52] Satyendra, K. S. (2016). “Vickers hardness test”, **Material hardness and hardness testing**. <https://www.ispatguru.com>. May 30, 2020.
- [53] Sidek, H. A. A. and et al. “Effect of PbO on the elastic behavior of ZnO-P₂O₅ glass systems”, **Results in Physics**. 6: 449-455; August, 2016.
- [54] Saddeek, Y. B. and Latif, L. A. E. “Effect of TeO₂ on the elastic moduli of sodium borate glasses”, **Physica B: Condensed Matter**. 348(1-4): 475-484; May, 2004.
- [55] Zou, X. and Toratani, H. “Compositional design of high modulus glasses for disk substrates”, **Journal of Non-Crystalline Solids**. 290(2-3): 180-188; September, 2001.
- [56] El-Moneim, A. A. “Correlation between acoustical and structural properties of glasses: Extension of Abd El-Moneim model for bioactive silica based glasses”, **Materials Chemistry and Physics**. 173: 372-378; February, 2016.
- [57] El-Moneim, A. A. “Oxyfluoro-zinc-tellurite glasses – Part I: Predicting the elastic properties and glass transition temperature under the substitution of AlF₃ by ZnO”, **Journal of Fluorine Chemistry**. 217: 97-104; January, 2019.

REFERENCES (CONTINUED)

- [58] El-Moneim, A. A. “BaF₂-contained tellurite glasses: Quantitative analysis and prediction of elastic properties and ultrasonic attenuation-Part I”, **Journal of Fluorine Chemistry**. 210: 156-165; March, 2018.
- [59] El-Moneim, A. A. “Theoretical analysis for ultrasonic properties of vanadate-phosphate glasses over an extended range of composition: Part II”, **Journal of Non-Crystalline Solids**. 465: 49-54; June, 2017.
- [60] El-Moneim, A. A. and El-Mallawany, R. “Analysis and prediction for elastic properties of quaternary tellurite Ag₂O-V₂O₅-MoO₃-TeO₂ and WO₃-B₂O₃-MgO-TeO₂ glasses”, **Journal of Non-Crystalline Solids**. 522: 119580; July, 2019.
- [61] Australian radiation protection and nuclear safety agency. “Gamma radiation”, **Understanding radiation**. <https://www.arpsa.gov.au>. May 29, 2020.
- [62] Hornyak, W. F. “II.A - The Interaction of Gamma Rays with Matter”, **Pure and Applied Physics**. 9(Part A): 211-227, September, 2013.
- [63] Ellis, D. V. and Singer, J. M. **Well Logging for Earth Scientists**. Netherlands: Springer, 2008.
- [64] Obodovskiy, I. **Radiation Fundamentals, Applications, Risks, and Safety**. Netherlands: Elsevier, 2019.
- [65] Cremer, J. T. “Chapter 4 – X-ray Optics”, In **Advances in Imaging and Electron Physics**. Peter W. Hawkes Editor. p. 497-559. Netherlands: Elsevier, 2012.
- [66] NDT resources center. (2001). “Radiography”, **NDT Course Material**. <https://www.nde-ed.org>. May 29, 2020.
- [67] Nelson, G. and Reilly, D. “The Fundamental Law of Gamma-Ray Attenuation”, **Gamma-Ray Interactions with Matter**. <https://fas.org>. June 1, 2020.
- [68] Sayyed, M. I. “Half value layer, mean free path and exposure buildup factor for tellurite glasses with different oxide compositions”, **Journal of Alloys and Compounds**. 695: 3191-3197; February, 2017.

REFERENCES (CONTINUED)

- [69] Waly, E. A., Fusco, M. A. and Bourham, M. A. “Gamma-ray mass attenuation coefficient and half value layer factor of some oxide glass shielding materials”, **Annals of Nuclear Energy**. 96: 26-30; October, 2016.
- [70] Sidhu, G. S. and et al. “Effect of collimator size and absorber thickness on gamma ray attenuation measurements for bakelite and perspex”, **PRAMANA Journal of Physics**. 53(5): 851-855; November, 1999.
- [71] Jahagirdar, H. A., Hanumaiah, B. and Thontadarya, S. R. “A new direct method to determine total atomic photoelectric cross sections at 123.6 keV”, **International Journal of Radiation Applications and Instrumentation. Part A. Applied Radiation and Isotopes**. 43(3): 399-404; March, 1992.
- [72] Jahagirdar, H. A., Hanumaiah, B. and Thontadarya, S. R. “Determination of narrow beam attenuation coefficients from a broad beam geometrical configuration for 320 keV photons”, **International Journal of Radiation Applications and Instrumentation. Part A. Applied Radiation and Isotopes**. 43(12): 1511-1514; December, 1992.
- [73] Jahagirdar, H. A., Hanumaiah, B. and Thontadarya, S. R. “Measurement of narrow beam attenuation coefficients using a broad beam geometry configuration for 145.4 keV photons”, **Applied Radiation and Isotopes**. 44(9): 1248-1252; September, 1993.
- [74] Hubbell, J. H. and Seltzer, S. M. **Tables of X-Ray Mass Attenuation Coefficients and Mass Energy-Absorption Coefficients**. Gaithersburg: National Institute of Standards and Technology, 1995.
- [75] Berger, M. J. and Hubbell, J. H. **XCOM: Photon cross sections on a personal computer**. Gaithersburg: National Bureau of Standards, 1987.
- [76] Gerward, L. and et al. “X-ray absorption in matter. Reengineering XCOM”, **Radiation Physics and Chemistry**. 60(1-2): 23-24; January, 2001.

REFERENCES (CONTINUED)

- [77] Odelami, K. A., Okunade, I. O. and Onimisi, M. Y. “Measurement of mass attenuation coefficient, effective atomic number and electron density of thermoluminescent dosimetric compounds”, **International Journal of Chemical Studies**. 4(1): 103-108, January, 2016.
- [78] Saloman, E. B. and Hubbell, J. H. **X-ray Attenuation Coefficients (Total Cross Sections): Comparison of the Experimental Data Base with Recommended Values of Henke and the Theoretical Values of Scofield for Energies between 0.1-100 keV**. Gaithersburg: National Bureau of Standards, 1986.
- [79] Souza, A. E. and et al. “Reuse of sugarcane bagasse ash (SCBA) to produce ceramic materials”, **Journal of Environmental Management**. 92(10): 2774-2780; October, 2011.
- [80] Saddeek, Y. B. “Ultrasonic study and physical properties of some borate glasses”, **Materials Chemistry and Physics**. 83(2-3): 222-228; February, 2004.
- [81] Singh, S. and et al. “Barium–borate–flyash glasses: As radiation shielding materials”, **Nuclear Instruments and Methods in Physics Research Section B: Beam Interactions with Materials and Atoms**. 266(1): 140-146; January, 2008.
- [82] Kaur, K., Singh, K. J. and Anand, V. “Structural properties of Bi₂O₃-B₂O₃-SiO₂-Na₂O glasses for gamma ray shielding applications”, **Radiation Physics and Chemistry**. 120: 63-72; March, 2016.
- [83] El-bashir, B. O. and et al. “Comprehensive study on physical, elastic and shielding properties of ternary BaO-Bi₂O₃-P₂O₅ glasses as a potent radiation shielding material”, **Journal of Non-Crystalline Solids**. 468: 92-99; July, 2017.
- [84] El Batal, H. A. and et al. “Gamma rays interactions with WO₃-doped lead borate glasses”, **Materials Chemistry and Physics**. 134(1): 542-548; May, 2012.

REFERENCES (CONTINUED)

- [85] Harraz, H. Z. (2013). “Topic 4: glass”, **Silica sand and glass industry**.
<https://www.slideshare.net>. June 2, 2020.
- [86] Martin, G. **Industrial and Manufacturing Chemistry**. London: Forgotten Books, 2018.
- [87] Vogel, W. **Glass Chemistry**. Heidelberg: Springer-Verlag Berlin and Heidelberg, 1994.
- [88] K. R., Fellers, T. J. and Davidson, M. W. “Human Vision and Color Perception”, **The Physics of Light and Color**. <https://www.olympus-lifescience.com>. June 3, 2020.
- [89] International Tungsten Industry Association. (2013). “The Beautiful Colours of Tungsten Oxides”, **Tungsten**. www.itia.info. June 3, 2020.
- [90] Tilley, R. J. D. **Colour and the optical properties of Materials**. England: John Wiley & Sons, Ltd, 2010.
- [91] National Center for Biotechnology Information. (2005). “Compound summary”, **PubChem**. <https://pubchem.ncbi.nlm.nih.gov>. June 5, 2020.
- [92] Kremer, P. (2015). “Periodic Table of the Elements”, **Chemglobe**.
<https://chemglobe.org>. June 5, 2020.
- [93] Friel1, J. J. and Lyman, C. E. “X-ray Mapping in Electron-Beam Instruments”, **Microscopy and microanalysis**. 12(1): 2-25; February, 2006.
- [94] Newbury, D. E. “Chemical compositional mapping by microbeam analysis at the micrometer scale and finer”, **Microelectronics Journal**. 28(4): 489-508; May, 1997.
- [95] Bhattacharya, S. **Metal oxide glass nanocomposites**. Washington: Elsevier, 2020.
- [96] Gautam, C., Yadav, A. K. and Singh, A. K. “A Review on infrared spectroscopy of borate glasses with effects of different additives”, **International Scholarly Research Network ISRN Ceramics**. 2012: 1-17; November, 2012.

REFERENCES (CONTINUED)

- [97] Anderson, S., Bohon, R. L., and Kimpton J, I. D. “Infrared spectra and atomic arrangement in fused boron oxide and soda borate glasses”, **Journal of the American Ceramic Society**. 38(10): 370-377; June, 2006.
- [98] Yadav, A. K. and Gautum, C. R. “Structural and optical studies of Fe₂O₃ doped barium strontium titanate borosilicate glasses”, **Indian journal of pure and applied physics**. 53: 42-48; January, 2015
- [99] Weir, C. E. and Schroeder, R. A. “Infrared spectra of the crystalline inorganic borates”, **Journal of research of the national bureau of standards-A. Physics and Chemistry**. 68A(5): 465-487; September, 1964.
- [100] Wang, M. and et al. “Structure and viscosity of soda lime silicate glasses with varying Gd₂O₃ content”, **Journal of Molecular Structure**. 1063(1): 139-144; April, 2014.
- [101] Singh, G. P. and et al. “Gamma ray effect on the covalent behavior of the CeO₂-BaO-B₂O₃ glasses”, **Physica B: Condensed Matter**. 450: 106-110; October, 2014.
- [102] Marzouk, S. Y. and ElBatal, F. H. “Ultraviolet–visible absorption of gamma-irradiated transition metal ions doped in sodium metaphosphate glasses”, **Nuclear Instruments and Methods in Physics Research Section B: Beam Interactions with Materials and Atoms**. 248(1): 90-102; July, 2006.
- [103] Kaur, K., Singh, K. J. and Anand, V. “Structural properties of Bi₂O₃-B₂O₃-SiO₂-Na₂O glasses for gamma ray shielding applications”, **Radiation Physics and Chemistry**. 120: 63-72; March, 2016.
- [104] Witke, K. and et al. “Vibrational spectroscopic investigations of lead borate and lead aluminoborate glasses”, **Glastechnische Berichte Glass science and technology**. 69(5): 143-153; July, 1996.
- [105] Singh, G. P. and et al. “Role of WO₃ in structural and optical properties of WO₃-Al₂O₃-PbO-B₂O₃ glasses”, **Physica B: Condensed Matter**. 406(24): 4652-4656; December, 2011.

REFERENCES (CONTINUED)

- [106] Dahiya, M. S., Khasa, S. and Agarwal, A. “Structural, optical and thermal properties of transition metal ions doped bismuth borate glasses”, **Physics and Chemistry of Glasses - European Journal of Glass Science and Technology Part B**. 57(2): 45-52(8); April, 2016.
- [107] Khanna, A. and et al. “Structural analysis of WO₃-TeO₂ glasses by neutron, high energy X-ray diffraction, reverse Monte Carlo simulations and XANES”, **Journal of Non-Crystalline Solids**. 495: 27-34; September, 2018.
- [108] Hargittal, M. and Hargittal, I. “Structure of Molecules and Assemblies”, **Croatica Chemica Acta**. 69(3): 1023-1038; December, 1995.
- [109] Singh, G. P. and et al. “Role of WO₃ in structural and optical properties of WO₃-Al₂O₃-PbO-B₂O₃ glasses”, **Physica B**. 406(24): 4652-4656; December, 2011.
- [110] Edukondalu, A. and et al. “Physical and optical studies on Li₂O-Na₂O-WO₃-B₂O₃ glasses”, **IOP Conference Series Materials Science and Engineering**. 73(1): 012127; February, 2015.
- [111] Hasnimulyati, L. and et al. “A comparative study of the experimental and the theoretical elastic data of Tm³⁺ doped zinc borotellurite glass”, **Materials Chemistry and Physics**. 192: 228-234; May, 2017.
- [112] Laila, S., Supardan, S. N. and Yahya, A. K. “Effect of ZnO addition and concurrent reduction of V₂O₅ on network formation and elastic properties of lead vanadate (55 - x)V₂O₅-45PbO-(x)ZnO glass system”, **Journal of Non-Crystalline Solids**. 367(1): 14-22; May, 2013.
- [113] Rajendran, V. and et al. “Characterisation of semiconducting V₂O₅-Bi₂O₃-TeO₂ glasses through ultrasonic measurements”, **Journal of Non-Crystalline Solids**. 320(1-3): 195-209; June, 2003.
- [114] Higazy, A. A. and Bridge, B. “Elastic constants and structure of the vitreous system Co₃O₄-P₂O₄”, **Journal of Non-Crystalline Solids**. 729(1): 81-108; June, 1985.

REFERENCES (CONTINUED)

- [115] Singh, N. and et al. “Comparative study of lead borate and bismuth lead borate glass systems as gamma-radiation shielding materials”, **Nuclear Instruments and Methods in Physics Research Section B: Beam Interactions with Materials and Atoms.** 225(3): 305-309; September, 2004.
- [116] Sopapan, P. and et al. “Feasibility study of recycled CRT glass on elastic and radiation shielding properties used as x-ray and gamma-ray shielding materials”, **Progress in Nuclear Energy.** 119: 103149; January, 2020.

APPENDICES

APPENDIX A
Raw materials and chemicals for research



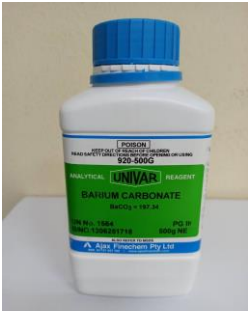


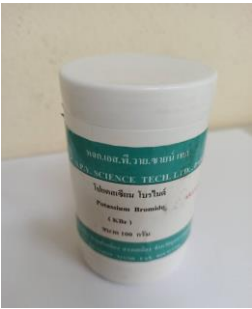
Figure no.	Name
 A I	Bagasse powder from Khon Kaen Sugar Industry Public Company Limited, 43 Moo 10, Nampong-Kranuan Rd., Nampong, Khon Kaen 40140, Thailand
 A II	Cassava rhizome powder from Cassava plantation, Sueang Khao, Si Rattana District, Si Sa Ket 33240, Thailand
 A III	Barium carbonate, Ajax Finechem Pty Ltd company, Purity of 95.0 %
 A IV	Dihydrogen borate, Fisher scientific company, Purity of 100.0 %

Figure no.	Name
 <p data-bbox="539 678 603 712">A V</p>	<p data-bbox="895 454 1348 548">Tungsten trioxide, Fisher scientific company, Purity of 95.0 %</p>
 <p data-bbox="531 1066 608 1099">A VI</p>	<p data-bbox="874 842 1369 936">Potassium bromide, S.P.Y. SCIENCE TECH. LDT. company, AR. Grade</p>

APPENDIX B

Scientific equipment and instruments for research




Figure no.	Name
 <p data-bbox="544 786 598 819">B I</p>	<p data-bbox="858 454 1382 712">Scanning Electron Microscopy, HITACHI Brand, S-3400N Model, Type II with EDAX element analyzer device, Genesis model at Scientific Equipment Center, Ubon Ratchathani University</p>
 <p data-bbox="539 1339 603 1373">B II</p>	<p data-bbox="874 981 1369 1238">Electric furnace: temperature of 1,800 °C, built by Glass Technology Excellent Center (GTEC), Department of Physics, Faculty of Science, Ubon Ratchathani University</p>
 <p data-bbox="533 1771 609 1805">B III</p>	<p data-bbox="866 1473 1377 1731">Electric oven: temperature of 1,000 °C, built by Glass Technology Excellent Center (GTEC), Department of Physics, Faculty of Science, Ubon Ratchathani University</p>




Figure no.	Name
 <p>A density measurement system consisting of a glass container with a liquid inside, placed on a digital scale. The scale's display shows a reading of 2740.49 g. The system is supported by a metal frame with clamps.</p> <p>B IV</p>	<p>Density measurement system, built by Glass Technology Excellent Center (GTEC), Department of Physics, Faculty of Science, Ubon Ratchathani University</p>
 <p>A glass grinding and polishing machine with a circular grinding wheel and a polishing disc. It is a yellow and black machine with a control panel. A red cable reel is visible next to it.</p> <p>B V</p>	<p>Glass grinding and polishing machine built by Glass Technology Excellent Center (GTEC), Department of Physics, Faculty of Science, Ubon Ratchathani University</p>
 <p>An X-ray analytical microscope setup on a desk. It includes a HORIBA Scientific XGT-5200 WR spectrometer, a computer monitor displaying a grid of images, a keyboard, and a mouse. A bottle of liquid is also visible on the desk.</p> <p>B VI</p>	<p>X-ray analytical microscope of energy dispersive X-ray fluorescence spectrometer, HORIBA Scientific brand, XGT-5200 WR model at Scientific Equipment Center, Ubon Ratchathani University</p>




Figure no.	Name
 <p data-bbox="523 757 608 790">B VII</p>	<p data-bbox="863 472 1377 674">Fourier Transform Infrared spectrometer (FTIR), Perkin Elmer brand, Spectrum RXI model at Scientific Equipment Center, Ubon Ratchathani University</p>
 <p data-bbox="523 1256 608 1290">B VIII</p>	<p data-bbox="863 931 1369 1245">Microhardness testing machine, Mitutoyo company, Mitsubishi brand, MVK- H1 model at Department of Industrial Engineering, Faculty of Engineering, Ubon Ratchathani University</p>
 <p data-bbox="531 1856 600 1890">B IX</p>	<p data-bbox="858 1487 1385 1744">X-ray Diffractometer, Phillips PANalytical brand, X'Pert Highscore model at Department of Physics, Faculty of Science, Ubon Ratchathani University</p>





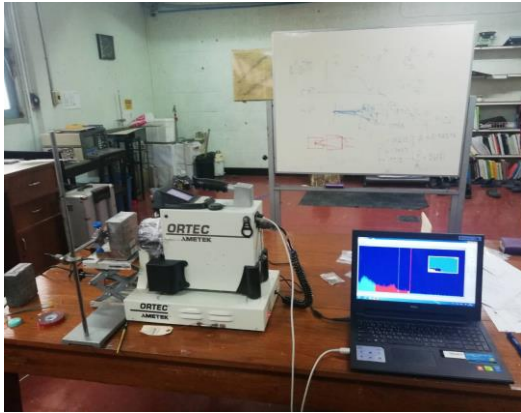



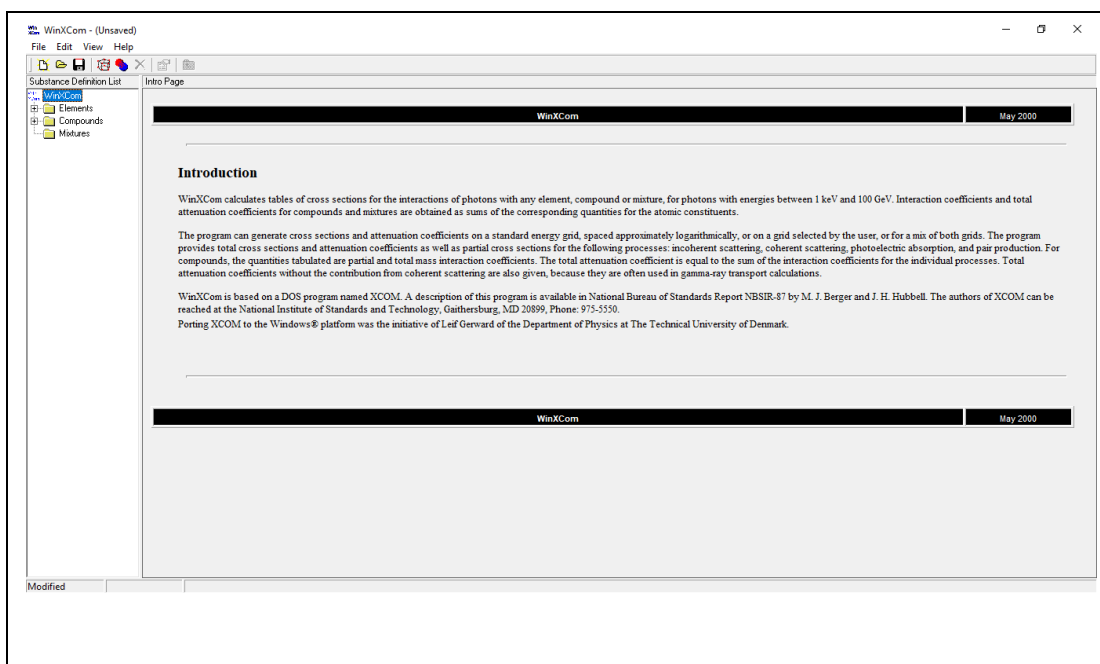
Figure no.	Name
 <p data-bbox="539 768 596 801">B X</p>	<p data-bbox="863 456 1382 712">Ultrasonic flaw detector, SONATEST brand, Sitescan 230 model with cable probe at Department of Physics, Faculty of Science, Ubon Ratchathani University</p>
 <p data-bbox="533 1200 603 1234">B XI</p>	<p data-bbox="874 940 1370 1137">Electrical balance, Denver Instrument company with accuracy 0.0001 at Department of Physics, Faculty of Science, Ubon Ratchathani University</p>
 <p data-bbox="526 1579 606 1612">B XII</p>	<p data-bbox="861 1337 1382 1534">Cutting machine, Benetec limited brand, labcut 1010 model at Department of Physics, Faculty of Science, Ubon Ratchathani University</p>
 <p data-bbox="526 1966 606 2000">B XII</p>	<p data-bbox="871 1747 1372 1890">Hydraulic press, SPECAC company at Scientific Equipment Center, Ubon Ratchathani University</p>

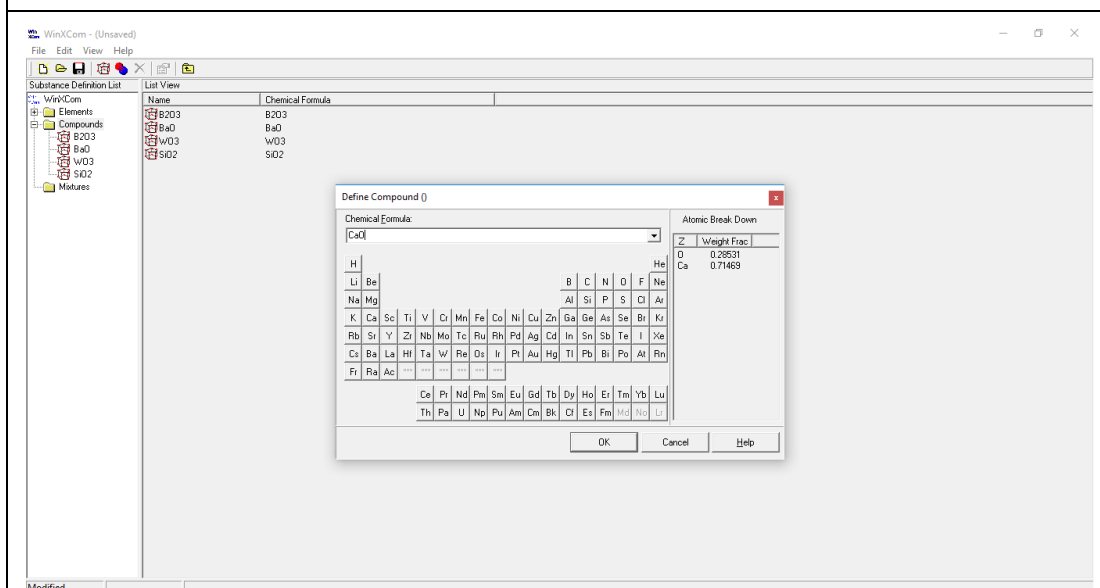
Figure no.	Name
 <p data-bbox="518 763 614 797">B XIII</p>	<p data-bbox="863 434 1380 689">The detector type NaI (Tl), ORTEC brand, a division of AMETEK model at Department of Nuclear Engineering, Faculty of Engineering, Chulalongkorn University</p>
 <p data-bbox="518 1151 614 1184">B XIV</p>	<p data-bbox="1007 987 1235 1021">Alumina crucible</p>
 <p data-bbox="518 1541 614 1574">B XV</p>	<p data-bbox="986 1375 1257 1408">Stainless steel molds</p>
 <p data-bbox="518 1928 614 1962">B XVI</p>	<p data-bbox="863 1706 1385 1854">lead glass (standard shielding), Kongsak X-ray Medical Industry CO., LTD. company</p>

APPENDIX C

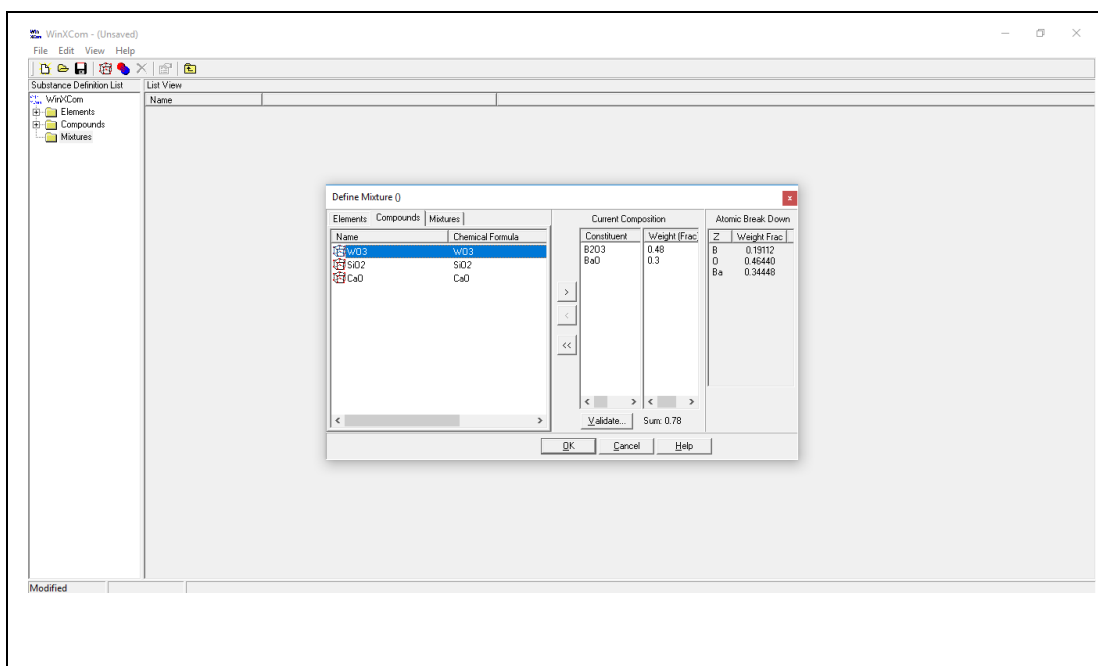
WinXCom program for research



C I Window of WinXCom program



C II Selection of elements for creating compound



C III Creating mixture of studied glass system

WinXCom - (Unsaved)

File Edit View Help

Substance Definition List

30BaO 50B2O3 10CaO 10SiO2 2W03

Partial Interaction Coefficients and Total Attenuation Coefficients

		Energy (MeV)	Coherent (cm ² /g)	InCoherent (cm ² /g)	Photo Electric (cm ² /g)	PAIR Nuclear (cm ² /g)	PAIR Electron (cm ² /g)	Sum (cm ² /g)	Sum NonCoherent (cm ² /g)
		1.000E-003	3.64E+000	9.81E-003	5.01E+003	0	0	5.01E+003	5.01E+003
		1.031E-003	3.62E+000	1.03E-002	4.65E+003	0	0	4.66E+003	4.65E+003
		1.062E-003	3.61E+000	1.08E-002	4.32E+003	0	0	4.33E+003	4.32E+003
56	M3	1.062E-003	3.61E+000	1.08E-002	4.61E+003	0	0	4.61E+003	4.61E+003
		1.099E-003	3.59E+000	1.14E-002	4.25E+003	0	0	4.26E+003	4.25E+003
		1.137E-003	3.57E+000	1.20E-002	3.92E+003	0	0	3.93E+003	3.92E+003
56	M2	1.137E-003	3.57E+000	1.20E-002	4.04E+003	0	0	4.04E+003	4.04E+003
		1.212E-003	3.54E+000	1.33E-002	3.47E+003	0	0	3.47E+003	3.47E+003
		1.293E-003	3.50E+000	1.47E-002	2.98E+003	0	0	2.99E+003	2.98E+003
56	M1	1.293E-003	3.50E+000	1.47E-002	3.05E+003	0	0	3.06E+003	3.05E+003
		1.500E-003	3.40E+000	1.84E-002	2.13E+003	0	0	2.13E+003	2.13E+003
		1.809E-003	3.24E+000	2.40E-002	1.33E+003	0	0	1.34E+003	1.33E+003
74	M5	1.809E-003	3.24E+000	2.40E-002	1.34E+003	0	0	1.34E+003	1.34E+003
		1.824E-003	3.23E+000	2.43E-002	1.31E+003	0	0	1.32E+003	1.31E+003
		1.839E-003	3.22E+000	2.46E-002	1.29E+003	0	0	1.30E+003	1.29E+003
14	K	1.839E-003	3.22E+000	2.46E-002	1.43E+003	0	0	1.43E+003	1.43E+003
		1.855E-003	3.22E+000	2.49E-002	1.41E+003	0	0	1.41E+003	1.41E+003
		1.872E-003	3.21E+000	2.52E-002	1.39E+003	0	0	1.39E+003	1.39E+003
74	M4	1.872E-003	3.21E+000	2.52E-002	1.39E+003	0	0	1.39E+003	1.39E+003
		2.000E-003	3.14E+000	2.75E-002	1.20E+003	0	0	1.21E+003	1.20E+003
		2.281E-003	3.01E+000	3.27E-002	8.63E+002	0	0	8.66E+002	8.63E+002
74	M3	2.281E-003	3.01E+000	3.27E-002	8.70E+002	0	0	8.73E+002	8.70E+002
		2.423E-003	2.94E+000	3.52E-002	7.44E+002	0	0	7.47E+002	7.44E+002
		2.575E-003	2.87E+000	3.79E-002	6.36E+002	0	0	6.39E+002	6.36E+002
74	M2	2.575E-003	2.87E+000	3.79E-002	6.38E+002	0	0	6.41E+002	6.38E+002
		2.694E-003	2.81E+000	4.00E-002	5.67E+002	0	0	5.70E+002	5.67E+002
		2.820E-003	2.76E+000	4.21E-002	5.04E+002	0	0	5.07E+002	5.04E+002
74	M1	2.820E-003	2.76E+000	4.21E-002	5.05E+002	0	0	5.08E+002	5.05E+002

C IV The results from processing of WinXCom program

APPENDIX D
Publications and Conferences

Year	Publications and Conferences
2015	<ul style="list-style-type: none"> • P. Gunhakoon, S. Pencharee, R. Laopaiboon. “The effect of lead to structural and elastic properties of recycle silica gel glass (RSG)”, Poster presentation, <u>Siam Physics Congress 2015 academic conference</u>, Sofitel Krabi Phokeethra Golf & Spa Resort, Krabi. • P. Gunhakoon, S. Pencharee, J. Laopaiboon, R. Laopaiboon. “Structural and elastic properties of Strontium lead silicate glass prepared from silica gel waste”, Poster presentation, <u>North Eastern Science and Technology Conference 2015</u>, Ubon Ratchathani University.
2016	<ul style="list-style-type: none"> • P. Gunhakoon, O. Jaiboon, S. Pencharee, J. Laopaiboon, R. Laopaiboon. “Investigation of strontium lead silicate glass prepared from silica gel used as gamma ray shielding materials”, Poster presentation, <u>International Scientific Conference on Engineering and Applied Sciences</u>, Beijing, China. • P. Gunhakoon, O. Jaiboon, S. Pencharee, J. Laopaiboon, R. Laopaiboon. “Investigation of lead silicate glass prepared from silica gel for used as gamma-ray shielding materials: a comparison between CaO and SrO”, <u>Journal of Science & Technology</u>, Ubon Ratchathani University, Special Issue, December 2016. Also, I participated a poster presentation of <u>Siam Physics Congress 2016 academic conference</u>, Baansuan Khunta Golf & Resort, Ubon Ratchathani.
2017	<ul style="list-style-type: none"> • P. Gunhakoon, O. Jaiboon, S. Pencharee, J. Laopaiboon, R. Laopaiboon and C. Yenchai. “Gamma-ray shielding and structural properties of stron-strontium-lead-silicate glasses”, Poster presentation, <u>Siam Physics Congress 2017 academic conference</u>, Rayong Marriott Resort & Spa, Rayong.

Year	Publications and Conferences
2018	<ul style="list-style-type: none"> • P. Gunhakoon, J. Laopaiboon, O. Jaiboon, S. Pencharee, R. Laopaiboon. “The effect of lead oxide on structural and elastic properties of strontium lead silicate glass from deteriorated silica gel”, <u>Journal of Engineering and Applied Science Research</u>, July-September 2018; 45(3): 230-234.
2019	<ul style="list-style-type: none"> • P. Gunhakoon, P. Sopapan, J. Laopaiboon, O. Jaiboon and R. Laopaiboon. “Influence of gamma ray on elastic and structural properties of recycled window glass doped with chromium oxide using ultrasonic contact technique and FTIR spectroscopy”, <u>Journal of Physics: Conf. Series</u>, 1285 (2019) 012033. Also, I participated a poster presentation of International Nuclear Science and Technology Conference, Centara Grand at Central Ladprao, Bangkok. • P. Sopapan, J. Laopaiboon, O. Jaiboon, P. Gunhakoon and R. Laopaiboon. “Effect of zinc oxide on elastic and structural properties of recycled window glass: a comparative study between before and after gamma irradiation”, <u>Journal of Physics: Conf. Series</u>, 1285 (2019) 012032.
2020	<ul style="list-style-type: none"> • P. Gunhakoon, T. Thongklom, P. Sopapan, J. Laopaiboon, R. Laopaiboon, O. Jaiboon. “Influence of WO_3 on elastic and structural properties of barium-borate-bagasse-cassava rhizome glass system”, <u>Journal of Materials Chemistry and Physics</u>, 243 (2020) 122587. • P. Sopapan, R. Laopaiboon, J. Laopaiboon, P. Gunhakoon, T. Thongklom and O. Jaiboon. “Study of bagasse and cassava rhizome effects on the physical, mechanical and structural properties of soda-lime borate glasses”, <u>Journal of SN Applied Sciences</u>, (2020), 2: 929.

APPENDIX E

Experiences

Year	Experiences
2012	<ul style="list-style-type: none"> • Internships, experience and inspiring about scientific research: Bio-physics, Mahidol University, Nakhon Pathom
2013	<ul style="list-style-type: none"> • Internships, experience and inspiring about scientific research: effect of polyvinylpyrrolidone on formation of Cu nanoparticles, King Mongkut's University of Technology Thonburi, Bangkok
2014	<ul style="list-style-type: none"> • Internships and experience, Physical Analysis Laboratory, Material Characterization Unit, National Metal and Materials Technology Center (MTEC), Pathum Thani. I was trained to analyze the material and scientific equipment such as grinding and polishing machine, Ball mill machine and Scanning electron microscope (EBSD).
2015	<ul style="list-style-type: none"> • Assistant lecturer of little scientist house project, Ubon Ratchathani University.
2017	<ul style="list-style-type: none"> • Internships and experience in experiment about radiation of materials, Department of Nuclear Engineering, Faculty of Engineering, Chula-longkorn University, Bangkok. • Training for the skill to operate the Conventional ultrasonic flaw detector and Phased Array, Ubon Ratchathani University by C.V.M. Group Co., Ltd.
2018	<ul style="list-style-type: none"> • KidBright Workshop for Trainer, Ubon Ratchathani University by National Electronics and Computer Technology Center (NECTEC)
2019	<ul style="list-style-type: none"> • Training for Radiation Safety Level 1, Thailand Institute of Nuclear Technology, Pathum Thani.
2020	<ul style="list-style-type: none"> • Assistant lecturer of Education Development Capacity Building Project in the utilization of x-ray, gamma ray and neutron for research and industrial applications

VITAE

Name	Miss Pattaranipa Gunhakoon
Date of Birth	29 June 1992
Address	36 Moo 2, Arun Prasert Rd., Na Mo Ma, Muang, Amnat Charoen, 37000
Phone	0930826429
Email	p.gunhakoon29@gmail.com
Education	2017 - Ph.D. candidate Ubon Ratchathani University Doctor of Philosophy (Physics) 2015 - 2017 Ubon Ratchathani University Master of Science (Physics) 2011 - 2015 Ubon Ratchathani University Bachelor of Science (Physics)
Scholarship	Science Achievement Scholarship of Thailand (SAST), Class 3, Phase 2 of the academic year 2011 (bachelor-master-doctorate)